UNIVERSITY OF
KWAZULU-NATAL
INYUVESI
YAKWAZULU-NATALI

THE DESIGN AND SYNTHESIS OF GOLD NANOPARTICLES AND ITS INTERACTION WITH MAMMALIAN CELLS IN CULTURE

By

Geraldine Genevive Lazarus

Submitted in fulfilment of the academic requirements for the degree of

DOCTOR OF PHILOSOPHY

In the School of Life Sciences

University of KwaZulu-Natal, Durban

December 2014

Supervisor: Dr. Moganavelli Singh

ABSTRACT

Cancer is a disease characterized by accelerated cell growth, resulting in healthy tissue being destroyed by the processes of invasion and metastasis. Non-viral gene delivery approaches have been extensively studied as a basic tool for intracellular gene transfer and gene therapy especially for genetic aberrations including cancer. Gold nanoparticles have attracted strong biomedical interest for drug delivery due to their low toxic nature, surface plasmon resonance and capability of increasing the stability of the payload. In the present study the synthesis of photoluminescent nanoparticles consisting of a gold core coated with polyethyleneimine, poly-L-lysine, cysteine and chitosan is reported. These functionalized gold nanoparticles (FAuNPs) were investigated at different pH values and ionic strength to identify the optimum conditions to produce stable monodisperse nanoparticles. FAuNPs showed good stability at low ionic strength which is important for the flexibility of the polymer chain. All nanoparticle/polymer formulations remained in the size range 11.9-195 nm with narrow particle distributions and low PDI (<1.2). TEM images revealed nanoparticles that were spherical and monodispersed. Nanoparticle and pDNA complexation was efficiently demonstrated in the band shift and ethidium bromide intercalation assays respectively. The serum nuclease digestion assay revealed that the nanoparticles provided partial protection to the complexed plasmid DNA (pCMV-*luc*). MTT cytotoxicity experiments indicated that the FAuNPs elicited a dose dependent cytotoxic effect with the four mammalian cell lines (HepG2, HEK293, HeLa and Caco2) tested responding differently. Au-PEI/pDNA maintained over 80% cell viability across all cell lines, while the Au-cys/pDNA exhibited a significant 91.8% (p<0.001) in Caco2 cells, Au-Chit/pDNA 126% (p<0.01) in HepG2 cells and Au-PLL/pDNA 104% in Hela cells. Transfection studies were accomplished using the luciferase reporter gene assay. Results showed that the FAuNPs produced greater transgene activity than the cationic polymer/DNA complexes on their own. This was evident for the Au-PEI/pDNA complex which produced a 12 fold increase in the HEK293 cells and a 9 fold increase in the HepG2 cells, compared to the PEI/pDNA complexes alone. The results of this study suggest that FAuNPs low cytotoxicity coupled with the ability to parametrically control particle size and surface properties, make these nanoparticles suitable non-viral gene delivery vectors. However further engineering and modifications of the FAuNPs may be required to enable *in vivo* gene delivery.

PREFACE

The experimental work described in this thesis was carried out at the: Chemistry Department, Faculty of Science and Agriculture, University of Zululand, Empangeni from October 2011 to December 2011, under the supervision of Prof. N. Revaprasadu; Applied Physics Department, Faculty of Science, University of Granada, Spain from January 2012 to July 2012 under the supervision of Dr. Julián López-Viota and at the Biochemistry Department, School of Life Sciences, University of KwaZulu-Natal, Durban from August 2012 to November 2014, under the supervision of Dr. M. Singh.

These studies represent original work by the author and have not otherwise been submitted in any form for any degree or diploma to any tertiary institution. Where use has been made of the work of others it is duly acknowledged in the text.

DECLARATION 1 - PLAGIARISM

I, Geraldine Genevive Lazarus declare that:

1. The research reported in this thesis, except where otherwise stated, is my original work.

2. This thesis has not been submitted for any degree or examination at any other university.

3. This thesis does not contain any person's data, pictures, graphs or other information, unless specifically acknowledged as being sourced from other persons.

4. This thesis does not contain others persons writing unless specifically acknowledged as being sourced from other researchers. Where other written sources have been cited, then:

   -Their words have been re-written but the general information attributed to them has been referenced.

   -Where their exact words have been used, then their writing has been placed in italics and inside quotation marks, and referenced.

5. This thesis does not contain text, graphics or tables copied and pasted from the internet unless specifically acknowledged, and the source being detailed in the thesis and in the Reference section.

Signed:

DECLARATION 2 – PUBLICATIONS

DETAILS OF CONTRIBUTION TO PUBLICATIONS that form part and/or include research presented in this thesis (include publications in preparation, submitted, *in press* and published and give details of the contribution of each author to the experimental work and writing of each publication).

Published work

Lazarus, GG., Revaprasadu, N., López-Viota., J and Singh M**.** 2014. The electrokinetic characterization of gold nanoparticles, functionalized with cationic functional groups, and its' interaction with DNA. *Colloids and Surfaces B: Biointerfaces.* **121**: 425–431. (Appendix A, pg. 121)

Submitted manuscript

Lazarus, GG., Singh, M. The influence of gold nanoparticles on polythyleneimine cytotoxity in kidney cells. (*Journal of Analytical Biochemistry*, Ref: ABIO-13-954)

Manuscript in preparation

Lazarus, GG., Singh, M. The *in vitro* transfection efficiency of functionalized gold nanoparticles and their transfection efficiencies in mammalian cells.

Conference presentation

The electrokinetic characterization of gold nanoparticles, functionalized with cationic functional groups, and its interaction with DNA. (ID: 80316). International Conference on Bioinformatics and Biomedical Engineering (iCBBE), Beijing China, Sep 26th -28th, 2013. (Appendix B, pg. 122)

Signed:

TABLE OF CONTENTS

LIST OF FIGURES

LIST OF TABLES

ABBREVIATIONS AND SYMBOLS

Amp^r	Ampicillin resistance
Au	Gold
AuNP	Gold nanoparticle
BCA	Bicinchoninic acid
Caco2	Human epithelial colorectal adenocarcinoma cells
Chit	Chitosan
CMV	Cytomegalovirus promoter
CP	Cationic polymer
Cys	Cysteine
DMSO	Dimethyl sulphoxide
EDTA	*N*, *N*, *N'*, *N'*-ethylenediaminetetra acetic acid
EMEM	Eagle's minimum essential medium
EtBR	Ethidium bromide
FAuNP	Functionalized gold nanoparticle
FCS	Fetal calf serum
HBS	Hepes buffered solution
HEK293	Human embryonic kidney cells
Hela	Human cervical cancer cells
HepG2	Human hepatocellular carcinoma cells
hr	Hour
kbp	Kilo base pair
L-lys	Lysine
luc	Luciferase
M	Molar
mM	Milli mole
MTT)	3-[4,5-dimethylthiazol-2-yl]-2.5-siphenyltetrazolium bromide

M_w	Molecular weight
nm	Nanometers
NTA	NanoSight tracking analysis
NP	Nanoparticle
PBS	Phosphate buffered saline
pCMV-*luc*	Plasmid containing the vector cytomegalovirus-luciferase
PDI	Polydispersity Index
pDNA	Plasmid DNA
PEI	Polyethylenemine
PL	Photoluminescence spectra
PLL	Poly-L-lysine
pSG5	Plasmid containing the vector pregnancy specific beta-1-glycoprotein 5
RLU	Relative luminescence units
rpm	Revolutions per minute
SD	Standard deviation
SDS	Sodium dodecyl sulphate
siRNA	Small interfering RNA
SPR	Surface plasmon resonance
*U*e	Electrophoretic mobility
UV	Ultraviolet spectroscopy
µg	Micrograms
µL	Microliters
$^{v}/_{v}$	Volume to volume ratio
$^{w}/_{w}$	Weight to weight ratio
λ	Wavelength (lambda)

ACKNOWLEDGEMENTS

I would like to express my appreciation to the following people who have contributed to the success of this project:

- My supervisor, Dr. Moganavelli Singh, (Biochemistry, University of KwaZulu Natal, Durban) for her advice, patience, time and guidance in revealing the fascinating field of gene delivery to me.
- Prof. Neerish Revaprasadu, (Chemistry, University of Zululand, Empangeni) for allowing me the use of the chemistry laboratory for the synthesis procedures.
- Prof. Ángel V. Delgado Mora and Dr. Julián López-Viota Gallardo, (Applied Physics, University of Granada, Spain) for their expertise in the electrokinetic characterization and for the use of the Nanosight and ZetaSizer instruments.
- The National Research Foundation (NRF) for their generous financial assistance.
- The Erasmus Mundus Program (EMA2SA) for awarding me the opportunity to gain international lab experience by studying abroad in Spain.
- To my colleagues at UKZN for their priceless memories and for creating an environment of fun and laughter. May God bless you as you reach for your dreams.
- To Dr. K. Naidoo, for her support and friendship.
- To my sisters, Jolene and Jacqueline, for their love and support.
- And most especially to my dear parents, Daniel and Margaret Lazarus, for being my pillar of strength and for their tremendous support throughout my life. Their prayers and encouragement have led to the completion of this thesis.
- Above all I want to thank my Lord Jesus, for granting me the wisdom and knowledge and courage to accomplish my goals and dreams.

DEDICATION

To my dearest parents Daniel & Margaret Lazarus

Thank you for your infinite love and care

Chapter One

Literature Review

Chapter One

Introduction and literature review

1.1 The beginning of gene therapy

Gene therapy has captured the attention of many researchers and medical practitioners in the scientific community. The perception that this approach can treat diseases by delivering exogenous DNA into the nuclei of target cells to express a therapeutic protein was first proposed in 1972 (Kim *et al.,* 2013). It is based on the transfer and expression of therapeutic genes in specific target cells (Mohr and Geissler, 2002). Although gene therapy sounds like a new and innovative field of research, the transfer of genetic material into living cells has been around for decades. However, this field is still in need of becoming an acceptable treatment as a cure for human diseases even though it has established therapeutic applications in infectious diseases, cancer and degenerative disorders. Each successful trial holds the prospect of successful treatment making it more feasible. Various examples of gene therapeutics include iron oxide nanoparticles, amino-modified silica nanoparticles, carbon nanotubes and gold nanoparticles (Kneur *et al.*, 2000; Xiang *et al.*, 2003; Bianco *et al.*, 2005 and Sandhu *et al.*, 2002). The significance of nucleic acid delivery for disease treatment is echoed in an abundance of clinical trials in scientific literature, with the approach being to transfect cells with plasmid DNA that are designed to replace a defective gene in the target cell genome.

Gene therapy trials have been implemented worldwide over the past twenty years, however, little progress has been made in curing diseases because a number of major steps must be overcome for successful clinical applications. Gene therapy must not only improve and enhance gene transfer but also gene expression. An ideal gene delivery system should be non-toxic, non-immunogenic, biodegradable, stable, accessible and suitable for efficient gene expression. A model system should meet three important criteria. Firstly, it should protect the therapeutic gene against degradation by nucleases in intercellular matrices, secondly it should transport the therapeutic gene (transgene) across the plasma membrane and into the nucleus of target cells and thirdly it should not be toxic or detrimental to the cell (Gao *et al.*, 2007). The transfer of nucleic

acids using carriers such as polymeric micelles, dendrimers, nanotubes or nanoparticles (NPs) has attracted increasing attention as a consequence of the low feasibility, stability, ease of large-scale production and lack of immunogenicity that characterize some of these nanomaterials (Cebrian *et al.*, 2011; Luo and Saltzman, 2000a; Pouton and Seymour, 2001 and Gemeinhart *et al.*, 2000). Many possible vectors are under intense scientific investigation (Godbey, 1999.) Two classes of vectors proposed for gene delivery are the viral and non-viral vectors which differ in their assembling processes. Viral dependent methods such as the retrovirus, adenovirus, adeno-associated virus and other viral vectors are still popular methods of gene delivery. They are assembled in the cell and are replication-defective viruses that have over the years presented many safety issues leading to the emergence of a variety of non-viral gene delivery vehicle approaches (Kim *et al.*, 1993). Although the use of viruses for gene therapy is highly effective in terms of its ease and feasibility, there are certain shortcomings associated with its practical use such as insufficient viral titers, toxicity and the potential replication of competent viruses which may result in lower efficacy in gene transfer and gene expression. (Huang *et al.,* 1999). Viral vectors have boundaries and therefore make synthetic vectors an attractive alternative. The successful system should selectively and competently deliver genetic material, with the ultimate goal being to cure inherited and acquired disorders and eliminating their causes, by adding, correcting or replacing genes (Mohr and Geissler, 2002).

Non-viral approaches have also been extensively studied for intracellular gene transfer and gene therapy and have an advantage over viral vectors due to their feasibility of being produced on a large scale, simplicity and low toxicity (Huang *et al.,* 1999). Liposomal assimilation into nanoparticles is preferred because of decreased side effects and prolonged drug exposure due to slow release. These are known as second and third generation carriers with ligands. The most important factors for applicability of the nanoparticle include particle sizes, particle surface functionalities and solubility in the desired media. At the nanoscale, the increase in the surface area to volume ratio is an exclusive phenomenon as it alters the mechanical, thermal and catalytic properties of the material. There is a still a need for better gene transfer technology, and its application holds possibilities for great developments in how we manage ailments today. It is apparent that understanding the molecular stages of surface binding, endocytosis, escape from

the endosome and delivery of the nucleic acid to the nucleus will provide us with vital signs towards improved designs of non-viral vectors that can evade viral-associated disadvantages. The need to understand endocytic pathways has never been more critical due to an increasing number of nanosized drug carriers (liposomes, nanoparticles and viral vectors), macromolecule drugs (proteins, oligonucleotides and synthetic polymers) and macromolecular conjugates (of polymers, proteins and antibodies) in research and development (Figure 1.1). A further benefit of the use of nanoparticles as non-viral vectors for gene delivery *in vitro* comes from their ability to sediment on the surface of target cells, which accelerates the transfer of biomolecules (Gemeinhart *et al.*, 2005).

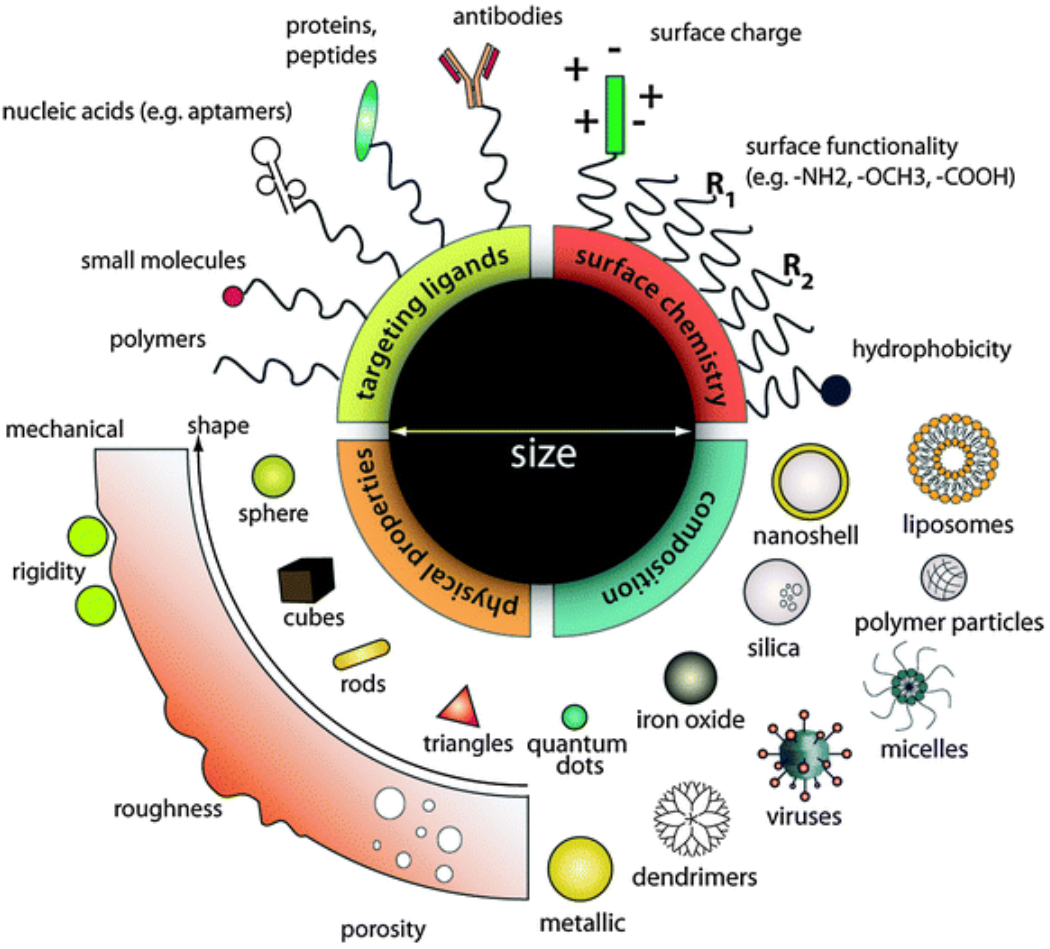

Figure 1.1: The assembling of nanoparticles with different material compositions and different physical and chemical properties, and functionalization with a myriad of ligands for biological targeting (Leo *et al.*, 2011).

1.2 Emerging trends in nanotechnology

Nanotechnology has emerged with new materials and products altering many aspects of our lives and generating international interest by academics and industrialists. It deals with nanoscale materials (1-100 nanometers) by developing novel technologies to probe and manipulate single atoms and molecules. A nanoparticle behaves as a whole unit in terms of its transport and properties and their small size allows them to penetrate cells and tissues. Materials at the nanoscale level often exhibit very different and desirable physical, chemical, and biological properties compared to their normal sized counterparts. These same properties may also contribute to their toxicity and to their ability to produce adverse side effects. Subsequently, countries and international organizations have raised safety concerns over the applications and exposure to these nanoparticles. The Organization for Economic Cooperation and Development (OECD), an inter-governmental organization, is an organization that plays a critical global role in ensuring that emerging technologies, including nanotechnology, are developed responsibly (Murashov *et al.*, 2011). A large range of materials with distinct properties are found in sunscreens, cosmetics, paint, remediation, water purification, batteries, lubricants, medical equipment and drug delivery treatments. Nanotechnology may help in transporting drugs across the blood brain barrier. Researchers have been building liposomes loaded with nanoparticles to gain access through the blood brain barrier. This new field is still being explored and holds promise for the application of nanotechnology in clinical neuroscience for treatment of disorders such as Alzheimer's and Parkinson's disease. Delivering drugs across the blood brain barrier is one of the most promising applications of nanotechnology in neuroscience. In essence nanoparticles could potentially carry out multiple tasks in a predetermined sequence, which is significant in the distribution of drugs across the blood brain barrier (Brigger *et al.*, 2002).

1.3 Cancer and associated diseases

Cancer is a serious disease in developing countries and is fast becoming the prime cause of death in industrialized counties as well. It is defined as a disease that causes uncontrollable growth of dysfunctional cells due to its aggressive growth profile. The distribution of a primary tumor to an anatomical site is defined as cancer metastasis. It remains a major challenge and cause of mortality despite the recent advances in cancer therapy. Oncogenes and tumor suppressor genes

play a crucial role in the growth and progression of cancer (Weir *et al.,* 2004). Tumors require a relatively short expression of therapeutically active proteins, whilst monogenic diseases such as cystic fibrosis need long term expression (Anson *et al.*, 2006). Four important targets have to be achieved by vectors in cancer gene therapy, viz. oncogene expression must be turned off, tumor suppressor expression must be enhanced to induce apoptosis of cancer cells, neo-angiogenesis must be inhibited and the immune system must be stimulated against the tumor cells (Morille *et al.*, 2008). The near infrared (NIR) laser in the region of 650-1000 nm has attracted increased attention as NIR laser irradiation can induce hyperthermia damage of cancer cells and tumors with deep tissue penetration and skin absorbance. In order to exploit new strategies for treatment of metastatic cancers, new avenues for efficient management are highly desired. Statistics reveal that head and neck carcinoma is the 6th most common cancer worldwide (Wang *et al.*, 2014). Approximately 600 000 new cases are reported yearly. Revealing a mortality rate of 50%, squamous cell carcinoma of the oral cavity accounts for close to 389 000 cases per year. Standard treatment such as radiation therapy, surgery and chemotherapy are effective but may cause significant side effects in patients. Often times this treatment is found to be ineffective due to infiltrating and progressive tumors. Surgical operations on squamous cell carcinoma cause unnecessary damage to adjacent or underlying anatomical structures, while radiotherapy can lead to complications such as osteoradionecrosis, soft tissue necrosis or spinal cord myelitis. Although there has been recent advances in modality therapy, the overall 5 year survival rate of patients with head and neck squamous cell carcinoma remains at 40-50%. Cancer research UK reported that prostate cancer is the fourth most common form of cancer in the country, with 40 841 new cases reported since 2009 (http://www.wired.co.uk, Accessed 31 October 2014). Therefore there is an urgent need to develop non-invasive methods with fewer side effects to treat patients suffering from cancer.

1.4 Mechanisms of gene delivery

Popular methods of transfection employed over the years include chemical or physical methods by calcium phosphate precipitation, electroporation, microinjection, and liposomal transfer. Non-viral gene delivery systems can either be non-targeted or targeted to a specific cell. Effective

delivery systems are required to promote targeted delivery of peptides, oligonucleotides and proteins to specific intracellular compartments. Non-targeted gene delivery methods would non-specifically deliver genes to all cells exposed to the delivery vehicle (Kim *et al.*, 1993). Macromolecular therapeutics and nanosized delivery systems are generally taken up by the process of endocytosis. Following internalization via ligand-stimulated cellular pathways such as clathrin-coated pits and membrane mechanisms, intracellular trafficking can lead to rapid removal out of the cell (5-10 min), trancytotic passage across an epithelial barrier, lysosomotropic delivery (30 minutes-1 hour) or delivery to the Golgi network. Physical approaches (carrier-free gene delivery) and chemical approaches (synthetic vector-based gene delivery have been explored. Physical approaches include needle injection (Wolff *et al.*, 1990) electroporation (Heller *et al.*, 2005 and Neumann *et al.*, 1982), gene gun (Yang *et al.*, 1990 and Yang *et al.*, 1995), hydrodynamic delivery (Liu *et al.*, 1999 and Zhang *et al.*, 1999) and ultrasound (Lawrie *et al.*, 2000).

1.5 Mechanical methods

There are several mechanical means of transfection and the three commonly employed are discussed below.

1.5.1 Microinjection

The direct injection of nuclei is perhaps the most simple, with respect to its practicality and has the advantage of not exposing DNA to the cellular compartments where degradation may occur. The drawback is that microinjection can be achieved only on a small scale i.e. one cell at a time which limits its use to applications in which individual cell manipulation is desired resulting in low levels of gene expression (Gao *et al.*, 2007). Though relatively efficient, this method is also laborious (Luo and Saltzman, 2000a). A pressure mediated naked oligonucleotide transfection method using controlled non-distending pressure was developed by Mann and colleagues (1999), and showed gene delivery efficiency of greater than 50% in cardiovascular tissue. Naked DNA-mediated gene delivery may not be conceivable because DNA is large in size and highly hydrophilic. This causes it to be kept out of cells in animals by barriers that include the

endothelium, interstitial matrices, the mucus lining, tightly specialized junctions of epithelial cells and the plasma membrane of all cells. Nucleases further reduce the chance that DNA eventually entering the nuclei will be intact and functional. Physical approaches can induce injuries and defects on cell membranes so that DNA can enter the cell by diffusion.

1.5.2 Gene gun method

Particle bombardment also called the biolistic particle delivery through a gene gun is an ideal method for gene transfer to skin, mucosa or surgically exposed tissue within a confined area (Yang *et al.*, 1990). It uses a high pressure helium gas surge to accelerate the cargo and deliver it into the cell. It was first described by Klein *et al*. in 1987 and used primarily to transfect plant cells. Due to the focus being on the DNA transfection efficiency, the fate and the localization has not been reported. This method has been used to transfer nanosensors into several adherent cells lines and the cells displayed a good nuclear uptake of the nanosensor according to the fluorescence levels and distribution as measured by confocal microscopy (Webster *et al.*, 2007). DNA coated on the surface of gold nanoparticles are fast-tracked by pressurized gas at high velocity, to penetrate a few millimeters into cell membranes and release DNA into cells (Gao, *et al.*, 2007; Yang *et al.*, 1990 and Yang and Sun., 1995). Bombardment is widely employed in DNA vaccination where limited local expression of delivered DNA is adequate to achieve immune responses (Luo *et al.*, 2000b). Further improvements could include chemical modifications on the surface of the gold particles to allow greater capacity and better stability for DNA binding and adjustment of the expelling force, for precise control of DNA deposition into cells in various tissues (Green and O'Brian *et al.*, 2000).

1.5.3 Electroporation

High voltage electric pulses to mammalian cells lead to the formation of nanometer-size pores in the plasma membrane. This approach permits cellular uptake of macromolecules and was first used to deliver DNA to mammalian cells in 1982 (Wong *et al.*, 1997 and Neumann *et al.*, 1982). DNA enters the cytoplasm of the cell through the pores as a consequence of the redistribution of membrane components that accompanies closure of the pores (Keating and Toneguzzo, 1990).

Electroporation has also been tested in several *in vivo* studies including the cornea, skin, endothelium and muscle (Banga *et al.*, 1998; Oshima *et al.*, 1998 and Alhara *et al.*, 1998). Rizzuto and colleagues (1999) used low voltage, high-frequency electric pulses to promote DNA uptake in muscle with only transient tissue damage. Gene transfer by electroporation showed less variation in efficiency across species sing direct DNA injection. Previous research demonstrated that electroporation increased transgene expression in isolated lung *ex vivo* organ culture showing that it also worked in live animals (Gao *et al.*, 2007). Single electroporation has produced long term expression that lasted for a year. Contributing factors to the efficacy of this method firstly include the amount of DNA and how well the injected plasmid DNA distributes within the treated tissue, and secondly the age of the recipient animal. Electroporation has been used to deliver DNA to a myriad of cell types *in vitro* including yeast and bacteria (Luo and Saltzman., 2000a). It is one of the most efficient gene transfer methods but is limited because of its high mortality of cells after high-voltage exposure and difficulty in optimization (Luo *et al.*, 2000a).

1.6 The history of gold nanoparticles

Dating back to the Middle Ages, base metals were converted into gold by using the philosophers' stone. The foundation of modern chemistry was laid by discovering the physical and chemical properties of the substances used (Kauffman, 1985). In the early 16th century alchemists focused on making gold drinkable which they believed would promote therapeutic applications. Women of royalty drank gold to add to the lustre of their beauty and youth. It was later found that when they died the gold was precipitated out into their hair creating strands of gold. The most common form of gold in artwork and decorative forms is the stained glass in numerous churches. Glass that shows a translucent ruby red colour in transmitted light and green colour in reflected light is due to the presence of gold colloids (Freestone *et al.*, 2007). At the dawn of the 18th century, gold was being employed in the treatment of syphilis and scrofula (Higby, 1982). In the late 90's gold sodium thimalate (Myochrysine) and gold thioglucose (Solgonal) were being used in the management of rheumatoid arthritis (Shaw, 1999). Currently a new glycopolymer mimicking the thiosugar ligand of the gold-based drug auronofin was designed (Pearson, 2015). Certain cultures worshipped the sun and the glow of gold was associated with the warmth of the sun and its life-

giving properties. Gold was seen as the earthly form of the sun and healers including religious believers from the east created jewellery that protected the wearer from the evil eye. Gold has a melting point of 1064 °C and it is the noblest of the metals because of its resistance to surface oxidation. Scientists have proven in some cases that gold does not obey quantum chemistry nor classical laws of physics (Higby, 1982).

1.6.1 Unique properties of gold nanoparticles in biomedical applications

Among the candidate nanomaterials, gold nanoparticles have emerged as therapeutic resolutions on account of their intrinsic properties and also because of their ease of synthesis and chemical functionalization of their surface (Ghosh *et al.*, 2008 and Krishna *et al.*, 2011). They can be easily functionalized by anchoring a thiol linker in their monolayers. A wide variety of functional bio-nanoconjugates have been obtained, including nanoparticles modified with peptides, proteins, antibodies, oligosaccharides and nucleic acids. This allows the nanomaterials to act as multifunctional platforms for both therapeutic and diagnostic purposes. To attain proper cellular applications using nanomaterials, it is critical not only to achieve efficient delivery to healthy cells but also to control the intracellular availability and the fate of the nanomaterial. When introduced into the body, nanostructures will at some level evoke a response from the body's protective machinery, primarily the immune system. Thus, the final goal of targeted nanostructures, can only be realized when we find ways to overcome or avoid these protective mechanisms. Using knowledge of physiologic, anatomic, and immunologic constraints combined with carefully designed nanomaterials of appropriate size and surface characteristics, gold nanoparticles have the potential to provide effective strategies for the development of effective, targeted gene/drug delivery (Papasani *et al.,* 2012).

In nanoscience and nanotechnology today, gold nanomaterials appear to be the most widely studied and used of all materials by both academics and industrialists. These nanoparticles are also synthesized with remarkable structural diversity, such as spheres, rods, wires, stars etc., with each structure exhibiting their own individual characteristics. Their potential application in cellular imaging (Murphy *et al.*, 2008) is due to their light scattering properties such as strong Raman enhancers which may also amplify fluorescence in certain cases, as previously applied in

optical microscopic imaging of cancer cells. They are bio-inert, non-toxic and readily synthesized (Daniel *et al.*, 2004), and their small size allows them to penetrate cells and tissues, making their application in medicine far reaching. They have become accepted as radiosensitizers in radiotherapy, because of their unique size and shape dependent optical properties and high extinction coefficient. The secondary electron caused by gamma or x-ray irradiation can accelerate DNA strand break (Zhang *et al.*, 2012). Gold nanoparticles, particularly gold nanorods, have shown promise owing to their strong absorption in the NIR "optical window" for biological samples. They have been used to ablate tumors located deep inside body tissues (Dickerson *et al.*, 2008; Choi *et al.*, 2011 and von Maltzahn *et al.*, 2009). The treatment involves introducing radioactive gold nanoparticles directly to a tumor causing it to shrink (Figure 1.2).

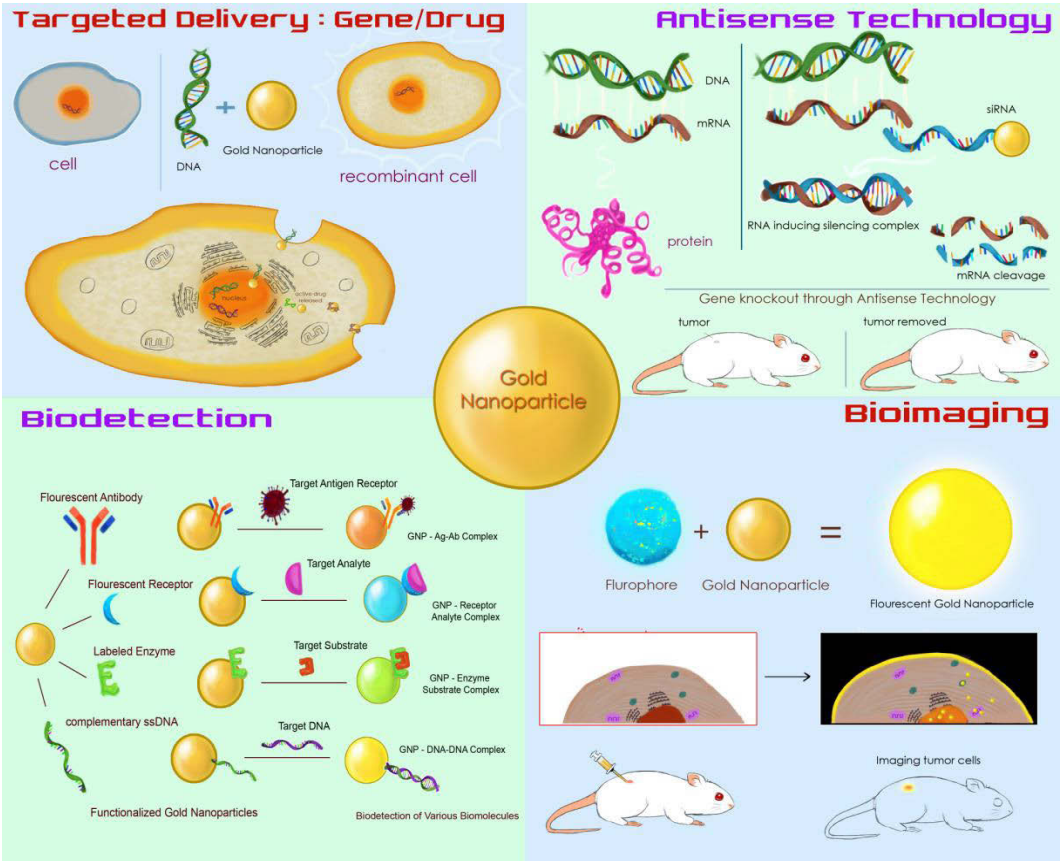

Figure 1.2: Types of functionalization of gold nanoparticles and their potential biomedical applications. Adapted from Tiwari *et al.*, 2011.

According to Sandra Axiak-Bechtel, an Assistant Professor of oncology at the University of Missouri (MU) College of Veterinary Medicine, gold nanoparticle prostate cancer treatment was found safe in dogs, (MU News Bureau) as gold nanoparticles have the potential to "tag" cancerous cells. This is due to coating of nanoparticles with imaging reagents before being introduced to brain tumor patients. The gold spheres drained out of the tiny blood vessels and lodged in nearby tumor material. Here the coated particles were selected using MRI, photoacoustic and Raman imaging, and used as a map for the brain tumors. AuNPs absorb and resonantly scatter visible and near-infrared light upon excitation of their plasmon oscillation. The photo-physical properties of gold nanoparticles can be exploited in ways that control the transport and release of drugs. Drugs can be released from a gold nanoparticle via internal stimuli that is operated by biologically controlled factors such as pH or glutathione or via external stimuli operated with the aid of stimuli-generating processes such as the application of light (Pissuwan *et al.*, 2011). AuNPs have also been utilized in gene guns where the AuNP was coated with DNA and transferred to a mylar carrier sheet (Yang *et al.*, 1990; Andree *et al.*, 1994 and Sun *et al.*, 1995). An electric arc generated by a high-voltage discharge, accelerated the nanocomplex to high velocities which enabled efficient penetration of target organs *in vivo* or single layers *in vitro*.

On a larger scale i.e. in its bulk form, gold is yellowish. It attained its noble status compared to other metals because it is resistant to surface oxidation. Gold nanoparticles have different properties to bulk molecules which render them attractive for medical purposes. Their importance is based on their surface to mass ratio that is larger than that of other particles. Furthermore, their quantum properties and their absorption abilities allow them to carry compounds such as drugs, probes and proteins. AuNPs hold promise in diagnostics and therapy, and are fast becoming one of the most popular nanomaterials worldwide. This can also be attributed to their extraordinary magnetic, optical and catalytic properties. There are a number of structural variations that can produce AuNPs in the form of rods, spheres, stars, wires and ribbons. Their industrial application is far reaching in terms of chemical processing, control of water pollution, hydrogen purification and oxidation of carbon monoxide for air purification

(McPherson and Thompson, 2009a). AuNPs offer possible suitable delivery mechanisms for gene therapy. DNA adsorption is maximized by the chemical modification of gold nanoparticles (Cebrian *et al.*, 2011). Cationic capping favours high-affinity electrostatic interactions with nucleic acids to ensure efficient binding and gene delivery to mammalian cells. It has been investigated and confirmed that the toxicity of gold nanoparticles in cancer treatment could be minimized by using less AuNPs, while exhibiting increased treatment efficiency. Rifampicin-conjugated gold nanoparticles greatly enhanced the rate as well as the efficiency of the accumulation of anticancer drugs bound to nanoparticles, and consequently their concentration inside the cancer cell. Cell viability results showed an impressive enhancement in the photothermal therapeutic effects of gold nanorods in the presence of rifampicin (Ali *et al.*, 2014).

1.7 The importance of gold nanoparticles in gene delivery

Gold nanoparticles (AuNPs) have attracted strong biomedical interest for drug delivery, due to their low toxic nature, surface plasmon resonance and capability of increasing the stability of the payload. Gene transfection represents yet another important biological application. Considering that cellular barriers keep enclosed their secret to deliver genes using nanoparticles, an important step can be achieved by studying the functionalization of gold nanoparticles because gold nanoparticles, by themselves, do not have target recognition abilities necessary for selective binding of analytes. In order to selectively detect analytes of interest, antibodies, proteins, short-chain organic acids, amine-thiols, or DNA, molecules have been used to modify the surface properties of AuNPs to provide target recognition sites (Daniel *et al.*, 2004 and Rosi *et al.*, 2005). This includes the delivery of drugs and of biomolecules such as peptides, proteins, and nucleic acids, and also for photo-thermal therapies. Major strides have been made towards the development of carrier systems based on gold nanoparticles. Current research shows that they can be functionalized and engineered using targeting ligands to accumulate in tumor cells for biological and biomedical applications including therapeutics, diagnostics, bio-imaging and bio-sensing (Ghosh *et al.*, 2008b). Figure 1.3 depicts the functionalization and various applications of AuNPs in gene and drug delivery. Prototypes have been in place in many areas of research, thus providing a tool for cancer diagnosis, tuberculosis and gene therapy (Lévy *et al.*, 2010).

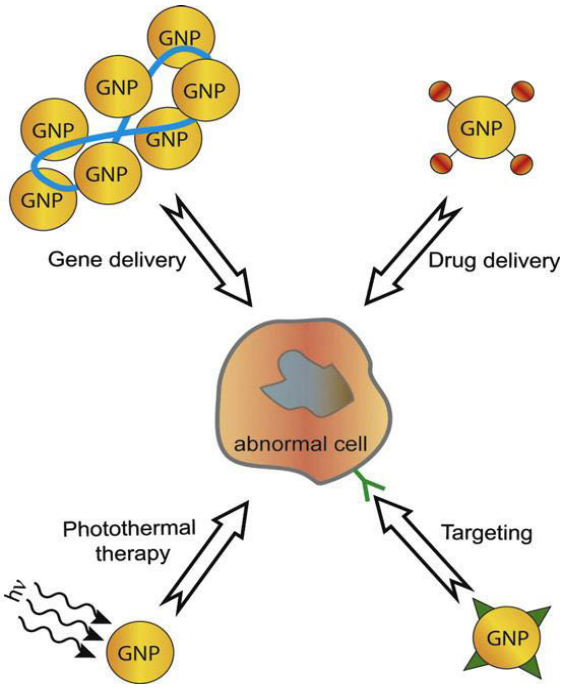

Figure 1.3: Various applications of gold nanoparticles in therapy indicating applications such as gene delivery, drug delivery, photothermal therapy and targeting. Adapted from Ghosh *et al.*, 2008b.

Currently the field of particle-based drug delivery is focused on two chemically distinct colloidal particles, liposomes and biodegradable polymers (Muller *et al.,* 2000; Jain *et al.,* 1998; Ogawa, 1997 and Maruyama *et al.,* 1998). These delivery systems can both encapsulate the active drug. In the case of liposomes, the drug is released from the particle as it lyses or it disintegrates similar to biodegradable polymers. Motivated by their relative non-toxicity and biocompatibility which are important in delivery applications, colloidal gold nanoparticles have been used for targeting cancerous cells *in vivo,* which is comparable to conventional diagnostic dyes that are known to be susceptible to photobleaching (Jain *et al.*, 1998). Cationic gold nanoparticles prepared by the $NaBH_4$ reduction in the presence of 2-aminoethaethiol were shown to form a complex structure with plasmid DNA containing a luciferase gene, and was able to deliver this gene to the target HeLa cells within 3 hours (Niidome *et al.*, 2004). The electrostatic binding of siRNA to gold nanorods by conjugation of cetyltrimethylammonium bromide (CTAB) gold nanorods to the siRNA (against DARPP-32 gene in dopaminergic neuronal (DAN) cells) and the uptake of these conjugates into the DAN cells were studied. The study confirmed that gold

nanoparticles can be used as innovative vehicles to deliver genes into neuronal cells and could provide the basis for nanotherapy to treat drug addiction in patients (Bonoiu *et al.*, 2009). The combination of phototherapy with conventional gene therapy offers great possibilities to improve the dexterity of gene delivery into cells (Mariko *et al.*, 2005).

1.7.1. Surface plasmon resonance of gold nanoparticles

The allure and fascination of AuNPS since the ancient times originates from their photophysical properties such as their intense colour. With regard to shape as a function of efficacy, the surface plasmon resonance (SPR) of gold nanostructures can be adjusted in the visible and near infrared region (Murphy *et al.*, 2005; Sau *et al.,* 2004a; Sau *et al.*, 2004b, Nikoobakht *et al.,* 2003). This phenomenon is termed surface plasmon resonance and can be explained as follows. On exposure to light the oscillating electromagnetic field of a metal particle induces a collective coherent oscillation of the free electrons of the metal. The electron oscillation around the particle surface causes a charge separation with respect to the ionic lattice. This forms a dipole oscillation along the direction of the electric field of the light. The amplitude of the oscillation reaches a maximum at a specific frequency and induces a strong absorption of the incident light which can be absorbed using a UV-visible absorption spectrophotometer. SPR bands are affected by particle size, shape, composition, structure and the type of the metal. As theory states, gold nanorods exhibit two SPR bands, the transverse band and longitudinal band that correspond to the oscillation of electrons along the short and long axis of the nanorod respectively. By increasing the aspect ratio of gold nanorods the longitudinal band can be adjusted from the visible to the NIR region causing a localized hypothermic effect that can be used in therapeutic applications (Gorov *et al.*, 2007; Jain *et al.*, 2007; Kattumuri *et al.*, 2007; Durr *et al.*, 2007; Kim *et al.*, 2007; Eghtedari *et al.*, 2007; Huang *et al.*, 2007).

1.7.2 Surface charge and zeta potential

Molecules that have been used to modify the surface properties of AuNPs can be incorporated into AuNPs through electrostatic attraction or covalent bonding. It is an effective way to enhance specificity and efficacy of nanoparticle based delivery systems (Tiwari *et al.*, 2011). For them to

be successfully utilized in medical applications their fundamental properties such as the forces that are responsible for nanoparticle-drug stabilization must be clearly understood. It is essential that the electrokinetic characterization be studied at the outset, because in order to design an ideal carrier, one needs to know the features and properties of the system that one is working with. These include hydrophobicity/hydrophilicity, size and most importantly charge. It is important to note that each time the surface of a nanoparticle is functionalized, any one of these (or all three at the same time) properties may change. Adsorption on the surface, commonly results in a modification of the charge. Therefore electrophoretic mobility (U_e) analysis determines and optimizes the preparation conditions of the final surface charge. Complementary to this feature, dynamic light scattering must also be performed in order to confirm the surface modification of the nanoparticle with an external agent. Size and surface charge of DNA complexes are two important factors in determining the efficiency of cellular uptake. Although there is a common theme in all vectors, each vector has to be suitably tailored and optimized to meet the needs of a specific application.

Zeta potential is the term given for the electrokinetic potential in a colloidal dispersion. It is the electrical potential at the slipping plane. This net electrical charge can be generated through the ionization of a surface functional group on the colloid, ion adsorption or by the ion dissolution of the colloid material bound by the slipping plane. This is largely dependent on the location of the plane. Zeta potential is often the only available path for characterization of the double layer (Caruso, 2004). Counter ions closest to the charged wall surface are strongly bound to the surface, forming what is called the stern layer. Adjacent to the stern layer, is the diffuse layer that contains loosely mobile ions. It is within this diffuse layer that there is an imaginary boundary where the ions and particles attain a stable form. This boundary is called the slipping plane (Figure 1.4). This is an extremely important parameter in the theory of interaction of particles (Caruso, 2004). The electrical potential of the double layer decreases as a reciprocal function of the distance from the particle and approaches zero as the counter ions gradually reduce the effect of the field created by the surface. If all the particles in suspension have a large negative or positive zeta potential then they will tend to repel each other and this will reduce the tendency for the particles to attract. In contrast, if the particles have low zeta potential values then there

will be no force to prevent the particles from aggregating. The dividing line between stable and unstable suspensions is either +30 or -30mV. Two important contributing factors that affect zeta potential are pH and conductivity. With regards to pH, one has to define the solution conditions, since addition of an acid to a suspension will cause the particles to acquire positive charge whilst if more alkali is added then the particles tend to acquire more negative charge (Jada and Salou, 2002). Conductivity is the ionic strength of a medium and is the second contributing factor. The higher the ionic strength, the more compressed the double layer becomes (Lyklema, 1998 and Bikerman, 1940). The double layer thickness is also influenced by the valency of the ions. A trivalent ion such as Fe^{3+} will compress the double layer to a greater extent than a monovalent ion such as K^{+}. At low concentrations the specific adsorption of ions onto a particle surface can have a dramatic effect on the zeta potential of the particle dispersion. Specific ion adsorption may even lead to charge reversal of the surface.

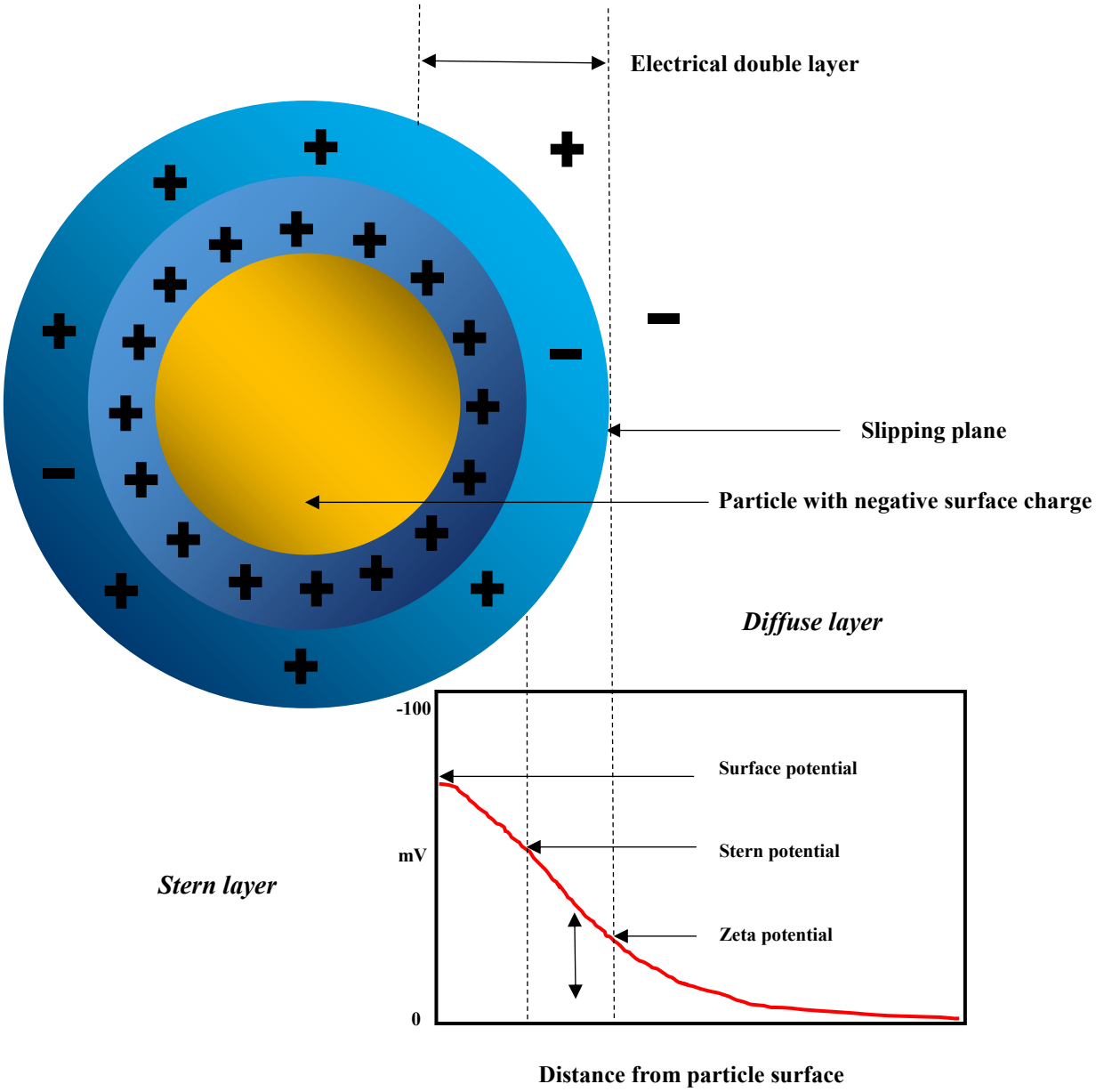

Figure 1.4: Diagram of zeta potential and slipping plane showing the ionic concentration and potential difference as a function of distance from the charged surface of a particle suspended in a dispersion medium.

1.7.3 Dynamic light scattering

Dynamic light scattering is the method of measuring the size distribution profile and the level of aggregation in gold nanoparticles. Particles in a colloid solution follow Brownian motion as a result of continuing particle collisions and movement. Based on Brownian motion, smaller particles will move quicker. A laser passing through the colloid will disperse, and the intensity of the dispersed light is dependent on the movement of the colloid particles. Hence particle size can be determined using the Stokes-Einstein relationship. Zeta potential is a powerful tool that is used to analyze the electrostatic forces within the bulk solution and on the surface of the nanoparticles and nanocomplexes, respectively (Rodríguez-Pulido *et al.*, 2009). Zeta potentials are calculated by applying the Smoluchowski model analysis based on the laser-Doppler micro-electrophoresis technique. There are many methods to determine the dimensions of nanoparticles. Some methods are direct like microscopy and others use relationships such as diffraction. Light scattering occurs when photon energy causes electron oscillations in the matter which emits photons in the form of scattered light. If this is at the same frequency, the incident light is known as Raleigh scattering or if it is at a shifted frequency it is called Raman scattering. The light absorption and scattering are strongly enhanced due to its SPR oscillation. This takes place at a rate of 5-6 orders of magnitude stronger than most strongly absorbing organic dye molecules and the emission obtained the same as that of the most strongly fluorescent molecules. The ratio of the scattering to absorption increases dramatically for larger sized particles. For imaging, larger nanoparticles are preferred because of higher scattering efficiency whilst for photothermal therapy smaller nanoparticles are preferred as light is mainly adsorbed by the particles. Gold nanoparticles possess non-radiative properties by converting the absorbed light into heat via a series of non-radiative processes. This has been extensively studied by the El-Sayed group (2005).

1.8 Characterization of gold nanoparticles for gene delivery

1.8.1 Synthesis of nanoparticles

Synthesis of nanoparticles must be done in a manner that produces the required size, shape, structure and composition (Aiken and Finke, 1999; Brus, 1984; Cushing *et al.*, 2004; Teranishi

and Miyake, 1998 and Watzky and Finke, 1997). In a two phase reaction, formation of ruby red colloidal gold solutions were observed by reducing gold salts with phosphorous in carbon disulfide. Colour changes were reported upon compression in the interactions of light and thin films of dried colloids. A description of the leading three methods; citrate-reduction, polyol method and the two-phase Brus-Schriffin (1984) are as follows.

1.8.1.1 Citrate reduction method

This is one of the most broadly used methods for manufacturing colloidal gold nanoparticles. It is both simple and scalable, and provides for the large scale production of colloidal gold nanoparticles. Gold nanoparticles with varying core sizes prepared by the reduction of chloroauric acid (Au^{+3}, $HAuCl_4$) to neutral gold (Au^0) by agents such as sodium citrate (Frens, 1972) (Figure 1.5). The addition of sodium citrate to the gold chloride initiates a series of well-described reduction reactions characterized by changes in the colour of the initial gold chloride solution (Frens, 1973). There has been vast interest in the study of the citrate-capped gold nanoparticle evolution of the colour changes. The colour changes range from pale yellow, colourless, dark blue, purple to ruby-red. The initial transition from dark blue to red on reduction of the gold (III) by citrate is associated with a decrease in particle size. The large particles are generally spherical in shape with a size range of 100-200 nm, while the smaller well-defined subunits range from 5-15 nm in size. The formation of small nanoclusters (5 nm) is a result of gold atoms that undergo nucleation. These nanoclusters assemble in a linear-like fashion into an extensive network of nanowires (Pan *et al.*, 2007). The diameter of the nanowires is increased when more gold adsorbs leading to destabilization. The wires then undergo fragmentation and divide into spherical particles.

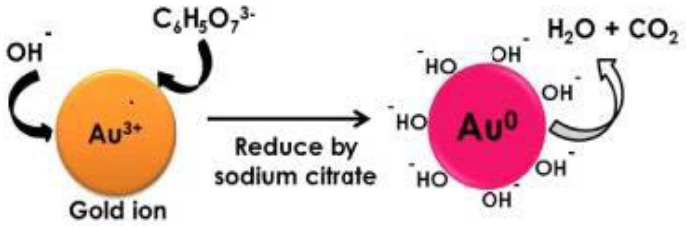

Figure 1.5: The characterization of gold nanoparticles by the reduction of sodium citrate. Adapted from Makhsin *et al.*, 2012.

1.8.1.2 Polyol reduction method

This method that has also gained popularity, involves the reduction of the metal salt in the presence of a protecting polymer usually polyvinyl pyrolidone (PVP). It was developed by Fievet and coworkers and entails refluxing the metal precursors (oxides, nitrates and acetates) in ethylene glycol or polyols (polyethyelene glycol) (PEG) in the presence of a polymer for a specific period of time (Fievet *et al.*, 1989). Therefore it is known as the polyol method. Investigations into the reaction mechanism revealed a solution based reduction pathway. This means that the nanoparticles are formed by nucleation and growth from the solution, with polyol acting as a solvent for the inorganic compound due to its high dielectric constant. Gold nanoparticles prepared via the polyol method demonstrated a pH dependent particle size effect, where an increase in particle size is associated with a rise in pH. Generally the use of the polyol is advantageous in that the glycol is adsorbed onto the nanoparticle surface, minimizing particle surface oxidation.

1.8.1.3 Two-phase reduction: Brust-schiffrin method

The use of alkanethiolates of different chain lengths can be used as capping agents for gold nanoparticles (Giersig and Mulvaney, 1993). The method developed by Brust and coworkers in 1994 has gained immense popularity in gold nanoparticle synthesis (Brust *et al.*, 1994). It is a two-phase redox reaction that involves dissolving $AuCl_4^-$ in water, and the transfer of $AuCl_4^-$ into a toluene layer by the action of a phase-transfer reagent, tetraocytylammonium bromide (TOABr). A one-phase reaction has also been reported as a modification of the two-phase protocol (Alivisatos, 1996). Since the advent of this study, a wide range of research has gone into developing other suitable capping ligands which include thiols-, amine-, silane-, phosphine and disulfide-based capping ligands (Weisbecker *et al.*, 1996; Green and O'Brien, 2000; Prasad *et al.*, 2003). Particles of sizes ranging from 1-10 nm could be synthesized by varying the stabilizer/gold ratio. The nanoparticle synthesized by this method showed tremendous stability. They could be dried and treated as simple chemical powders and re-dispersed in solvents as colloids (Brust *et al.*, 1994; Faraday, 1857).

1.8.2 Stabilization of gold nanoparticles

The first synthesis of gold colloids was reported 150 years ago when Michael Faraday used phosphorous to reduce $AuCl_4^-$ ions (Yang *et al.*, 2007). Since then numerous procedures have been proposed to synthesise AuNPs of different sizes, and shapes, and in different dispersion media depending on the application (Rossi, 2006 and Durcan *et al.*, 2008). Aqueous dispersions are the most common preparation method for biomedical applications. The most common and simplest method is the citrate reduction technique which was introduced by Turkevich in 1951, via reduction of hydrogen tetracholoaurate ($HAuCl_4$) in boiling sodium citrate. It was also reported that nanosized AuNPs from 15 to 150 nm could be obtained through an adequate control of the ratio of trisodium citrate to $HAuCl_4$, with higher ratios yielding smaller particles (Frens, 1973; Handley, 1989). The citrate ions have dual functions, in that they act as reducing agents to reduce Au^{+3} to Au^0, and they also act as stabilizing agents by forming a layer of citrate anions on top of the nanoparticle surface which repels the particles from contacting each other and thus preventing the aggregation of the particles. The main differences between steric and electrostatic stabilization are listed below in Table 1.1. Briefly, steric stabilization is simple and requires the addition of a suitable polymer that is relatively insensitive to the presence of electrolyte dyes due to the steric hindrance of the polymer chain (Figure 1.6). In contrast and electrostatic-stabilized dispersion will be unstable and will coagulate. They are less effective in non-aqueous dispersion media than they are in aqueous media. This coagulation induced by an electrolyte is usually irreversible, while the flocculation of a sterically stabilized dispersion can be usually reversed.

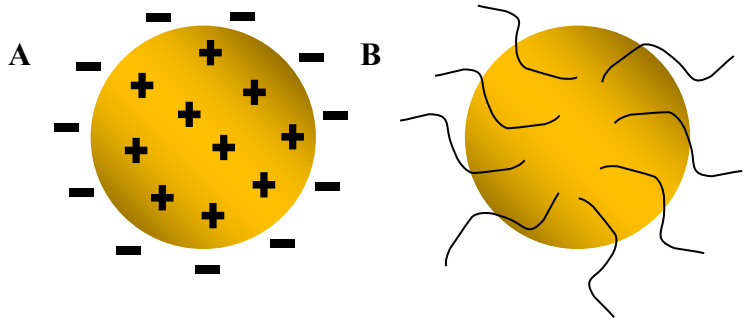

Figure 1.6: Illustration of the **A**) electrokinetic stabilization where charged ions adsorb on the surface of the metal nanoparticle creating an electrostatic double layer and **B**) steric stabilization by bulky ligands or polymers.

Table 1.1: A comparison of electrostatic and steric stabilization.

Constituent	Electrostatic	Steric
Media	Optimal in aqueous dispersion	Optimum in both aqueous and non-aqueous solution
Electrolyte	Aggregates on addition of electrolyte	Insensitive to electrolyte
Stability	Dependent on the ionic strength and pH of the solvent	Independent of ionic strength and pH
Colloid	Ineffective at high concentration of colloid	Effective at high and low colloid concentrations.
Aggregation	Irreversible coagulation	Reversible coagulation

1.8.3 The biosynthesis route

The idea of taking nanoparticle synthesis through a biosynthetic route requires the development of environmentally safe protocols. To ensure safety and efficacy, a minimum number of steps should be included using less toxic materials, and fewer reagents under appropriate laboratory conditions. This has led to widespread approaches for the synthesis of nanomaterials and the subsequent growth of advanced structures (Ahmad *et al.*, 2009). Inorganic metal salt ions are generally toxic to microorganisms once in contact with these foreign species. The foreign ions inside the cell trigger a change of redox states. This fundamental characteristic of microorganisms is being applied in areas such as bioremediation, nanoparticle synthesis and microbial corrosion (Dameron *et al.*, 1989). Studies show that eukaryotic and prokaryotic microorganisms produce nanoparticles within their cell walls. Gold and silver nanoparticles have been synthesized by reacting the metal salts with *Verticullium,* a family of fungi in the genus of *Ascomycota*, resulting in the intracellular deposition of nanoparticles. *Klebsiella aerogenes* bacterium has also been used to synthesize CdS nanoparticles (Holmes *et al.*, 1985).

Lactobacillus strains which are present in buttermilk have also been used for large scale production of Au and Ag when exposed simultaneously to the metal salts of both elements (Nair and Pradeep, 2002).

1.9 Integration of organic molecules with nanoparticles

Zhou *et al.*, 1991; Gao *et al.*, 1993 and Kupfer *et al.*, 1994 have shown that several cationic polymers can form complexes with DNA and that linear and branched structures of poly L-lysine (PLL) and polyethyleneimine (PEI) do not have a major effect on transfection efficiency. A complex can easily be formed between cationic polymers and DNA because of charge interaction. Amino acids hold the promise to be used in bio-functionalization of gold nanoparticles. Amino acids stabilize the AuNPs because their functional groups have a high affinity for gold. These groups are commonly known for their sulfhydryl groups (-SH) and amine groups ($-NH_2$). One of the simplest representations of protein surfaces are gold nanoparticles capped with amino acids (You *et al.*, 2005). Citrate-capped gold nanoparticles have been functionalized by ligands for improving stability. Mangeney and coworkers (2002) covalently derivatized a hydrophilic polymer monolayer bearing terminal disulfide groups. The resulting colloidal particles were found stable and ready for biological use. They successfully converted negatively charged citrate-capped gold nanoparticles into positively charged ones, by displacing the citrate and chloride on the particles by thioctic acid (TA), and then exchanged TA with thiols possessing the desired functionality. Brust and coworkers (1994) produced monolayer-protected gold nanoparticles of reduced dispersity and controlled size. The resulting compounds exhibited great stability when dispersed in organic solutions. This procedure was further explored and a wider range of monolayer-protected gold clusters (MPC's) were synthesized. These MPCs capping layers containing the thiol ligands can be straight-chain alkanethiolates of different length, glutathione (Schaaf *et al.*, 1998), tiopronin (Kohlmann *et al.*, 2001 and Templeton *et al.*, 1999), thiolated polyetheylene glycol (Bartz *et al.*, 1999), p-mercatophenol (Brust *et al.*, 1995) and other systems (Templeton *et al.*, 2000).

1.10 Functionalization of gold nanoparticles with amino acid and cationic polyelectrolytes

An ideal approach is to functionalize the surface of AuNPs with biocompatible ligands to yield gene delivery systems that simultaneously yield low toxicity and high gene transfer efficiency in living cells (Ahmed *et al.*, 2009). The non-covalent approach is seen as ideal for the attachment of nucleic acids, as it prevents denaturation of the nucleic acids, and it also enhances the release of the nucleic acid from the AuNP complex into the cell (Ahmed *et al.*, 2009).

Poly-L-lysine (PLL) is a linear polymer of the amino acid lysine which is essential for human health (Kim *et al.*, 2013). It has shown pronounced activity with DNA and cell membranes and is a positively charged amino acid polymer with approximately one HBr per lysine residue (Figure 1.7). The hydrobromide allows the poly-L-lysine to be in a crystalline state so that it can be soluble in water. A small amount of product may be found in the beta conformation because the HBr interferes with hydrogen bonding between the amino and / or carboxyl groups, or with N or O containing moieties. PLL exhibits stimulatory activity towards production of immunoglobulin, and has found to increase the production of interferon-beta without influencing cell proliferation. It can assume different conformations such as random coil, α-helix and β-sheet of its secondary structure depending on temperature and pH. In general at neutral pH, PLL forms an extended random coil due to repulsions between protonated amine groups. The interaction between DNA and PLL were identified to be electrostatic when the lysine residues of PLL were positively charged and to be hydrogen bonding when the residues were deprotonated. AuNPs can be functionalized with PLL through covalent attachment via an amide group. PLL possesses many active amino groups which makes it useful in promoting cell adhesion (Zhang *et al.*, 2006). As the functional group on the AuNP it provides advantages, such as good compatibility, abundance of active amino groups, a flexible molecular backbone and relatively good solubility in water (Zhang *et al.*, 2006). Some free amino groups on the PLL molecular chains can cross link with the carboxyl group of AuNP, whilst the other residual free amino group can act as a relatively friendly and form a soft linker between the AuNP and bioactive molecules such as DNA (Zhang *et al.*, 2006).

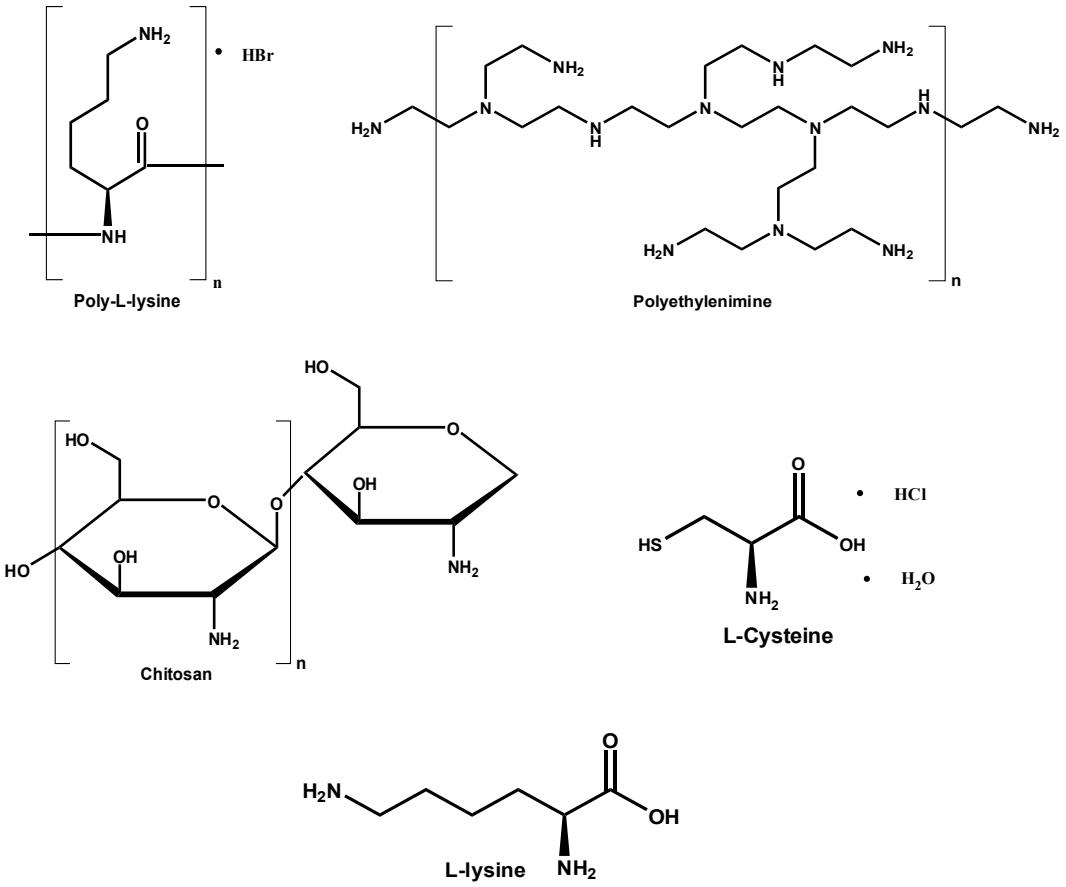

Figure 1.7: Common cationic polymers for functionalization of anionic AuNPs.

The good biocompatibility and water solubility of PLL, coupled to the abundance of available active amino groups for DNA attachment, indicates that PLL functionalized AuNPs may be a potential viable option as future non-viral gene delivery systems (Zhang *et al.*, 2006).

Polyethylenimine (PEI) is a branched polymer that is used as a polyelectrolyte multilayer on charged surfaces to provide a biocompatible coating. There has been a flurry of interest in this polycation and its role as a gene carrier due to its "proton-sponge" effect in the endosomal compartment ensuing high transfection efficiency. It has hence a privileged place in the components of non-viral gene delivery. It is composed of ethyleneimine monomers with the tertiary amine of PEI acting as a reductant and stabilizer. The amine functional groups bind tightly to colloidal gold by virtue of the available electron lone pair. PEI in its branched form is produced by cationic polymerization from aziridine monomers via a chain-growth mechanism,

with branch sites arising from specific interactions between two growing polymer molecules. The branched form of PEI has yielded significantly greater success in terms of cell transfection and is therefore the common form of PEI currently used in gene delivery. PEI is non-degradable and its molecular weight tends to correlate with its cytotoxicity and gene transfer activity. High molecular PEI >25 kDa exhibits a high transfection efficiency and high toxicity. In contrast PEI with low molecular weight <25 kDa is less toxic and cannot be used as a gene delivery vector because of its low transfection efficiency (Kim *et al.*, 2013). Due to its abundant positive surface charges, PEI is able to condense the negatively charged DNA into complexes with a net positive charge. PEI/DNA complexes can act as 'proton sponges' after they cross the cellular membrane via the endocytic pathway (Kim *et al.*, 2013). PEI has a backbone of 2 carbons followed by 1 nitrogen atom and 3 amine groups each with the potential to be protonated. This gives PEI the attribute of serving as an effective buffer through a wide pH range. Coating of AuNPs with ligands having buffering capacity such as PEI provides effective release of the nucleic acid payload through the "proton sponge effect" (Niidome *et al.*, 2008 and Thomas *et al.*, 2003).

Protonation of the ionisable amino groups of PEI leads to an influx of counter ions such as chloride, which in turn increases the endosomal osmotic pressure, causing rupture of the endosomal membrane and release of its contents (Figure 1.8). PEI raises the endolysosomal pH which alters protein folding within the endolysosome, and possibly inactivates degradative enzymes thereby inducing a water influx into the endosome causing the PEI/DNA complex to escape (Behr, 1997). To describe PEI's proton ability, one needs to obtain its pKa. To obtain PEI's pKa requires an ionization constant for every amino group (Godbey *et al.*, 1999). Depending on the molecular weight of PEI being analysed the number of amine groups can easily exceed 1000. PEI-mediated gene delivery has the potential to transfect cells with large sizes of genetic material (Abdallah *et al.*, 1995). One of the problems for *in vivo* gene delivery mediated by PEI and liposomes is that the transfection efficiency is inhibited by serum (Goldman *et al.*, 1997). Studies have shown that PEI-mediated transfection decreased in the presence of 10% serum (Erbacher *et al.,* 1998). The deposition of oppositely charged alternate layers of siRNAs and polyethyleneimine on the gold surface resulted in the active delivery of siRNAs to

the cytoplasm and the conjugates showed no cytotoxicity (Elbakry *et al.*, 2009). They also demonstrated high stability and effective transfection in multiple myeloma cells (Crew *et al.*, 2012 and Lee *et al.*, 2008).

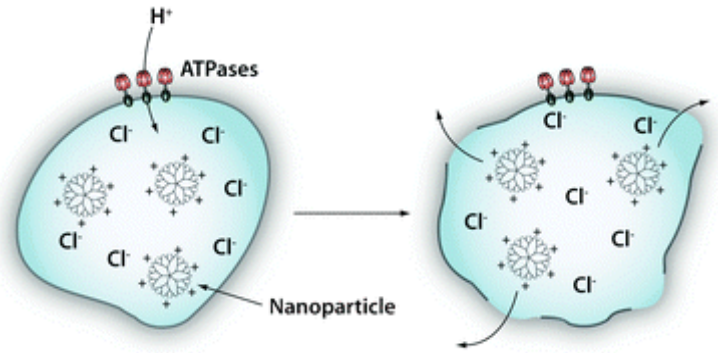

Figure 1.8: Diagram showing endosomal escape by the "proton-sponge effect". The proton pumps eg. ATPase, pumps H^+ ions into the lumen of the endosome. A parallel influx of Cl^- ions and water accompanies the influx of protons to maintain electric neutrality. This swells and eventually ruptures the endosomal membrane allowing its contents to escape. Sourced from Fuller *et al.*, 2008.

Chitosan (Chit) is a natural carbohydrate polymer found in the exoskeleton of marine zooplankton. They are also used in dietary supplements, water treatment, food preservation and medicinal applications. A large increase in chitosan research has been carried out mostly due to its biocompatibility, biodegradability, non-toxicity and other unique properties. It has been investigated as a non-viral vector offering several advantages including high cationic potential. The properties of chitosan are dependent on its molecular weight and viscosity (Islam *et al.,* 2011). Chitosan is produced by the hydrolysis of the aminoacetyl groups of chitin from crabs or shrimps in aqueous alkaline solution. The functional groups allow simple coupling of extracellular and intracellular targeting ligands. It is one of the most reported non-viral naturally derived polymeric gene carriers with a strong affinity for DNA. It is insoluble in water but soluble in dilute aqueous acids such as acetic acid. Lower molecular weight chitosan (poly-D-glucosamine), 5400 g/mol in its physical form, with a 75-85% degree of deacetylation was employed in this study.

Chitosan with higher molecular weight seem to be more effective as food preservatives than those with lower molecule weight (Dutta *et al.*, 2004). It is a flocculent, protein precipitating, encapsulating agent and an aqueous thickener, that forms gels with multivalent anions and can be

used as a heavy metal trapper (Lee *et al.*, 2002). Factors affecting transfection efficiency of chitosan/DNA complexes include the optimum pH of 6.8-7, charge ratio (optimum being 3-5) and optimum serum content (10-20 wt %). Degree of deacetylation and molecular weight has a major influence on its biological and physicochemical properties. Chain entanglement has been attributed to the formulation of chitosan with DNA (Kiang *et al.*, 2004). High molecular weight chitosan entangle free DNA more easily once the initial electrostatic interaction has occurred. It is capable of protecting the condensed DNA from degradation by DNases and serum components. At acidic pH the primary amines become positively charged reflecting a pKa of around 6.3-6.4 (Li *et al.*, 1996). Protonated amines of chitosan facilitate its binding to negatively charged DNA and condense into particles through phase separation. At pH 6.9 chitosan/DNA are positively charged and can bind with the negatively charged cells through electrostatic interaction (Kima *et al.*, 2007).

Cysteine (Cys) is commonly used as a coating agent that wraps AuNPs intended for biomedical application. Figure 1.9 depicts cysteine binding to citrate capped gold nanoparticles. Cysteine is a major biological source of sulphur and is one of the two common sulphur-containing amino acids with a thiol group (-SH) on the side chain. It is a neutral polar amino acid with limited hydrophilic properties with pKa values of 1.96, 8.18 and 10.28 respectively. The biosynthesis of cysteine occurs through the initial condensation of homocysteine and serine via cystathionine synthase to form cystathionine, which in turn undergoes cleavage by cystathionase to give cysteine and α-ketobutyrate. The addition of the cysteine solution to the colloidal gold leads to a colour change of bluish-black. This kind of colour change as an effect of aggregation, is a well understood phenomenon (Mayya *et al.,* 1997). When the inter-particle distance in the aggregates decreases to less than average particle diameter, the electric dipole-dipole interaction coupling between the plasmons of neighbouring particles in the aggregates results in the bathochromic shift of the absorption band. This supports the observation and existence of covalent interaction between sulphur and gold (Aryal *et al.,* 2006).

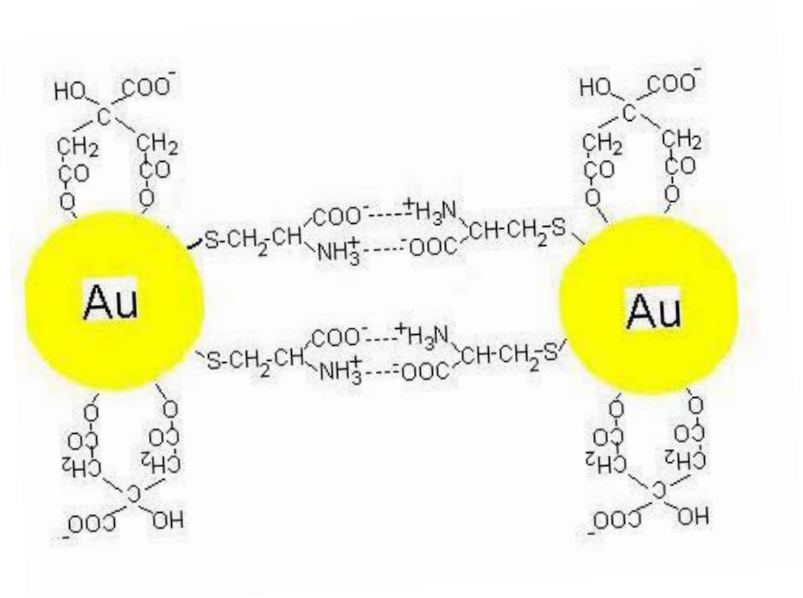

Figure 1.9: Scheme of cysteine binding to citrate capped gold nanoparticles and bonds formation between particles. Adapted from Petean *et al.*, 2008.

L-lysine (Lys) is one of the three essential amino acids with basic side chains and is hydrophilic in nature. It contains an N-butyl amino group in its side chain which is protonated at physiological pH. It is also one of the two purely ketogenic amino acids with a carboxyl group of pKa 2.2 and two amino groups with pKa's of 9.0 and 10.2 respectively, which are significantly high. So a fully protonated lysine molecule has a +2 net charge. Direct interaction of lysine residues with the gold surface stabilizes the gold nanoparticle in solution. However at neutral pH, the complexation of lysine to gold is fairly weak (Joshi *et al.*, 2004).

1.11 Formation of cationic nanocomplexes with plasmid DNA

There are three techniques commonly used to determine the size of the nanoparticles viz. Transmission electron microscopy (TEM), dynamic light scattering (DLS) and differential centrifugal sedimentation. Electron micrographs can be used to physically measure the size of the colloidal gold particles. Dynamic light scattering determines particle size by measuring the angles at which an incident light beam is scattered as a function of Brownian motion of the colloidal gold particle. Differential centrifugal sedimentation measures particle size by determining the time required for the colloidal gold to traverse a sucrose density gradient created

in a disc centrifuge. Both DLS and DCS methods use calibrated particle reference standards to estimate the size of the colloidal gold preparation. Colloidal AuNPs that are formed remain in suspension by their mutual electrostatic repulsion that is generated and maintained by a net negative charge on their surface. Cations present in the salt solution negate this charge repulsion and cause these "naked particles" to agglomerate and eventually precipitate out of solution. Binding of other stabilizing agents or proteins to the particles' surface maintains the sol state by blocking the salt-induced precipitation of the colloidal gold particles. The binding of proteins to colloidal AuNP is dependent on the pH of the colloidal gold and the protein solution. DNA is susceptible to a variety of environmental challenges such as enzymatic, physical and chemical degradation during the transfection processes. If cleavage occurs in the gene-expressing sequence, fragmentation may result from strand breakage in the DNA which will lead to the reduction or elimination of gene expression. Therefore for recognition and delivery of DNA it is essential to cationically functionalize DNA. Cationic nanoparticles can bind to DNA which is a negatively charged molecule through a combination of electrostatic interactions, intercalation and groove binding. This binding induces changes in the DNA strand. If a nanoparticle has a high positive surface charge density, the DNA is likely to wrap and bend upon binding to the nanoparticle as in the case of chromatin. If the nanoparticle has a weak charge it will not induce dsDNA compaction (Railsback *et al.,* 2012).

1.12 Mechanisms of cellular uptake

A gene/drug delivery carrier can affect the bio-distribution through passive or active targeting (Figure 1.10). With regard to passive targeting, this occurs as a result of the intrinsic physiochemical properties of the carrier. Size and charge are critical properties that need to be taken into account (Jeong *et al.*, 2006). One approach *in vivo* involves the use of direct local delivery of the agents to the affected cell. It is an advantageous method since it protects the drug from the systemic circulation, but it is also very invasive since it involves surgical procedures and injections. The biggest challenge is the inability to accumulate large enough quantities of the nanocomplex on the tumor cells, resulting in low therapeutic efficacy (Ferrari, 2005). Active targeting is based on specific interactions such as ligand-receptor, lectin-carbohydrate and

antibody-antigen. Active targeting improves the distribution of nanomedicine within the tumor interstitum (Drummond *et al.*, 1991). The exact mechanism and pathways of how the body rids itself of the nanoparticle is still a subject of intense investigation. It is assumed that the liver is most likely the destination of spent nanoparticles, but they generally travel freely to other organs and are commonly captured and retained in the spleen or by macrophages in the liver (Pei *et al.*, 2001).

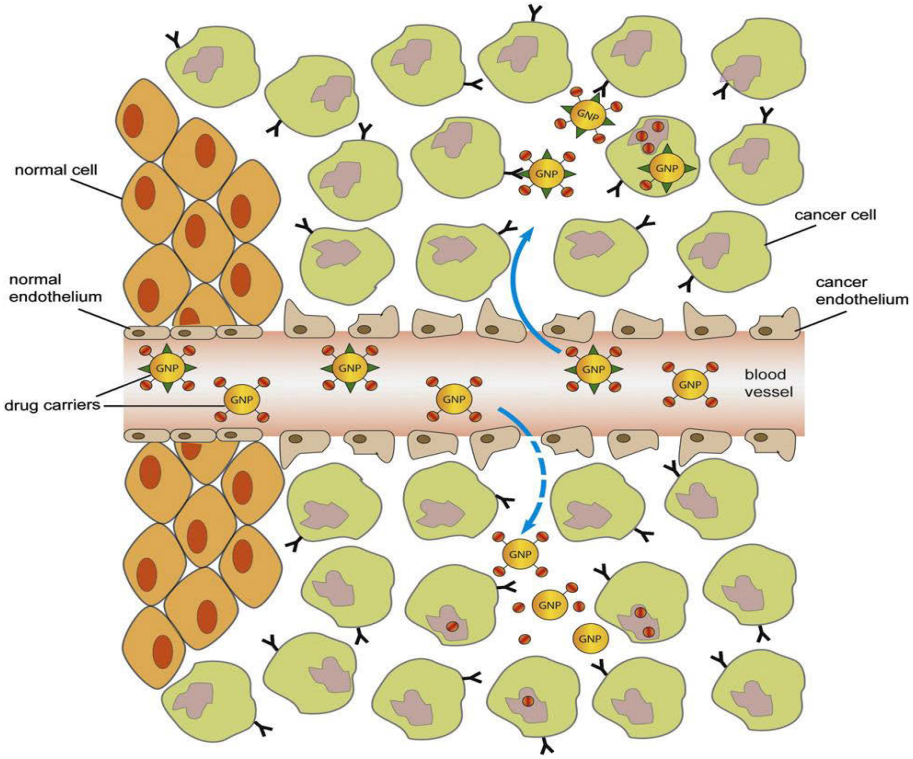

Figure 1.10: A representation of drug delivery via 'active' and 'passive' targeting, solid and dotted line respectively. Adapted from Ghosh *et al.*, 2008b.

The process of phagocytosis is usually involved in the uptake of particles larger than 500 nm. This was observed in macrophages, dendritic cells, monocytes and basophils. Most inorganic nanoparticles are synthesized to within the 1-100 nm range and are thought to be taken up by the cell via endocytosis. The size of these particles usually remains at less than 200 nm regardless of surface modification. Understanding the uptake of nanoparticles into cells is of crucial importance. Conjugates of gold nanoparticles with antibiotics provide promising results in the treatment of intracellular infections (Check, 2002; Ghosh *et al.*, 2008b; Luo *et al.*, 2000b and

Zhang *et al.*, 2006). Magnetic nanoparticles, liposomes and carbon nanotubes have been of great interest as non-viral carriers for gene delivery. As described previously, gold nanoparticles are attractive because of their unique properties. From early studies it was shown that gold nanoparticles functionalized with cationic quaternary ammonium groups can electrostatically bind to plasmid DNA, afford protection to the DNA from enzymatic degradation and could regulate DNA transcription of the T7 RNA polymerase (Boyer *et al.*, 2010; Gao *et al.*, 2006; Suzuki *et al.*, 2008).

1.13 Gold nanoparticles as potential transfection agents

Functionalized AuNPs (FAuNPs) have demonstrated their use as delivery platforms for antisense oligonucleotides (ON) or small interfering RNA (siRNA) for targeted gene knockdown (Rosi *et al.*, 2006 and Giljohann *et al.*, 2009). The oligonucleotide:FAuNP complexes showed poor gene knockdown. However the siRNA: AuNPs complexes showed improved stability of the bound siRNA and were effective in transfecting cells and releasing the siRNA in a controlled manner. This method resulted in an extended gene knockdown when compared to lipofectamine mediated transfection of siRNAs (Giljohann *et al.*, 2009). The initial indications regarding the cellular uptake mechanism of gold nanoparticle conjugates suggest that the particles enter cells via several routes as seen in Figure 1.11. When incubated with cells *in vitro,* the serum proteins such as albumin, fibrinogen and globulin that are present in the media interact with the AuNPs (Lacerda *et al.*, 2010, Ghitescu *et al.*, 1986 and Wang *et al.*, 2010). Data describing thermodynamic parameters indicate that the interactions between gold nanoparticles and serum albumin are mainly hydrophobic in nature. It was further shown that when gold nanoparticles are incubated with cell culture media they become coated with serum proteins which favourably mediates the uptake of these gold nanoparticles by cells (Chithrani *et al*., 2006). The interaction of serum proteins with AuNPs is an interesting area of research that will have implications in cellular uptake processes *in vitro* and *in vivo*.

1.14 Intracellular trafficking of nanoparticles

Nanostructures in the extracellular space may be internalized via mechanisms and structures that include macropinocytosis, clathrin-coated pits, caveolae or via nonspecific uptake (Figure 1.11) (Conner and Schmid, 2003). These pathways initially traffic nanostructures into the cell and eventually to the early endosomes. Some nanostructures may be trafficked along regressive transport pathways ie. via the Golgi apparatus and endoplasmic reticulum, whilst others may be carried through from the late endosomes to lysosomes where they may be degraded (Dobrovolskaia and McNeil, 2007). The hypothesis that nanostructures escape into the cytoplasm from endosomes and lysosomes still needs validation and further study. Most nanoparticle preparations suffer from poor characterization of their size distribution. The physiochemical properties of nanoparticles strongly effect their cellular uptake. The nano-bio interface comprises many physiochemical interactions between nanoparticles and biological systems. The components that shape these interactions are still far from being completely studied. A major barrier for nanoparticles delivering any kind of cargo molecules into cells is their cellular uptake (Alkilany *et al,* 2009). For every delivery vehicle/particle an optimal size exists which accelerates cellular entry, membrane wrapping at the cell surface and intracellular passage. The uptake of gold nanoparticles into HeLa cells was investigated at sizes of 14, 30, 50, 74 and 100 nm (Chithrani *et al.*, 2006 and 2007) and revealed that the cellular uptake of gold nanoparticles coated with the ligand transferrin was observed to enter the cells via receptor mediated endocytosis.

Factors contributing to low transfection ability may be related to the inefficient release from the endosomes into the cytoplasm. This can be seen by the differences in buffering capacities between PEI and chitosan due to its comparatively weak endo-lysosomolytic “proton sponge effect”. The escape of the polyplex from the endosome is an integral step for the release of the therapeutic drug or gene. Several endosomal disruptive agents have been suggested to overcome the endosomal barrier and to enhance transfection (Mao *et al.*, 2010). These include fusogenic peptides, pH-sensitive neutral lipids and lysosomotropic chloroquine. Chloroquine, however may cause side effects making them impractical for *in vivo* gene therapy. Fusogenic peptides that

exist in a random coil conformation can undergo transition to an amphiphilic α-helical structure which facilitates penetration and leads to endosomal disruption. Furthermore, helper lipids such as dioleoylphosphatidylethanolamine (DOPE) commonly used in liposomal formulations, interact with the endosomal membrane and promotes fusion of the lipid/DNA complexes with the membrane thereby facilitating escape of DNA (Mao *et al.*, 2001).

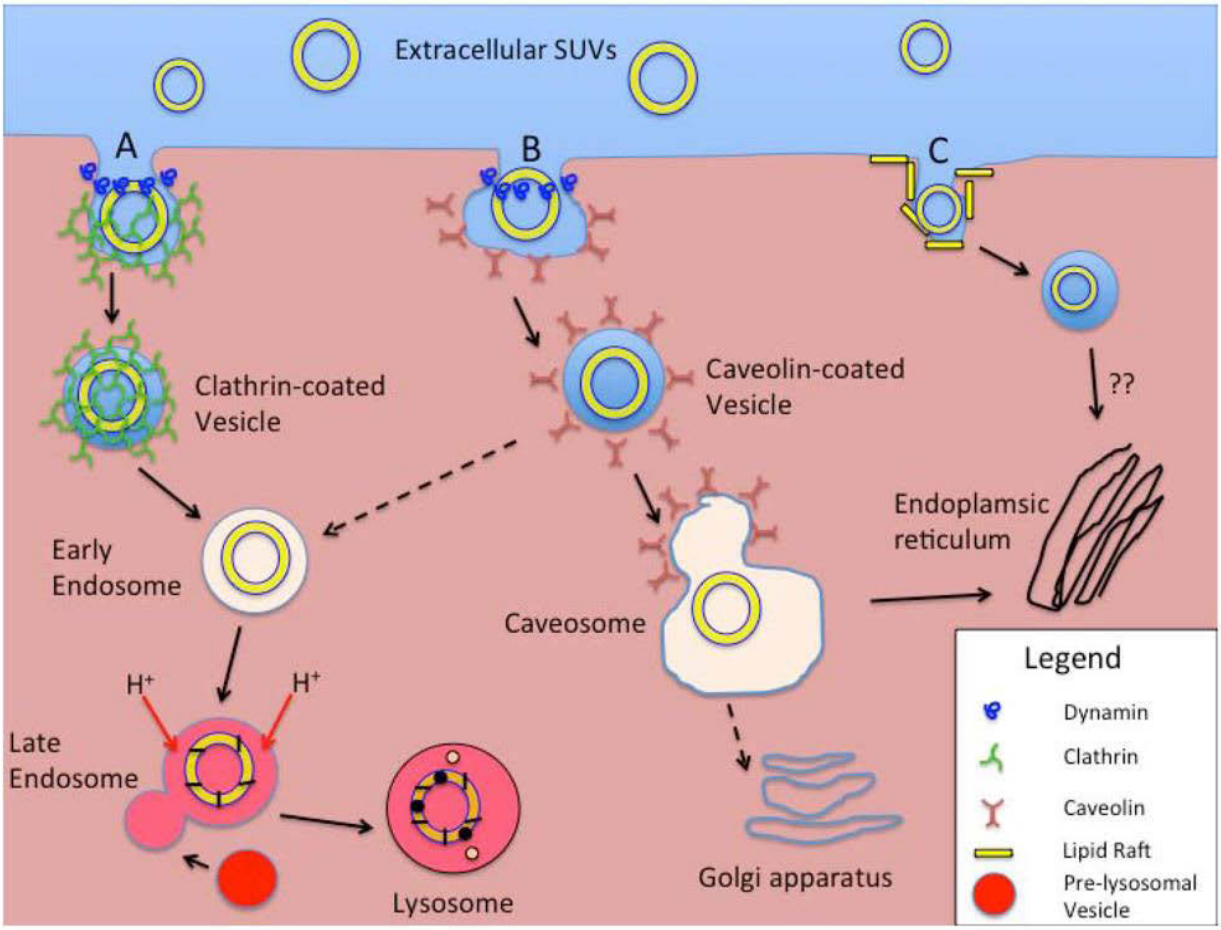

Figure 1.11: Possible endocytosis pathways for cellular uptake of nanostructures. Nanostructures in the extracellular space may be internalized via mechanisms and structures that include macropinocytosis, clathrin coated pits, caveolae, or via nonspecific uptake. These pathways initially traffic nanostructures to early endosomes (Massimo *et al*., 2011).

1.15 Aims

Owing to its safety, non-viral gene therapy approaches are fast becoming popular compared to viral vectors in the scientific world. This study aims to design and synthesize gold nanoparticles (AuNPs) and to elucidate their biological effects on selected mammalian cells in culture. Furthermore these nanoparticles were functionalized with different polymers and complexed with plasmid DNA (pCMV-*luc*) in order to identify the safest and most efficient nanocomplex *in vitro*.

1.16 Objectives

- Gold nanoparticles will be synthesized and characterized
- Morpho-isoform plasmid DNA pSG5 and pCMV-*luc* (circular, linear and nicked) will be purified
- Functionalization and electrophoretic characterization of gold nanoparticles (FAuNPs) coated with amino-acids L-lysine and cationic polymers (CP); polyethylenemine (PEI), poly-L-lysine (PLL), chitosan (Chit) and cysteine (Cys) will be carried out
- FAuNPs and CP will be incubated respectively with pDNA intended for gene delivery
- Electrophoretic characterization, effect of the pH, concentration and ionic strength of the FAuNPs/pDNA and CP/pDNA will be assessed
- DNA binding studies, cell culture, cytotoxicity and transfection studies will be investigated in four cell lines *in vitro*

Novelty of work: The current study holds novelty in that the functionalized gold nanoparticles incorporates a range of different polymers and the effect of its interaction with four mammalian cell lines is observed.

1.17 Outline of thesis

Chapter 1 provides a review of the literature, background information, interest in the proposed study and the important use of gold nanoparticle in gene delivery applications. It also includes

the most widely used synthesis methods of gold nanoparticles and a description of the cellular mechanics involved in the uptake of these particles into the cell.

Chapter 2 focuses on the experimental work that is involved namely the design and synthesis of the gold nanoparticles and their characterization. The preparation of the cationic polymers and functionalization of the AuNPs are discussed in detail. Characterization protocols using TEM, particle sizing, zeta potential, and electrokinetic studies are described. The methods used in DNA binding studies such as the band shift, nuclease protection and ethidium bromide intercalation assays are also discussed. Lastly the methodology for the *in vitro* studies in human embryonic kidney cells (HEK293), human cervical cancer (HeLa), human epithelial colorectal adenocarcinoma cells (Caco2) and human hepatocellular carcinoma cells (HepG2) are outlined.

Chapter 3 details the results obtained from all the experimental analyses followed by discussions and interpretations of the results.

Chapter 4 concludes the research study and offers possible alternatives for future advancement of the current research in pharmaceutical and medical applications.

Chapter Two

Materials and Methods

Chapter Two

Materials and Methods

2.1 Materials

2.1.1 Chemical reagents

Gold (III) chloride trihydrate ($HAuCl_4.3H_2O$), 3-[4,5-dimethylthiazol-2-yl]-2.5-siphenyltetrazolium bromide (MTT), tris (hydroxymethyl)-aminomethane (M_w 121.2 g/mol, Tris base), sodium dihydrogen phosphate (NaH_2PO_4) agarose, glycerol, dimethylsulfoxide (DMSO), phosphate buffered saline (PBS) tablets, ethidium bromide (EtBr, M_w 394.3 g/mol), sodium dodecyl sulphate (SDS, M_w 288.4g/mol), isopropanol, sodium borohydride ($NaBH_4$), 2-[4-(2-hydroxyethyl) piperazin-1-yl] ethanesulphonic acid (HEPES, $C_8H_{18}N_2O_4S$), sodium sulphate (Na_2SO_4), sodium chloride (NaCl), sodium bicarbonate ($NaHCO_3$), sodium citrate trisbasic dehydrate ($C_6H_5Na_3O_7.2H_2O$), EDTA disodium salt), xylene cyanol and sodium dihydrogen phosphate (M_w 120 g/mol, NaH_2PO_4) were acquired from Merck, Darmstadt, Germany. Polyethylenimine branched (H $(NHCH_2CH_2)_n$ NH_2, M_w 25,000 kDa), poly-L-lysine (M_w 1,000-5,000), L-lysine ($C_6H_{14}N_2O_2$, M_w 149.19 g/mol), L-cysteinhydrochloride-monohydrat ($C_3H_8C_lNO_2S.H_20$, M_w 175.64 g/mol), chitosan *>75%* deacetylated and bromophenol blue were purchased from Sigma-Aldrich Chemical Co. (St. Louis, USA). *N*, *N*, *N'*, *N'*-ethylenediaminetetra acetic acid (M_w 372.2 g/mol, Ultrapure (18 Mohm) deionized water (Milli-Q Academic, Millipore, France) was used in the preparation of all reagents. All other chemicals and reagents were of analytical grade or higher and purchased commercially.

2.1.2 Plasmid DNA, cell lines and cell culture reagents

Plasmid pCMV-*luc* DNA (6.2 kbp) was purchased from Plasmid Factory (Bielefeld, Germany). The plasmid was amplified in *E.coli* strain JM109 (Promega Corp.,Madison, USA) according to standard protocol. Plasmid pSG5 (4.1 kbp) was prepared at the San Cecilio Hospital, Granada Spain (Figure 2.1 A, B). Eagle's Minimum Essential Medium (EMEM) with L-glutamine (4.5 g/L), penicillin (10000 U/mL) streptomycin (10000 µg/mL) amphotericin B (25 µg/mL) mixture and trypsin-versene mixture were purchased from Lonza BioWhittaker (Verviers, Belgium).

Fetal calf serum (FCS) was purchased from Hyclone GE Healthcare (Utah, USA). Reporter lysis buffer (5x) and luciferase assay reagent were purchased from Promega Corp. (Madison, USA). The Bicinchoninic acid (BCA) assay kit was obtained from Sigma-Aldrich Chemical Co. (St. Louis, USA). Human embryonic kidney cells (HEK293) was obtained from the Anti-viral Gene Therapy Unit, Medical School, University of the Witwatersrand, human cervical cancer (HeLa), human epithelial colorectal adenocarcinoma cells (Caco2) and human hepatocellular carcinoma cells (HepG2) were purchased from Highveld Biologicals (Pty) Ltd, Kelvin, SA. All tissue culture plastic ware, consumables and cryogenic storage vials were obtained from Corning Incorporated (New York, USA). All glassware used was cleaned and rinsed thoroughly with distilled H_2O prior to use.

2.2 Methods

2.2.1 Synthesis of colloidal gold nanoparticles by citrate reduction

Approximately 0.45 x 10^{-3} M of an aqueous colloidal gold solution was prepared by $HAuCl_4$ reduction with trisodium citrate according to the method of Turkevich *et al.*, 1951. Figure 2.1 shows the schematic representation of the citrate reduction of $HAuCl_4$ followed by stabilization and functionalization via the ligand exchange reaction, leading to the formation of anionic gold nanoparticles (Remant Bahadur *et al.,* 2013).

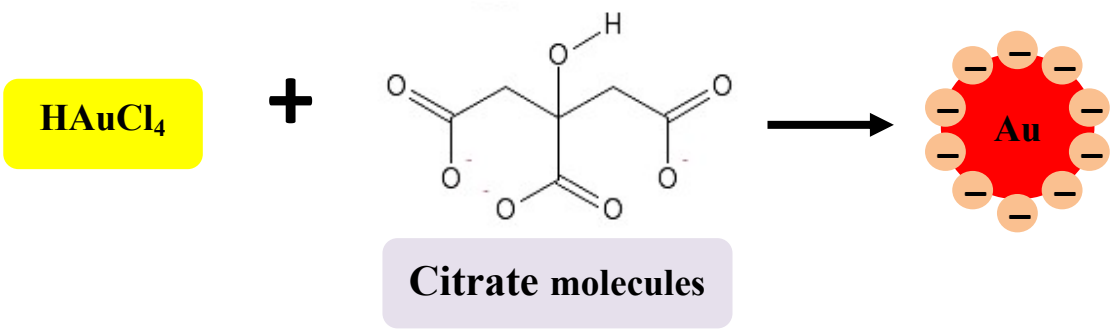

Figure 2.1: The citrate reduction of $HAuCl_4$ by the method of Turkevich, 1951.

Briefly, a solution containing 0.11 mL gold colloidal in 25 mL water was boiled for 15 minutes in a 50 mL round bottomed flask. Thereafter 1 mL of 1% sodium citrate was added rapidly to the

vortex of the solution. Upon addition of the citrate to the boiling tetrachloroaurate solution, the colour changed from pale yellow to dark blue within the first 3 minutes, gradually darkening over a period of about 5 minutes. After 15 minutes of reaction time the final colour of a deep wine red was obtained (Figure 2.3). This was boiled for a further 5 minutes on the heating mantle, removed, cooled to room temperature and thereafter stored in a dark bottle. The synthesis process is outline in Figure 2.2.

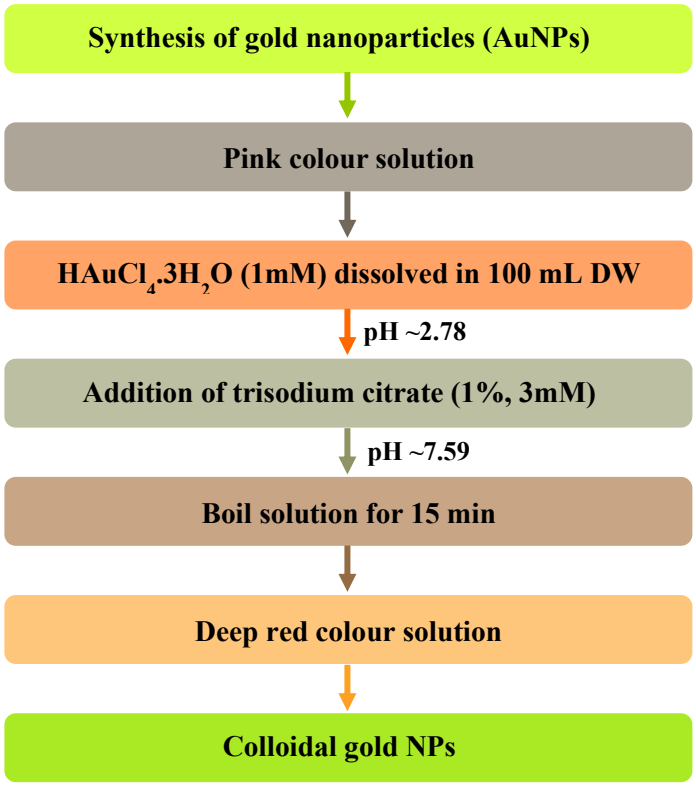

Figure 2.2: Flow chart for the synthesis of AuNPs.

Figure 2.3: The synthesis of gold nanoparticles by the method of Turkevich *et al.*, 1951.

2.2.2 Functionalization with amino acids and cationic polyelectrolytes

A primary stock solution (100 mg/mL) of poly-L-lysine coated AuNPs were prepared, from which concentrations of 0.8, 1, 5, and 10 mg/mL were set up. The resulting Au-PLL nanoparticles were purified by centrifugation (Hettich Zentrifugen Mikro 220R) and filtered to remove the unbound PLL (Cebrian *et al.*, 2011). For experimental purposes a stock solution of 10 mg/mL Au-PEI was diluted to the desired concentrations of 1, 2, 5, 7 and 10 mg/mL and stored at room temperature. A chitosan stock (0.1 mg/mL) in H_2O was diluted to 0.0125 µg/µL for experimental use. Due to poor solubility of chitosan, the solution was kept for 24 hours overnight under constant vortexing until a clear solution was obtained. Adsorption of L-cysteine onto Au was carried out by the modified method of Petean *et al.*, 2008. Briefly, 1 mL of the gold colloidal solution was added drop wise to 1 mL of the cysteine solution (20 mg/mL in water) under constant but moderate vortexing. This was washed three times with distilled water to remove any free polyelectrolytes that remained in solution. In the case of lysine, dilutions (0.01, 0.1, 5, 10, 100, 200 mg/mL) were prepared from a stock solution of L-lysine (20 mg/mL) for experimental use.

2.2.3 Nanoparticle preparation and nanocomplex formation

Nanoparticle suspensions were sonicated for 1 minute prior to use. The pCMV-*luc* DNA reporter gene (0.25 µg) was added to varied amounts of the cationic polymers (CP) and functionalised gold nanoparticles (FAuNP) respectively to produce a range of CP/FAuNP:pDNA ($^{w}/_{w}$) mass ratios. The mixtures were brought up to volume of 11 µL with sterile HBS (20 mM Hepes, 150 mM NaCl ,pH 7.4), gently vortexed and incubated for 60 minutes at room temperature for complexation. The formation of the complexes with pDNA was confirmed using band shift assays (section 2.4.1).

2.3 Particle imaging and analysis

2.3.1 UV-vis optical spectrophotometry analysis

The qualitative analysis of uniformity and stability of the gold nanoparticles were followed up by examining the absorption spectra of the individual nanoparticles and to correlate with literature that the expected surface plasmon resonance (SPR) absorption of the nanosized gold particles occurred at 534 nm. UV-vis absorption measurements were conducted and the spectra recorded by measuring dilute samples in a quartz cell with a path length of 1 cm (Malvern Instruments, Worcestershire, UK). Assuming no aggregation, these densities could then be used with the Beer-Lambert law to determine the concentration of gold nanoparticles.

2.3.2 Imaging and size distribution analysis

Particle size and morphology were determined using a transmission electron microscope Jeol (T 1010) (Electron Microscopy Unit, UKZN and Applied Physics Department, University of Granada). One drop of the nanoparticle suspension was placed on a 400 mesh carbon coated copper grid (Ted Pella Inc. Redding, USA) which was covered by a carbon-supported film and allowed to air dry at room temperature before it was viewed at a magnification of 60 000x. The average diameter of particles was calculated by measuring 100-300 individual particles using the iTEM Soft Imaging Systems (SIS) MegaView III side-mounted 3 megapixel digital camera. The AuNPs were also viewed using the (NTA) NanoSight tracking analysis (Nanosight LM10, Malvern Instruments, UK). For this visualisation, one drop of the required sample was placed on

a metal surface and observed using the microscope. The zeta potential measurements were also performed in triplicate at pH 7. Briefly, one drop of the gold suspension coated by the respective amino acid and poly-electrolyte as described in section 2.2.3 above, was added to 10 mL of an aqueous solution of pH 3-9 and desired ionic strength. After 24 hours of incubation the pH was re-adjusted and the electrophoretic mobility was measured. Zeta potentials were calculated from the mean electrophoretic mobility by applying the Smoluchowski model based on the laser-Doppler micro-electrophoresis technique. Citric acid and sodium hydroxide were used to adjust the pH.

2.3.3 Photoluminescence spectra (PL)

A drop of the required sample was placed into an empty cuvette and diluted with deionized water. The fluorescence spectrometer LS55 (FL WinLab, Perkin Elmer) was adjusted and the excitation set at 240 nm. Spectra were recorded by measuring dilute samples in a quartz cell with a path length of 1 cm.

2.3.4 Ionic strength studies

Ionic strength studies were performed to determine the compactness of the adsorbed layer. To achieve this we investigated the effect of electrolyte concentrations on the electrophoretic mobility (U_e). Essentially in the presence of layers the mobility should tend towards zero because of the electric double layer compression at high ionic strength. The dispersion medium, sodium chloride, was prepared at different ionic salt concentrations of ($1x10^{-4}$; $1x10^{-3}$; $2.5x10^{-3}$; $5x10^{-3}$; $7.5x10^{-3}$; $1x10^{-2}$; $2.5x10^{-2}$; $5x10^{-2}$ mg/mL).

2.3.5 Plasmid amplification

Plasmid pCMV-*luc* DNA (Amp^r) expresses the firefly luciferase (*luc)* reporter gene and is driven by the cytomegalovirus (CMV) promoter (Figure 2.4 A). The plasmid was amplified using *E. coli* strain JM109 according to a standard transformation protocol. The plasmid pSG5 (Amp^r) is a eukaryotic expression vector constructed by combining pKCR2 and the Agilent pBS vector (Figure 2.4 B). Because of the high copy number of this plasmid, large quantities of double-stranded DNA are obtained. The pCMV-*luc* vector contains the cDNA of the firefly luciferase

(l*uc*) gene and the pSG5 vector is a pregnancy specific beta-1-glycoprotein 5 protein-coding gene. Both express the beta-lactamase for ampicillin resistance (Amp^r). Agarose gel electrophoresis and UV spectroscopy were used to confirm the species and purity of the DNA. Concentration of the DNA was confirmed using a NanoDrop 2000c spectrophotometer (Thermo Scientific, Wilmington, USA). Stock concentrations of the DNA (0.25 µg/µL) were prepared with ultrapure (18 Mohm) deionized water and stored at -20°C.

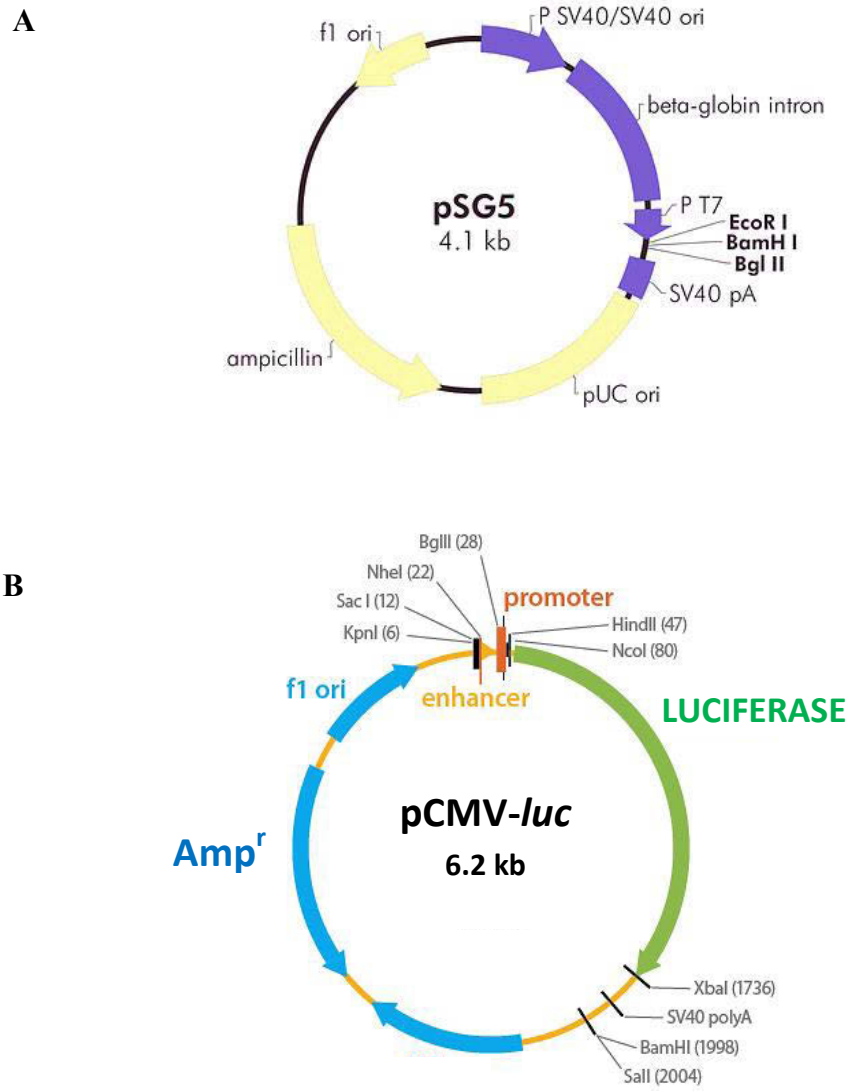

Figure 2.4: Plasmid maps of **A)** pSG5 and **B)** pCMV-*luc*.

2.4 DNA binding studies

2.4.1 Band shift assay

The ability of the cationic nanoparticle and cationic polymers to bind plasmid DNA to form stable complexes was observed by the band shift or gel retardation assay. Agarose gels (1%) containing 1.5 µL ethidium bromide (10 mg/ ml) were prepared [(0.28 g agarose, 25.2 mL ultrapure deionized 18 Mohm water, 2.8 mL of 10 x electrophoresis buffer (0.36M Tris-HCl; 0.3M Na_2HPO_4 and 0.1 M EDTA in 1 litre Mohm water, pH 7.5)] and poured into a sealed UV gel tray fitted with an 8 well comb and allowed to set for a minimum of 60 minutes. Nanocomplexes were prepared separately by incubating the reporter gene pCMV-*luc* DNA (0.25 or 0.5 µg/µL) with increasing amounts of the respective CP or FAuNP at varying CP/FAuNP:pDNA weight ratios ($^{w}/_{w}$) for 60 minutes at room temperature (Table 2.1 and 2.2). All complexes were made up to a constant volume of 11 µL in HEPES buffered saline (HBS) in micro-centrifuge tubes. After the 60 minute incubation period, 3 µL of gel loading buffer (glycerol 50%, bromophenol blue 0.05% and xylene cyanol (0.05%) was added to the complexes and 11 µL of each sample was loaded into the wells and then placed in a Mini-Sub® electrophoretic apparatus (BioRad Laboratories, Richmond, USA). Electrophoresis was performed at 50 V for 90 minutes in 1x electrophoresis buffer at room temperature. CP and FAuNP interaction with the pDNA was viewed and images captured at exposure times of 1-2 seconds using the Vacutec Syngene G: Box BioImaging system (Syngene, Cambridge, UK).

Table 2.1: Varying amounts of the FAuNPs and pCMV-*luc* DNA used in the band shift assay.

Components	**AuNP-PEI**							
	1:0	**1:6**	**1:8**	**1:10**	**1:12**	**1:14**	**1:16**	**1:18**
Sample (µL) (w/w)	0	0.75 (1.5)	1 (2)	1.25 (2.5)	1.5 (3)	1.75 (3.5)	2 (4)	2.25 (4.5)
DNA (0.25 µg/µL)	1	1	1	1	1	1	1	1
HBS	10	9.25	9	8.75	8.5	8.25	8	7.75
Components	**AuNP-PLL**							
	1:0	**1:3.2**	**1:3.4**	**1:3.5**	**1:3.7**	**1:3.8**	**1:4**	**1:4.2**
Sample (µL) (w/w)	0	2 (1.60)	2.1 (1.68)	2.2 (1.76)	2.3 (1.84)	2.4 (1.92)	2.5 (2)	2.6 (2.08)
DNA (0.25 µg/µL)	2	2	2	2	2	2	2	2
HBS	9	7	6.9	6.8	6.7	6.6	6.5	6.4
Components	**AuNP-Cys**							
	1:0	**1:40**	**1:41**	**1:42**	**1:43**	**1:44**	**1:45**	**1:46**
Sample (µL) (w/w)	0	1 (20)	1.02 (20.5)	1.05 (21)	1.07 (21.5)	1.1 (22)	1.12 (22.5)	1.15 (23)
DNA (0.25 µg/µL)	2	2	2	2	2	2	2	2
HBS	9	8	7.98	7.95	7.93	7.9	7.88	7.85
Components	**AuNP-Chitosan**							
	1:0	**1:0.04**	**1:0.08**	**1:0.16**	**1:0.2**	**1:0.24**	**1:0.28**	**1:0.36**
Sample (µL) (w/w)	0	1 (0.01)	2 (0.02)	3 (0.04)	4 (0.05)	5 (0.06)	6 (0.07)	7 (0.09)
DNA (0.25 µg/µL)	1	1	1	1	1	1	1	1
HBS	10	9	8	7	6	5	4	3

Table 2.2: Varying amounts of the Cationic polymer and pCMV-*luc* DNA used in band shift assays.

Components	**PEI**							
	1:0	**1:4**	**1:6**	**1:8**	**1:10**	**1:12**	**1:14**	**1:16**
Sample (µL) (w/w)	0	0.5 (1)	0.75 (1.5)	1 (2)	1.25 (2.5)	-	-	-
DNA (0.25 µg/µL)	1	1	1	1	1	-	-	-
HBS	10	9.5	9.25	9	8.75	-	-	-
Components	**PLL**							
	1:0	**1:0.12**	**1:0.24**	**1:0.38**	**1:0.50**	**1:0.62**	**1:0.74**	**1:0.88**
Sample (µL) (w/w)	0	1 (0.06)	2 (0.12)	3 (0.19)	4 (0.25)	5 (0.31)	6 (0.37)	7 (0.44)
DNA (0.25 µg/µL)	2	2	2	2	2	2	2	2
HBS	9	8	7	6	5	4	3	2
Components	**Cys**							
	1:0	**1:33**	**1:34**	**1:35**	**1:36**	**1:37**	**1:38**	**1:39**
Sample (µL) (w/w)	0	0.82 (16.5)	0.85 (17)	0.87 (17.5)	0.9 (18)	0.92 (18.5)	0.95 (19)	0.97 (19.5)
DNA (0.25 µg/µL)	2	2	2	2	2	2	2	2
HBS	9	8.18	8.15	8.13	8.1	8.08	8.05	8.03
Components	**Chitosan**							
	1:0	**1:0.05**	**1:0.08**	**1:0.16**	**1:0.2**	**1:0.24**	**1:0.28**	**1:0.36**
Sample (µL) (w/w)	0	1 (0.01)	2 (0.02)	3 (0.04)	4 (0.05)	5 (0.06)	6 (0.07)	7 (0.09)
DNA (0.25 µg/µL)	1	1	1	1	1	1	1	1
HBS	10	9	8	7	6	5	4	3

2.4.2 Nuclease protection assay

To confirm whether the cationic polymers on their own or the functionalized gold nanoparticles could provide adequate protection to the adsorbed plasmid DNA from nuclease degradation, foetal bovine serum (FBS)-mediated digestion was assessed using agarose gel electrophoresis. The PEI and Chitosan based complexes contained increasing amounts of nanoparticle concentrations and a constant amount of pCMV-*luc* DNA (0.25 µg/µL) while the PLL and Cysteine based complexes contained 0.5 µg/µL of pCMV-*luc* DNA, made up to a volume of 14 µL in HBS (pH 7.4) at room temperature. Three ratios (sub-optimal, optimal, supra-optimal) were selected based on the band shift assay results as set out in Table 2.3 and 2.4. A positive control (C1) containing naked DNA with no FBS and negative control (C2) containing FBS treated DNA were set up. The complexes were incubated for 30 minutes and thereafter treated with FCS (excluding positive control) to a final concentration of 10% (1 µL) and incubated further at 37 °C for 4 hours in a temperature controlled water bath. Thereafter EDTA (1.1 µL, 10mM) was introduced to stop the nuclease reaction. Approximately 0.5% SDS (1.33 µL, $^{w}/_{v}$) was then added to the complexes which were incubated for a further 20 minutes at 55°C to facilitate release of the DNA. At the end of the incubation, gel loading buffer (3 µL) was added to each sample. Agarose gel electrophoresis at 50 V for 2 hours was carried out as described in 2.4.1.

Table 2.3: Weight ratios of the FAuNPs used in the FCS-mediated digestion assay.

Components	Volume (µL)					
	AuNP-PEI			AuNP-PLL		
	1:8	**1:10**	**1:12**	**1:3.2**	**1:3.4**	**1:3.5**
Sample (µL) (w/w)	1 (2 µg)	1.25 (2.5 µg)	1.5 (3 µg)	2 (1.6 µg)	2.1 (1.68 µg)	2.2 (1.76 µg)
HBS	8	7.75	7.5	7	6.9	6.8
Components	**Volume (µL)**					
	AuNP-Cys			**AuNP-Chitosan**		
	1:40	**1:41**	**1:42**	**1:0.04**	**1:0.08**	**1:0.16**
Sample (µL) (w/w)	1 (20 µg)	1.02 (20.5 µg)	1.05 (21 µg)	1 (0.01 µg)	2 (0.02 µg)	3 (0.04 µg)
HBS	8	7.98	7.95	8	7	6

Table 2.4: Weight ratios of the CPs used in the FCS-mediated digestion assay.

Components	Volume (µL)					
	PEI			PLL		
	1:4	**1:6**	**1:8**	**1:0.62**	**1:0.74**	**1:0.88**
Sample (µL) (w/w)	0.5 (1 µg)	0.75 (1.5 µg)	1 (2 µg)	5 (0.31 µg)	6 (0.37 µg)	7 (0.44 µg)
HBS	8.5	8.25	8	4	3	2
Components	**Volume (µL)**					
	Cys			**Chitosan**		
	1:36	**1:37**	**1:38**	**1:0.05**	**1:0.08**	**1:0.16**
Sample (µL) (w/w)	0.9 (18 µg)	0.92 (18.5 µg)	0.95 (19 µg)	1 (0.01 µg)	2 (0.02 µg)	3 (0.04 µg)
HBS	8.1	8.08	8.05	8	7	6

2.4.3 Ethidium bromide intercalation assay

The ethidium bromide intercalation assay was carried out to determine the level of pDNA condensation. Approximately 100 µL HBS was dispensed into a control and test well in a 96-well FluorTrac flat-bottom black plate. To each well 2 µL ethidium bromide (100 µg/µL) was added. The fluorescence value at excitation and emission wavelengths of 520 nm and 600 nm respectively was then read in a GloMax®-Multi Detection System (Promega BioSystems, Sunnyvale, USA) to provide a baseline relative fluorescence of 0%. Thereafter, DNA (1.2 µg) was introduced to both wells and this fluorescence intensity reading was set at 100%. Cationic polymers (CP) and the functionalized Au nanoparticles (FAuNP) (1 µL aliquots) were added to the respective EtBr/pDNA solutions followed by a 30 second brisk vortex to promote uniformity in the solution prior to recording the respective fluorescence intensities. This was continued until a plateau in fluorescence readings was reached. All measurements were conducted in triplicate at 25°C and the relative fluorescence (F_r) was plotted against CP or FAuNP mass ratios using the equation F_r (%) = (Fi – F_0)/ (F_{max} - F_0) x 100 where F_0 is the fluorescence intensity of un-intercalated EtBr in the absence of pDNA, F_{max} is the fluorescence intensity of fully intercalated EtBr in pDNA and in the absence of CP or FAuNP, and F_i is the fluorescence intensity for a given concentration of nanoparticle (Sun *et al.,* 2009).

2.5 *In vitro* cell culture and transfection studies

2.5.1 Growth and maintenance of cell lines

All media preparations and cell culture work were performed in an Airvolution Class II Biosafety cabinet. All surfaces were wiped with 70% ethanol and only sterile pipettes, disposable tubes, 25 cm^2 flasks, multi-well plates and pipettes tips were used for cell culture studies. Cells were initially grown in 25 cm^2 tissue culture flasks containing 5 mL of EMEM supplemented with 10% ($^v/_v$) gamma-irradiated FBS and antibiotics (100 U/mL penicillin, 100 µg/mL streptomycin) at 37 °C in a HEPA Class 100 Steri-Cult CO_2 incubator (Thermo-Electron Corporation, Waltham, Massachusetts, USA). Cell growth was monitored daily under a Nikon TMS (Nikon Corp., Tokyo, Japan) inverted microscope. Medium was changed approximately every 2-3 days or when required.

2.5.2 Reconstitution of frozen cells

Frozen vials of cells were removed from the biofreezer (-80°C) and placed immediately in a water bath at 37 °C to thaw. Thereafter the cell suspension was transferred aseptically to a micro-centrifuge tube (2 mL) and microfuged at 3000 rpm for 1 minute. The supernatant containing DMSO was thereafter decanted and the pellet resuspended in 1 mL of fresh pre-warmed medium. The reconstituted cell suspension was introduced to a flask containing 5 mL of growth medium. The flask was then placed in the incubator overnight at 37 °C under a humidified atmosphere and 5% CO_2. The medium was replaced the following day to remove traces of DMSO which is toxic to cells above 4 °C. Cells were left to grow and maintained in culture until confluent and could be used or experimental purposes.

2.5.3 Trypsinization

Complete growth medium and trypsin were pre-warmed in a 37 °C water bath. Spent medium was decanted and cells were washed with 5 mL PBS (150 mM sodium chloride, 2.7 mM potassium chloride, 1 mM potassium dihydrogen phosphate, 6 mM disodium hydrogen phosphate, pH 7.5) Trypsin-versene (1 mL) was added to cover the cells in the flask. The flask was allowed to stand for 1-5 minutes depending on the trypsinization time required for the cell line used. The process of trypsinization which is driven by the proteolytic enzyme trypsin, catalyses the cell dissociation and digests the proteins that allow the cells to adhere to the flask. Cells were viewed under the inverted microscope to observe rounding off during trypsinization. Dislodging of the cells from the flask was aided by gently tapping of the flask against the palm of the hand. The activity of trypsin was inhibited by the addition of 2 mL medium containing serum. Cells were split according to pre-determined ratios into 25 cm^2 flasks or multi-well plates, or alternatively cryopreserved. Cell counting was facilitated using a Millipore Scepter™ handheld automated cell counter (Millipore Corporation, Billerica, MA, USA) prior to plating of cells for the respective assays.

2.5.4 Cryopreservation

After trypsinization of adherent cells, cells were pelleted by configuration at 3000 rpm for 1 minute. The pelleted cells were re-suspended in 0.9 mL growth medium and 0.1 mL DMSO (10 %) which is a cryoprotective storage medium. The suspension was vortexed and aliquoted into sterile 2 mL cryogenic storage vials. Cells were frozen at a rate of -1°C per minute in a Nalgene^{TM} "Mr Frosty" Cryo 1°C freezing container containing isopropanol to a temperature of -70°C. Cells were stored temporarily in a -80°C biofreezer (Nuaire, Lasec Laboratory and Scientific Equipment) or in liquid nitrogen for long term storage.

2.5.5 *In vitro* MTT reduction assay

Cells at or near confluency were trypsinized and seeded into clear 48-well plates at a seeding density of 2.4 - 2.9 x 10^4 cells/well. Cells were incubated at 37 °C for 24 hours to allow for attachment. Thereafter the medium was replaced and the respective CP / FAuNP:pCMV-*luc* DNA complexes were added and cells allowed to incubate for 48 hours at 37 °C in 5% CO_2. Complexes were prepared as set out in Tables 2.5 and 2.6. A positive control was set up which contained only cells and no pDNA or complexes and assumed to have 100% cell survival. The assay was done in triplicate. After 48 hours the spent medium was removed and 200 µL fresh growth medium plus 200 µL MTT reagent (5 mg/mL in PBS) was added to each well. After a 4 hour incubation at 37°C the MTT infused growth medium was removed from each well and discarded. The insoluble formazan crystals were solublized by the addition of 200 µL DMSO and gently shaken. Absorption was read at 570 nm in a Mindray MR-96A microplate reader (Vacutec, Hamburg, Germany).

Table 2.5: MTT cytotoxicity weight ratios of FAuNPs/pDNA complexes.

Components	Volume (µL)					
	AuNP-PEI			AuNP-PLL		
	1:8	**1:10**	**1:12**	**1:3.2**	**1:3.4**	**1:3.5**
Sample (µL) (w/w)	1 (2 µg)	1.25 (2.5 µg)	1.5 (3 µg)	2 (1.6 µg)	2.1 (1.68 µg)	2.2 (1.76 µg)
HBS	6	5.75	5.5	5	4.9	4.8

Components	Volume (µL)					
	AuNP-Cys			AuNP-Chitosan		
	1:40	**1:41**	**1:42**	**1:0.04**	**1:0.08**	**1:0.16**
Sample (µL) (w/w)	1 (20.5 µg)	1.02 (21 µg)	1.05 (21.5 µg)	1 (0.01 µg)	2 (0.02 µg)	3 (0.04 µg)
HBS	6	5.98	5.95	6	5	4

Table 2.6: MTT cytotoxicity weight ratios of CP/pDNA complexes**.**

Components	Volume (µL)					
	PEI			PLL		
	1:4	**1:6**	**1:8**	**1:0.62**	**1:0.74**	**1:0.88**
Sample (µL) (w/w)	0.5 (1 µg)	0.75 (1.5 µg)	1 (2 µg)	5 (0.31 µg)	6 (0.37 µg)	7 (0.44 µg)
HBS	6.5	6.25	6	2	1	0

Components	Volume (µL)					
	Cys			Chitosan		
	1:36	**1:37**	**1:38**	**1:0.05**	**1:0.08**	**1:0.16**
Sample (µL) (w/w)	0.9 (18 µg)	0.92 (18.5 µg)	0.95 (19 µg)	1 (0.01 µg)	2 (0.02 µg)	3 (0.04 µg)
HBS	7.9	6.08	6.05	6	5	4

2.5.6 Transfection analysis

After reaching confluency, cells were trypsinized and plated in 48-well plates as outlined in 2.5.5. All nanocomplexes were freshly prepared as set out in Tables 2.5 and 2.6. The assay was conducted in triplicate. Two cell controls were set up, one unexposed to nanoparticles/cationic polymers or pDNA and one exposed to free naked pDNA in the absence of nanoparticles/cationic polymers (0.25 μg/μL per well). After 24 hours the nanocomplexes were added to the cells, and cells incubated for 48 hours at 37°C in 5% CO_2. Thereafter the cells were subjected to the luciferase assay (2.5.7).

2.5.7 Luciferase Assay

Cells were washed twice with 0.2 mL PBS and lysed with 80 μL reporter lysis buffer (1x) (25 mM tris-phosphate, pH 7.8; 2 mM dithiothreitol, 2 mM 1,2-diaminocyclohexane – N, N, N'N'-tetra-acetic acid, 10% (v/v) glycerol, 1% (v/v) triton X-100). The plates were rocked gently on a STR 6 platform shaker (Stuart Scientific, Staffordshire, UK) for 15 minutes at 30 rpm. Thereafter the cells were gently scraped from the wells and the cell suspensions transferred to 1 mL micro-centrifuge tubes and centrifuged in an Eppendorf 5418 centrifuge for 30 seconds at 12000 x g. Approximately 20 μL of the cell free extracts were transferred to white 96 well plates, to which 50 μL of luciferase assay reagent (20 mM tricine, 1.1 mM magnesium carbonate hydroxide, pentahydrate, 2.7 mM magnesium sulphate, 0.1 mM EDTA, 33.3 mM dithiothreitol, 270 μM coenzyme A , 470 μM luciferin, 530 μM ATP) was added just before bioluminescence was read. Prior to this the PMT detector (photomultiplier tube) on a GloMax®-Multi Detection System (Promega BioSystems, Sunnyvale, USA) operated by Instinct software was activated for 5 minutes. The plates were gently shaken and relative light units (RLU) of all samples were immediately measured at room temperature. Light units were normalized against soluble protein content in the cell lysates, which was determined colorimetrically by the BCA protein assay at 562 nm. Each data point was averaged over three replicates (n=3) and results were presented as means ± SD.

2.5.8 Statistical analysis

All data is presented as mean ± standard deviation (± SD n=3). Multi group comparisons of means were carried out using one-way analysis of variance (ANOVA) followed by Dunnett's *post hoc* test for the MTT assay and the Tukey-Kramer *post hoc* test for the luciferase activity assay. Statistical significance for all tests was set at ***p<0.001 (high significance), **p<0.01 (medium significance) and *p<0.05 (low significance). Each experimental value was compared to its corresponding control. Graphpad Instat Prism 4.0.3 software was used for statistical analysis. All graphs were plotted in Origin 7.0.

Chapter Three

Results and Discussion

Chapter Three

Results and Discussion

3.1 Synthesis and characterization of gold nanoparticles

The electrokinetic characterization of the AuNPs functionalized with PEI, PLL and L-lysine was carried out at the Applied Physics Department, University of Granada, Spain as part of the Erasmus Mundus (EMA2SA) Fellowship Award. The objective of the research was to study the role that size, concentration, type of morpho-isoform of the DNA molecule, pH and ionic strength play in determining the specificity and charge of the nanosensors for the analytes (Sections 3.1.-3.2).

3.1.1 Nanoparticle tracking analysis

The gold nanoparticles were synthesized and viewed using nanoparticle tracking analysis (NTA). This unique technique directly sizes and visualizes nanoscale particles in liquids with high-resolution in real-time and with minimal sample preparation. The system provided count and concentration measurements by utilizing a laser light source to illuminate nanoscale particles that appeared individually as point scatters moving under Brownian motion. Below are images that show the distribution of the gold nanoparticles (Figure 3.1), confirming their strong light scattering ability and surface plasmon resonance.

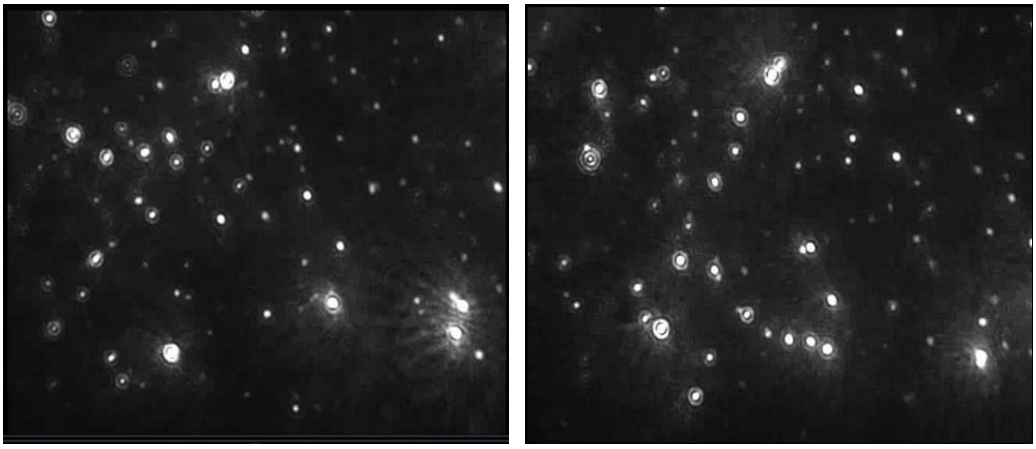

Figure 3.1: Sample photo frame of the colloidal gold nanoparticles as captured by NTA software.

Size distribution of the non-functionalized gold nanoparticles averaged <100 nm. The total concentration was 36.65 particles/frame or 5.75 x 10^8 particles/mL. The laser light completed 723 tracks at 23.75 frames per second (14240 frames with a drift velocity of 2491 nm/s) at a temperature of 25.5 °C. The plot seen below in Figure 3.2 is a 3-dimensional representation of the particle size and relative intensity as a function of the number of particles.

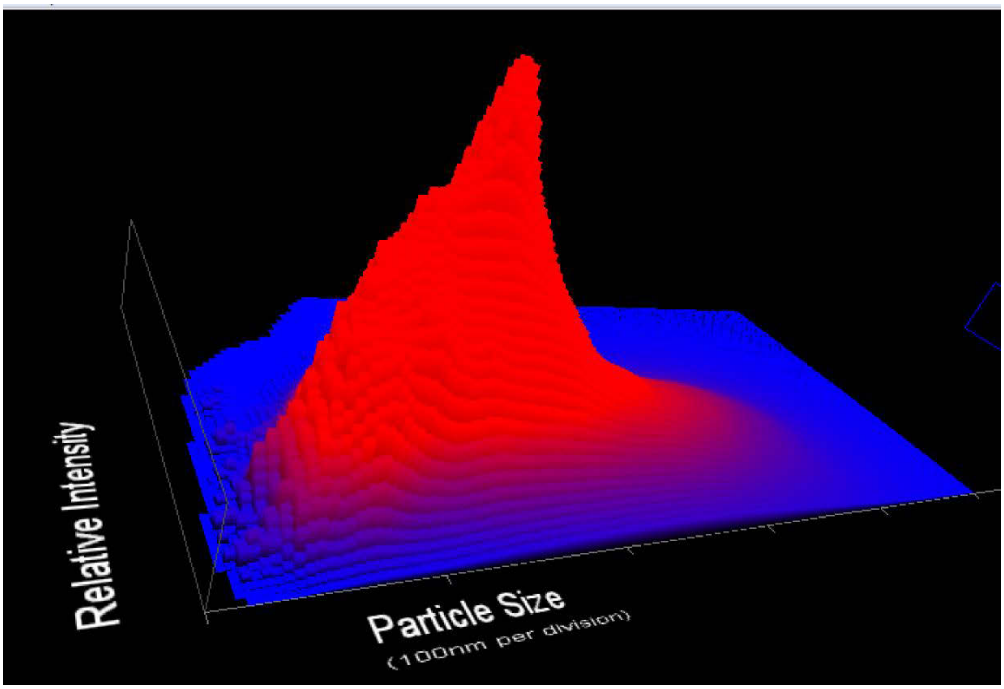

Figure 3.2: Particle Size / Relative Intensity 3D plot of the gold nanoparticles.

3.1.2 Photoluminescence spectra of Au

The design and synthesis of fluorescent side-chain conjugated polymers which assemble supramolecularly, and are able to exhibit either chromogenic or fluoregenic responses due to non-covalent interactions, have gained considerable attention. Understanding the photo-physical processes are essential in order to improve the efficiency of our complexes. In order to understand the dynamics of the excited states of Au, photoluminescence (PL) was measured which is due to photo induced exciton states that undergo radiative recombination (Figure 3.3). The measurement of photoluminescence quenching gives a strong indication of the potential of a particular material for a charge transfer and also provides an understanding of its morphological

properties and quenching radius. Gold nanoparticles are highly attractive models for biological and fluorescent conjugated polymers. High performance fluorescence assay methods have been developed by taking advantage of this super-quenching ability of gold nanoparticles for optically sensing biologically important ions and molecules. The quenching of fluorophores that are attached to monolayer-protected gold nanoparticles and also the electron transfer from excited fluorophores to gold nanoparticles have been investigated (El-Sayed *et al*, 2010; McIntosh *et al*., 2001). Direct binding between a fluorophore and a metal surface often results in the quenching of the fluorophores excited states. Energy transfer and electron transfer processes are considered to be the major deactivation pathway for excited fluorophores on a metal surface (Ipe *et al.*, 2002). The AuNPs were excited at 240 nm and emission was observed at 530 nm and 726 nm respectively, indicating a red shift.

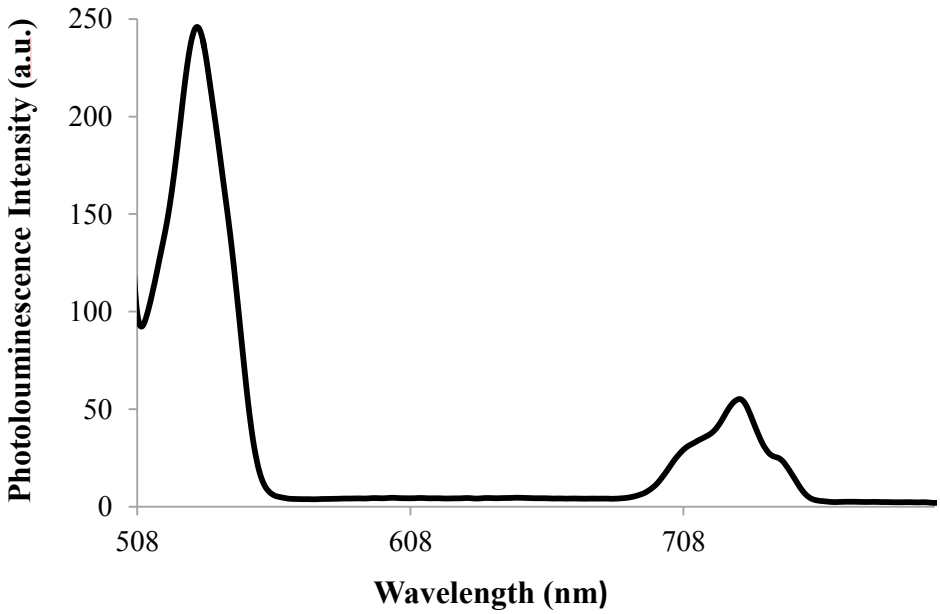

Figure 3.3: Fluorescence quenching spectra of Au nanoparticles excited at 240 nm. The emission peaks were at 530 nm and 726 nm. Photoluminescence intensity was expressed as arbitrary units (a. u.).

3.1.2.1 TEM analysis of Au, Au-Lys and Au-Lys with pDNA respectively

TEM micrographs revealed that the non-functionalized gold nanoparticles appeared spherical with smooth shapes and surfaces that were homogenous in the nanosized range of 25–50 nm with relatively monodisperse distributions (Figure 3.4). Subsequent observations showed no structural modifications such as aggregation or absorption changes for the particles after six months of storage at room temperature. The transition in colour of the AuNPs from pale yellow to ruby red confirmed the formation of citrate-capped gold nanoparticles (Turkevich *et al.*, 1951). When the pale yellow colour faded it signified the formation of the gold atoms which nucleated to form dark red nanowires (Lazarus *et al*., 2014). The citrate reduction route remains an attractive and reliable method of preparation, using a solvent such as water and no additional passivating ligand. The control over the nanoparticle size is related to the ratio of the agents used during preparation. The more reducing agents added, the smaller the nanoparticle produced. TEM micrographs of the L-lysine functionalised AuNPs and The Au-Lys NPs appeared as aggregates in the size range of 25–50 nm (Figure 3.5)

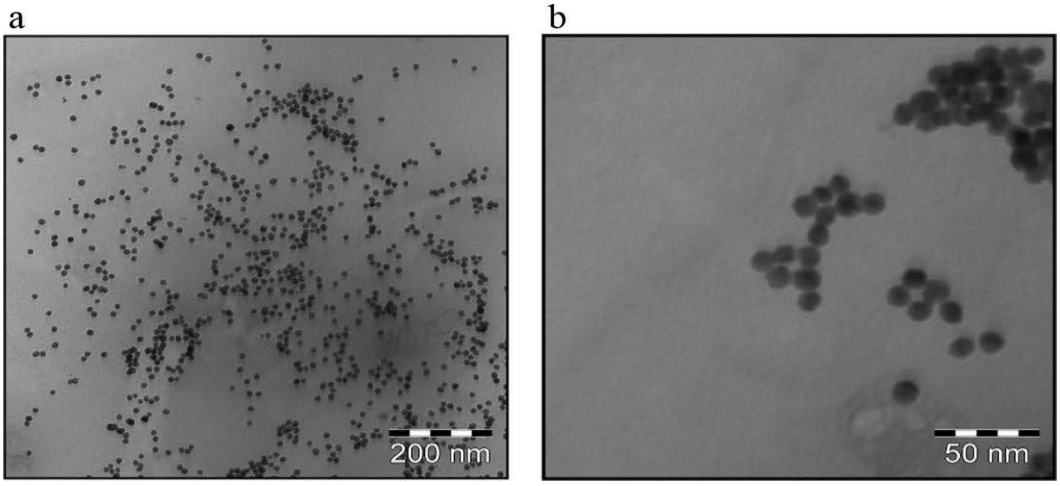

Figure 3.4: TEM analysis of AuNP at **a)** 40 000X and **b)** 60 000X magnification.

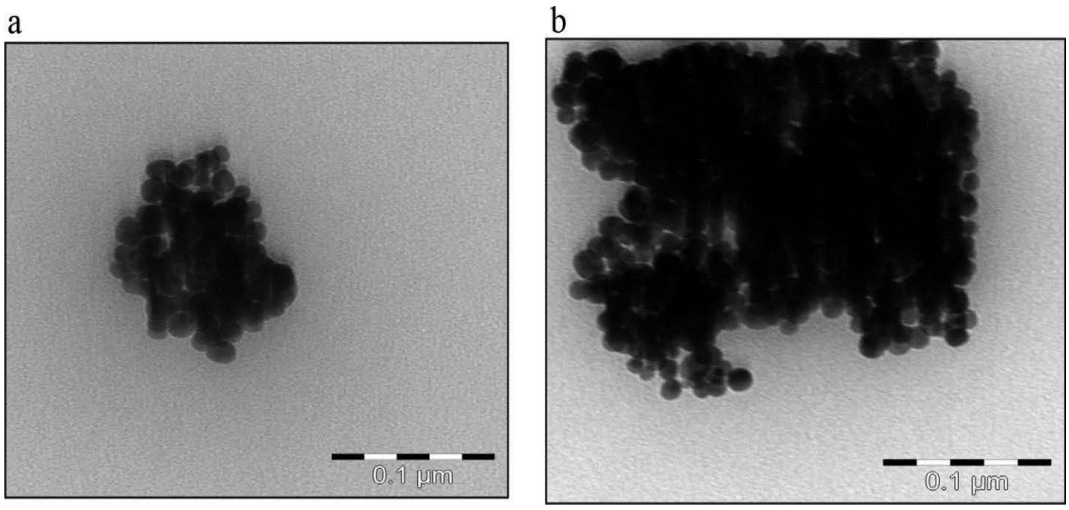

Figure 3.5: TEM of **a)** L-lysine bound to gold displaying aggregation **b)** Au-Lys/pDNA nanocomplex.

3.1.3 UV–visible spectrophotometry

The UV–vis absorption spectra in Figure 3.6 shows the absorbance peak of citrate-reduced colloidal Au nanoparticles. The surface plasmon resonance (SPR) absorption of the nanoparticles was observed presenting a well-defined absorption band with a maximum at wavelength λ_{max} = 534 nm. This value is characteristic and in agreement with the expected SPR absorption of the nanosized gold particles at this wavelength (Turkevich *et al*., 1951). The adsorption of L-lysine onto the surface of the gold particle was confirmed by a decrease in the absorbance peak to 519 nm. A blue shift can be observed by the decrease in wavelength which also denotes an increase in particle size (Lazarus *et al*., 2014). Particle size and shape of the nanoparticles are of major importance as they influence the internalization of the delivery complex by the cell.

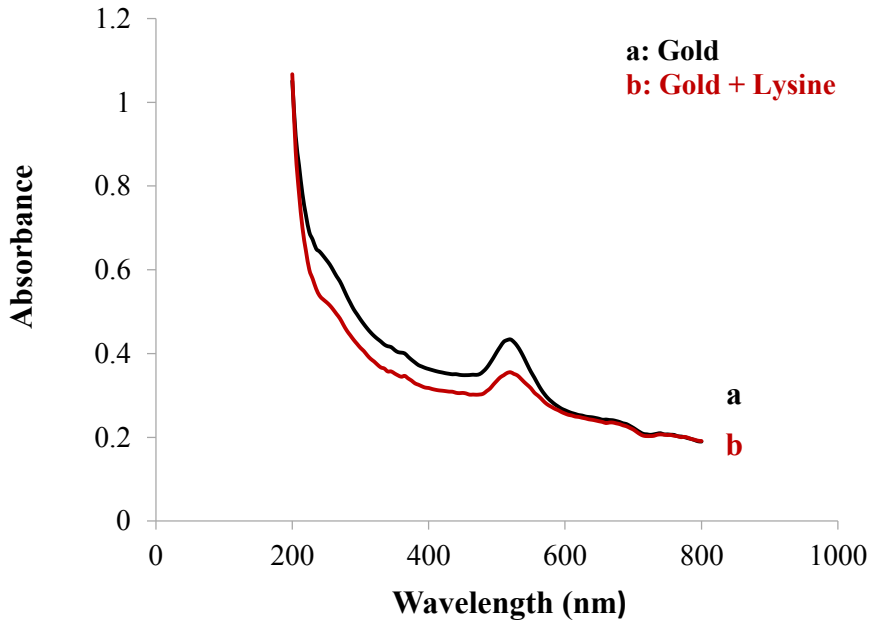

Figure 3.6: UV-*visible* spectrophotometry of gold nanoparticles at absorbance 534 nm indicating a blue shift change to 519 nm confirming the adsorption of L-lysine.

3.2 Gold nanoparticle and cationic polymer interaction

3.2.1 Effect of pH and concentration of cationic functional groups

Due to the anionic nature of the citrate reduced AuNPs it was of critical importance to functionalize the AuNPs with suitable cationic polymers (CPs) which will have a high affinity for the negatively charged cell membrane and enhance cell-mediated uptake processes (Wieber *et al.,* 2012). The polymers chosen for this initial study were polyethyleneimine (PEI), poly-L-lysine (PLL) and L-lysine. The chemistry of the functionalization of the AuNPs is of importance and the objective was to ensure that the bound molecule retained its biorecognition property such as light scattering and strong plasmon bands (Nikoobakht *et al.,* 2003 and Jans *et al.*, 2009). Surface functionalization of AuNPs is essential in order to target them to specific areas, organs or tissues of disease in order for them to effectively interact with cells or biological molecules.

Aggregation of particles is a huge problem in most cases of biological systems. Normally colloidal AuNPs are stabilized by using long hydrocarbon ligand chains that contain various functional groups. For example mercaptocarboxylic acid is popular in the stabilization of AuNPs due to the strong affinity of sulphur for gold (Uson *et al.*, 1978). It also has a photoluminescence property. There are several ways that have been employed to attach biological molecules to nanoparticles. The easiest method to functionalize and stabilize AuNPs is using electrostatic interactions.

3.2.2 Electrophoretic mobility (U_e) of Au-Lys

There are several theories that link electrophoretic mobility with zeta potential. L-lysine was initially chosen for its preference as an amino acid because it binds to the hydroxyl groups on citrate by its two amine groups. L-lysine exhibited positive electrophoretic mobility predominantly at pH 3 (Figure 3.8). This correlated to previous literature (Viota *et al.*, 2012). Researchers investigated the adsorption of amino acids onto the surface of magnetite cores by measuring the electrophoretic mobility of the amino acid-coated magnetite particles and comparing the results with the ones obtained for the unmodified magnetite cores. Likewise in order to explain L-lysines' particular pH dependence and its effect on *U*e, we coated the gold nanoparticles with this amino acid and took into consideration the pKa of its ionized groups. L-lysine has pKa values of 2.2; 8 and 10. At pH 3 the Au-lys NPs were protonated and L-lysine showed an overall +2 net charge. Therefore, there was attraction and adsorption between the L-lysine and gold nanoparticles. The isoelectric point with minimum electrostatic repulsion, shifted 4 units back (pH 3) from the norm (pH 7) after the gold was placed into contact with L-lysine. At pH 7, the *U*e became negative because L-lysine bound to gold, forming cross bridges with each other resulting in aggregation (Figure 3.8). As the pH increased to 9, deprotonation followed owing to the negative *U*e. The Au-Lys NPs experienced repulsion resulting in little or no adsorption. The difference in pH trend was further studied by modifying the surface adsorption of the AuNPs and varying the concentration of L-lysine in solution. As a result, at low L-lysine concentrations of 0.01 and 0.05 mg/mL the values corresponded to the gold particles. In Figure

3.8 there was a distinct adsorption on the AuNP with the L-lysine coated particles, showing a significant negative mobility irrespective of pH.

This again can be attributed to the fact that at high pH, L-lysine was deprotonated and any further increase in the concentration of L-lysine in solution led to saturation of the AuNP, resulting in cross-binding, aggregation and negative mobility (Figure 3.9A). The size distribution (Fig. 3.9 B) by intensity, correlated to the size by zeta sizing (Table 3.1). This was evident by the colour changes of the nanocomplex in solution (Figure 3.7A). It showed a distinct change from red to purple. It is likely that an increase in L-lysine concentration may have caused bridging leading to aggregation. At the lowest concentration of L-lysine (0.1-10 mg/mL) the colour was ruby red. Red is indicative of small particles of size 20–40 nm. After 24 hours the Au-Lys (Figure 3.7 B, C) turned purple indicating aggregation and instability. As the concentration of L-lysine increased (100–500 mg/mL) the colour changed to a deeper purple which indicated the formation of clusters and larger particles around 70–80 nm.

Figure 3.7: The instability of Au-Lys to bind to pDNA is confirmed by the image above. **A)** The increase in L-lysine concentration resulted in aggregation which shows bigger particles. This is indicated by the change in colour from red to violet. **B)** Au-Lys and **C)** Au-Lys after 24 hours.

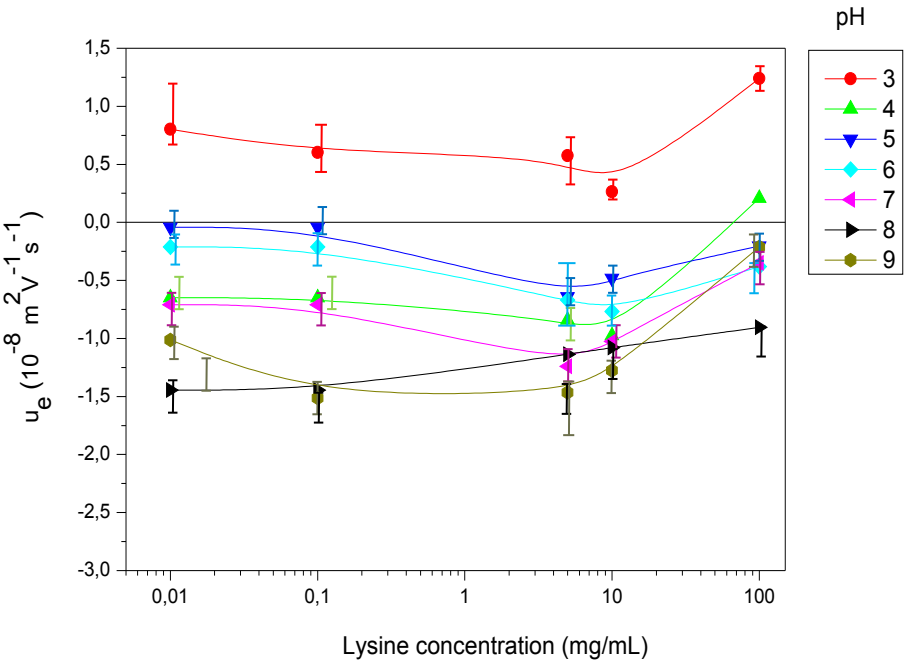

Figure 3.8: Electrophoretic mobility (U_e) of Au-Lys as a function of pH. Error bars represents the mean ± SD, n=3.

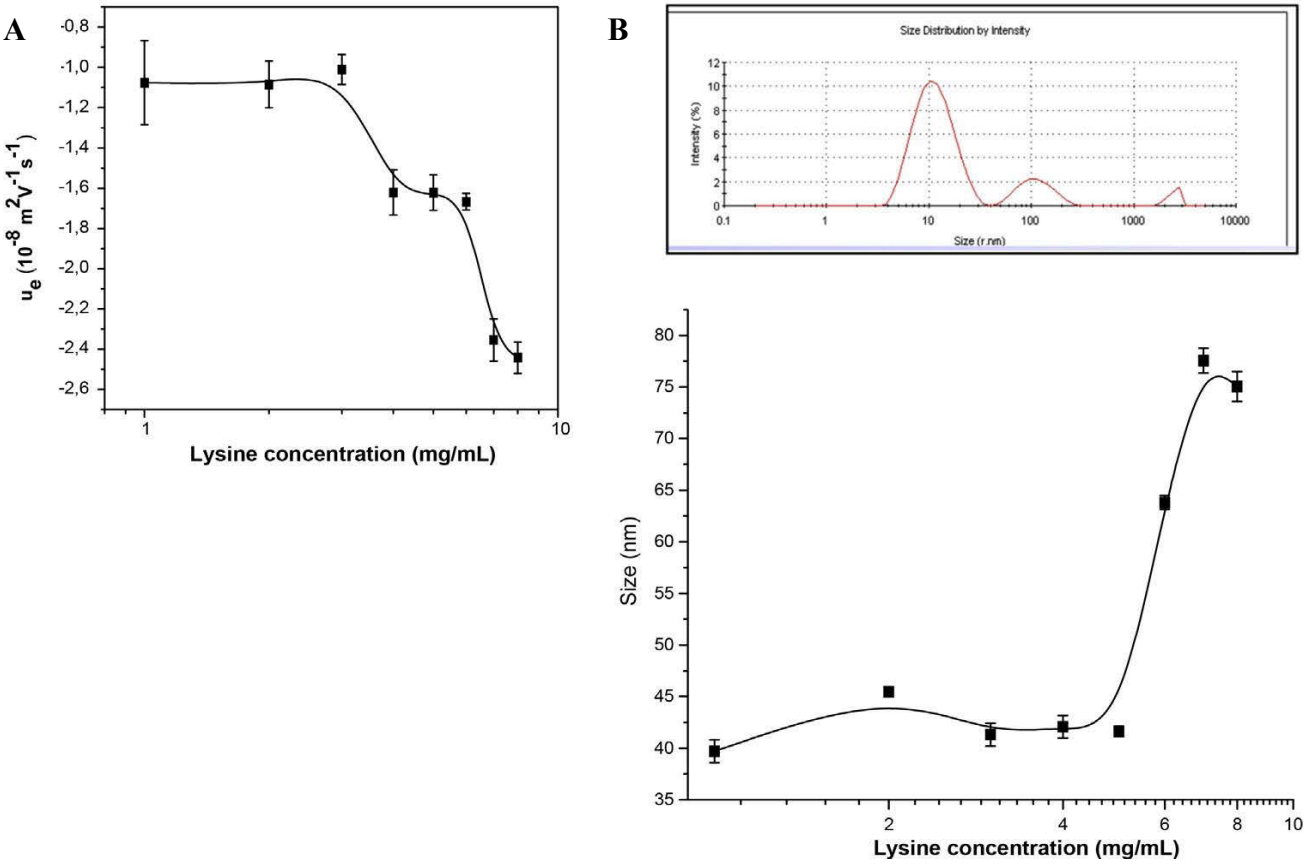

Figure 3.9: A) Electrophoretic mobility (U_e) and **B)** Size distribution of Au-Lys as a function of L-lysine concentration. Error bars represents the mean ± SD, n=3.

3.2.3 Electrophoretic mobility (U_e) of Au-PEI and Au-PLL

PEI and PLL were investigated for their interaction and relationship with gold nanoparticles and to determine whether gold may reduce the toxicological effects of these cationic polymers. The AuNPs were combined with PEI and PLL to prepare (1, 2, 5, 7 and 10 mg/mL) of PEI-coated AuNPs and (1, 10 and 100 mg/mL) of PLL-coated AuNPs respectively. Au-PEI NPs displayed sizes in the range 70–120 nm (Figure 3.10 B) which was more acceptable to that of the Au-PLL NPs which was in the range 350–500 nm (Figure 3.10 A). Au-PEI nanoparticles were coupled to the three different isoforms of pDNA. The pDNA conjugates with the functionalised AuNPs (FAuNPs) were found to be positively charged with a considerable increase in particle size (Figure 3.10 A). The electrophoretic mobility of Au-PLL and Au-PEI as a function of its concentration in solution is shown in Figure 3.11. The results obtained show considerable increase in electrophoretic mobility of the cationic functionalized groups when adsorbed onto gold nanoparticles. The particle size of the complexes increased with increasing weight ratios, and the rise in positive electrophoretic mobility was due to the cationic character of both polymers.

This result shows that PEI can condense pDNA into nanosized particles that are appropriate for gene delivery. A positive charge of the nanocomplex is necessary for the binding of the negatively charged phospholipids in the cellular membrane which will lead to efficient intracellular trafficking. Zeta potentials of the Au-PEI and Au-PLL NPs rapidly increased and reached a plateau above 1 mV, at weight ratios between 1 and 10 mg/mL. In the case of both CPs, the higher the concentration of the polymer the greater the positive charge (Figure 3.11). It is important to note that at the various concentrations of the PEI, the gold nanoparticles were already close to the saturation region as predicted in the law of Lambert Beer (Figure 3.11 B). It was not necessary to prepare the Au-PLL and Au-PEI nanoparticles at varying pH's as they were positively charged entities.

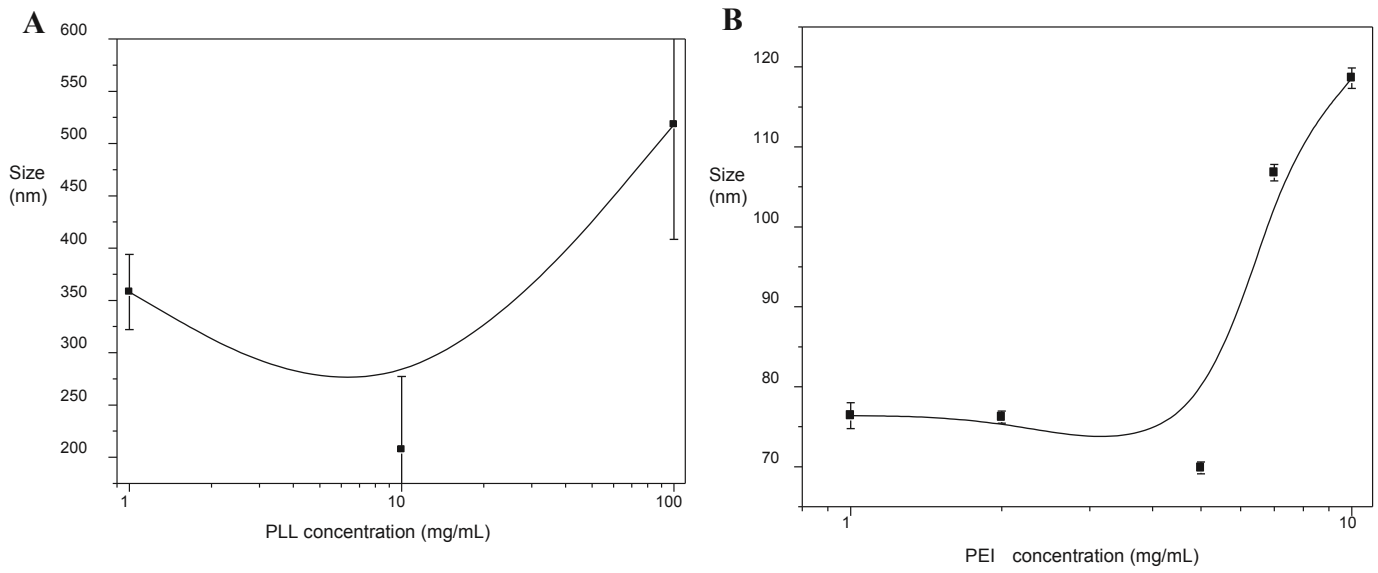

Figure 3.10: Zeta sizing by dynamic light scattering of **A)** Au-PLL and **B)** Au-PEI as a function of its concentration in solution. Error bars represents the mean ± SD, *n*=3.

A

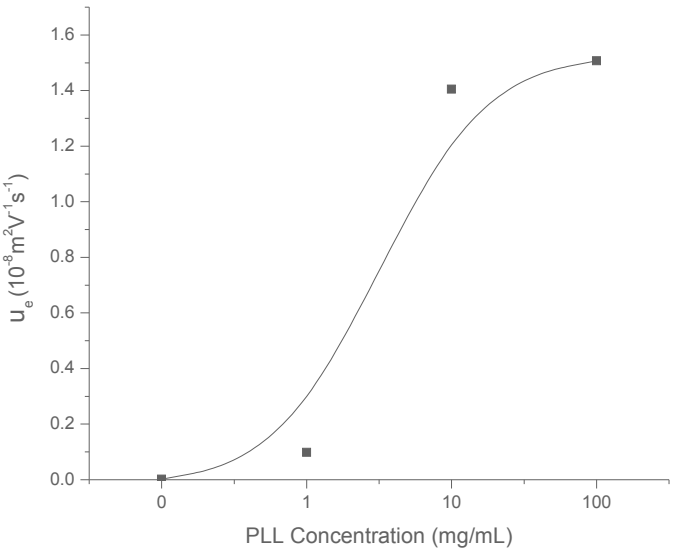

B

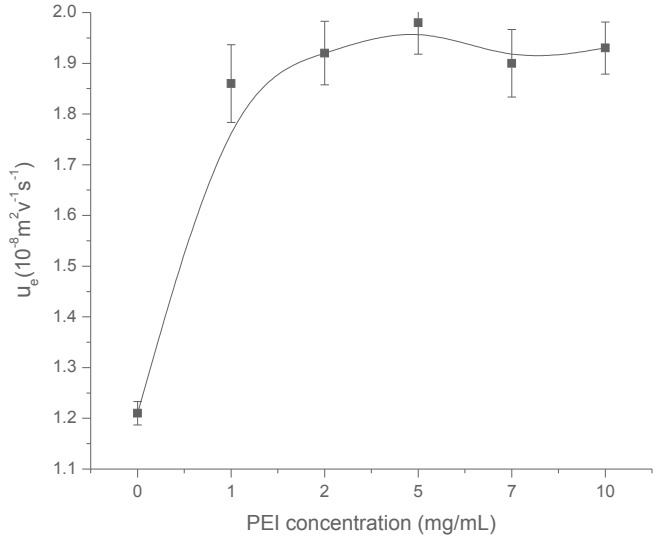

Figure 3.11: Electrophoretic mobility U_e of **A)** Au-PLL and **B)** Au-PEI as a function of its concentration in solution. Error bars represents the mean ± SD, n=3.

3.2.4 Au-PLL interaction with pSG5 DNA

Nanoparticle binding can facilitate DNA compaction in addition to partial strand separation (Ghosh *et al*., 2008a). We did not incubate the Au-Lys NPs with DNA because L-lysine was positive only at pH 3, which is too acidic for the proper physiological functioning of the body. Furthermore, the pH of blood is 7.4 and in order for the nanocomplexes to enter the cell and circulate in the body it has to be neutral or slightly positively charged. This study of Au-PEI/DNA interaction was not continued due to the early literature citing toxicity to cells in vitro (Lee, 2007). However, Au-PEI revealed size distributions within the desired size range and positive electrophoretic mobility, and was only employed further with DNA plasmids in later studies, where its cytotoxicity and biological activities were assessed. Hence studies with Au-PLL were conducted where Au-PLL was incubated with DNA pSG5. It exhibited size distributions in the range of 110–290 nm (Figure 3.13 B). As the concentration of PLL increased, the DNA strands wrapped tighter around the Au-PLL complex compacting it as seen in the TEM images (Figure 3.18 D), with a size decrease of more than 50% (Figure 3.13 B). An illustration is shown below in Figure 3.12 of the functionalization of AuNPs with CP and pDNA. Given that the smallest particle size was at 10 mg/mL, the Au-PLL NPs was prepared accordingly and incubated with DNA pSG5 of different isoforms as a function of their concentration. Results obtained (Figure 3.13 A) indicated that the *U*e of linear and supercoiled isoforms tended towards zero. When supercoiled DNA was complexed to PLL it yielded a much lower effective charge than linear DNA, since the polyelectrolyte was compacted with a large amount of counter ions.

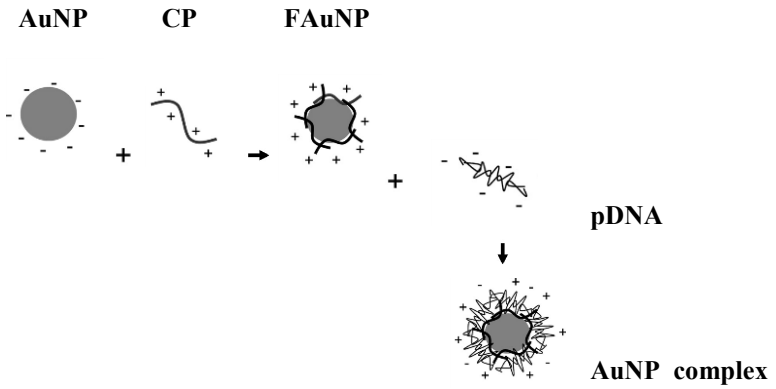

Figure 3.12: A simple illustration of the AuNP/cationic polymer nanoscaffold condensed with pDNA.

A

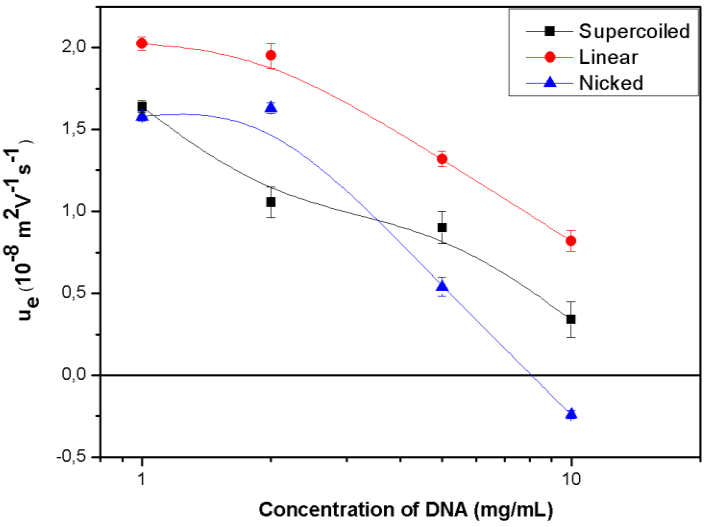

B

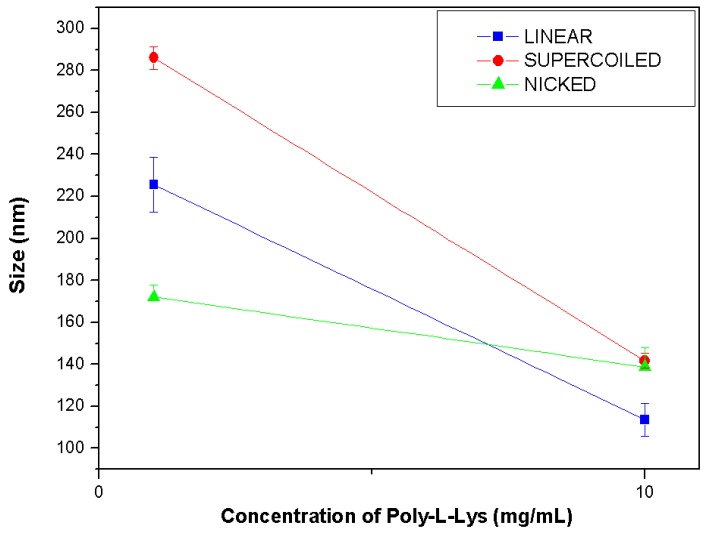

Figure 3.13: U_e of **A)** Au-PLL and DNA pSG5 as a function of DNA concentration and **B)** Size distribution of Au-PLL and DNA pSG5 as a function of PLL concentration. Error bars represents the mean ± SD, n=3.

3.2.5 Effect of ionic strength

The ionic strength of the Au-PEI complex was investigated, with and without pDNA, to determine how compact the adsorbed layer was. To achieve this, we investigated the effect of

electrolyte concentrations on the U_e. Theoretically, in the presence of layers the mobility should tend towards zero because of the electric double layer compression at high ionic strength. The dispersion medium, sodium citrate, was prepared at different ionic salt concentrations of ($1x10^{-4}$; $1x10^{-3}$; $2.5x10^{-3}$; $5x10^{-3}$; $7.5x10^{-3}$; $1x10^{-2}$; $2.5x10^{-2}$; $5x10^{-2}$ mg/mL). The result in Figure 3.14 showed that at higher salt concentrations, the mobility of the nanocomplexes approached zero which indicated that the overall charge was neutral. This suggested, that during transfection studies the complex should easily pass through the cell membrane. The results also revealed that at high ionic strength, electroneutrality was achieved and can be interpreted that the electric double layer was compact and stable. When the surface of the gold core was covered by PLL-DNA and PEI-DNA (Figure 3.14), the particles did not display soft electrokinetic behaviour. The formalization derived by Sennato *et al*. (2004) which is in turn based on the complexation theory developed by Nguyen and Shklovskii (2001a and 2001b), describes the complexation of long polyelectrolytes with oppositely charged spherical bodies to a single negative molecule of DNA. The theory predicts that in a system, equilibrium is reached by the DNA concentration with lipoplexes. The same can be said for metal nanoparticles which allows us to predict the isoelectric point where the nanocomplex is almost neutrally charged (Rodríguez-Pulido *et al*., 2009).

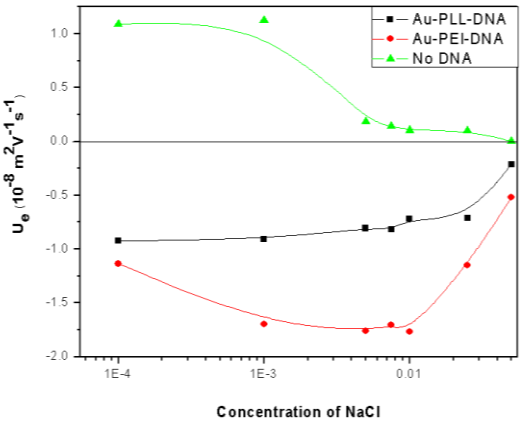

Figure 3.14: U_e of Au-PLL and Au-PEI and its interaction with supercoiled DNA as a function of ionic strength. Error bars represents the mean ± SD, n=3.

3.3 Nanocomplex binding and stability

The size of nanoparticles determine their cellular uptake, endocytosis, cytotoxicity, bio-distribution, and clearance pathway (Chithrani *et al.,* 2006; Hirn *et al.,* 2011; Pan *et al.,* 2007; Semmler-Behnke *et al.,* 2008; Sonavane *et al.,* 2008). Citrate-stabilized AuNPs were not appropriate for biological purposes due to their lack of stability in the presence of salt. Hence, cationic polymers were employed as capping agents to enhance biocompatibility to cells.

3.3.1 Sizing by dynamic light scattering and zeta potential analysis

Nanoparticles with cationic surfaces have a high cellular uptake, low toxicity, and renal clearance rate compared to those with an anionic surface. A positive surface charge can support electrostatic interactions and attachment to anionic cell membranes, as cells are known to take up positively charged nanocomplexes more efficiently. An acceptable size for circulation of AuNPs is 45 nm (Wang *et al*., 2010). Small nanoparticles also show greater transfection efficiency (Zhang *et al*., 1999). TEM images showed that the nanoparticles were spherical and monodispersed in many cases with an average size of 76 nm. Mean particle size distribution and zeta potential of the nanoparticles and corresponding nanocomplexes are summarized in Table 3.1. Dynamic light scattering characterization revealed the nanosized nanoparticles and nanocomplexes are accompanied by narrow SD (in brackets) as follows: Au-PEI 76 nm (0.269), Au-PEI/pDNA 217 nm (0.509); Au-PLL 207 nm (0.475), Au-PLL/pDNA 130 nm (0.217); Au-Cys 9.6 nm (0.012), Au-Cys/pDNA 15.7 nm (0.098) and Au-Chit 29.8 nm (0.391), Au-Chit/pDNA 186 nm (0.261). From these results there appears to be a correlation between nanocomplex size and zeta potential. The size increase of the non-functionalized AuNPs (25 nm) validated the success of polymer adsorption and functionalization (Table 3.1). Of particular interest is the size increase when the CP was adsorbed onto the AuNP. When the AuNPs were functionalized with PEI there was an increase in zeta potential and an increase in size. PEI has many residues with positive moieties, therefore the higher the PEI concentration the higher the surface charge of the nanocomplex. As noted in the Au-Lys, Au-Cys and Au-Chit samples, zeta potential decreases as the size of the nanocomplex increases. The AuNPs displayed an increase in zeta potential upon PLL addition and a drastic decrease in size as seen in TEM images (Figure

3.15). In addition this size decrease was confirmed by the ability of PLL to create a condensed network (Figure 3.12).

Table 3.1: Surface characteristics of the different AuNPs functionalized with cationic polymers and complexed to pCMV-l*uc* DNA.

Nanoparticle (NP)	Particle Composition (µg/µL)			Gel Retardation DNA:NP ($^{w}/_{w}$) Optimum Binding	EtBr Intercalation DNA:NP (w/w)	Size (nm) ± SD	Zeta Potential (mV) ± SD
	Au	NP	pDNA				
Au	1	0	0	ND	ND	**25** ± 0.733	**-17.0** ± 12.48
Au-Lys	1	1	0	ND	ND	**77.6** ± 0.334	**-46.5** ± 6.764
Au-Lys/pDNA	1	1	0.25	ND	ND	**200** ± 0.429	**-24.5** ± 6.764
Au-PEI	1	2	0	ND	ND	**76** ± 0.269	**42.4** ± 5.390
PEI/pDNA	0	2	0.25	**1:4** (0.25:1)	0.25:6	**182** ± 1.210	**46.2** ±2.123
Au-PEI/pDNA	1	2	0.25	**1:10** (0.25:2.5)	0.25:22	**217** ± 0.509	**53.8** ± 9.541
Au-PLL	1	10	0	ND	ND	**207** ± 0.475	**39.2** ± 4.565
PLL/pDNA	0	10	0.5	**1:0.88** (0.5:0.44)	0.5:48	**195** ± 0.987	**21.6** ± 2.315
Au-PLL/pDNA	1	10	0.5	**1:3.4** (0.5:1.60)	0.5:46	**130** ± 0.217	**47.9** ± 5.142
Au-Cys	1	20	0	ND	ND	**9.6** ± 0.012	**21.4** ± 0.019
Cys/pDNA	0	20	0.5	**1:37** (0.5:18.5)	0.5:320	**11.9** ± 0.875	**18.9** ± 0.256
Au-Cys/pDNA	1	20	0.5	**1:40** (0.5:20)	0.5:140	**15.7** ± 0.098	**16.4** ± 0.496
Au-Chit	1	0.0125	0	ND	ND	**29.8** ± 0.391	**32.5** ± 8.142
Chit/pDNA	0	0.0125	0.25	**1:0.05** (0.25:0.01)	0.25:0.25	**94** ± 0.569	**43.9** ± 4.156
Au-Chit/pDNA	1	0.0125	0.25	**1:0.08** (0.25:0.025)	0.25:0.24	**186** ± 0.261	**28.4** ± 4.921

ND denotes NOT DETERMINED

3.3.2 TEM of FAuNPs and nanocomplexes

Surface modification is important for the endocytosis of AuNPs, since AuNPs without ligands cannot efficiently interact with nucleic acids and with the cell surface. Small gold nanoparticles approach the size of typical protein ligands and may inadvertently activate cell surface receptors. When endocytosis of AuNPs occurs, the AuNPs become wrapped within the vesicles. From previous studies (Wang *et al*., 2010), the optimal size of AuNPs required for efficient uptake by cells was around 45 nm, suggesting that this size could probably have the highest efficiency for drug delivery. On the other hand, large AuNPs which remain bound to the cell membrane can be used to reconstruct the morphology of the cell.

TEM images of Au-PEI and Au-PLL appeared as oval, individualized shaped particles (Figure 3.15 A, C). Upon addition of pDNA, the nanoparticles assumed a gel-like structure which can be identified as the nanocomplex. The particles sizes were altered due to the interaction of pDNA as seen in Table 3.1. Of striking interest is the Au-Cys TEM (Figure 3.16 A). Au-Cys revealed chain-like structures that are known to be characteristic upon its addition to the citrate-stabilized gold aqueous dispersion. The citrate molecules are replaced by cysteine, resulting in the formation of an organic double layer (Majzika *et al.*, 2010). The addition of cysteine to the gold colloidal mixture led to a blue to black colour change. This colour change is generally regarded as a sign of aggregation (Mayya *et al*., 1997 and Petean *et al.,* 2008). Gold nanoparticles are particularly notorious for binding thiol ligands because of the high electronegativity of gold and electro-positivity of sulphur. Thus gold will preferentially bind sulphur containing compounds like cysteine. The formation of a covalent bond Au-S is due to the interaction of the positively charged amino group in cysteine (NH^{3+}) and the negative charge on the surface of the gold nanoparticles bound by their –SH groups. This phenomenon could be explained through the zwitterion-type electrostatic interaction where assemblies are formed and is in agreement with reported data on the adsorption of cysteine onto AuNP (Petean *et al*., 2008). Also characteristic for cysteine mediated assembly of gold nanoparticles is the linear arrangement. This is seen in the TEM (Figure 3.16 B). Au-Chit appeared as round nanoparticles that were well dispersed and appear far apart (Figure 3.16 C, D).

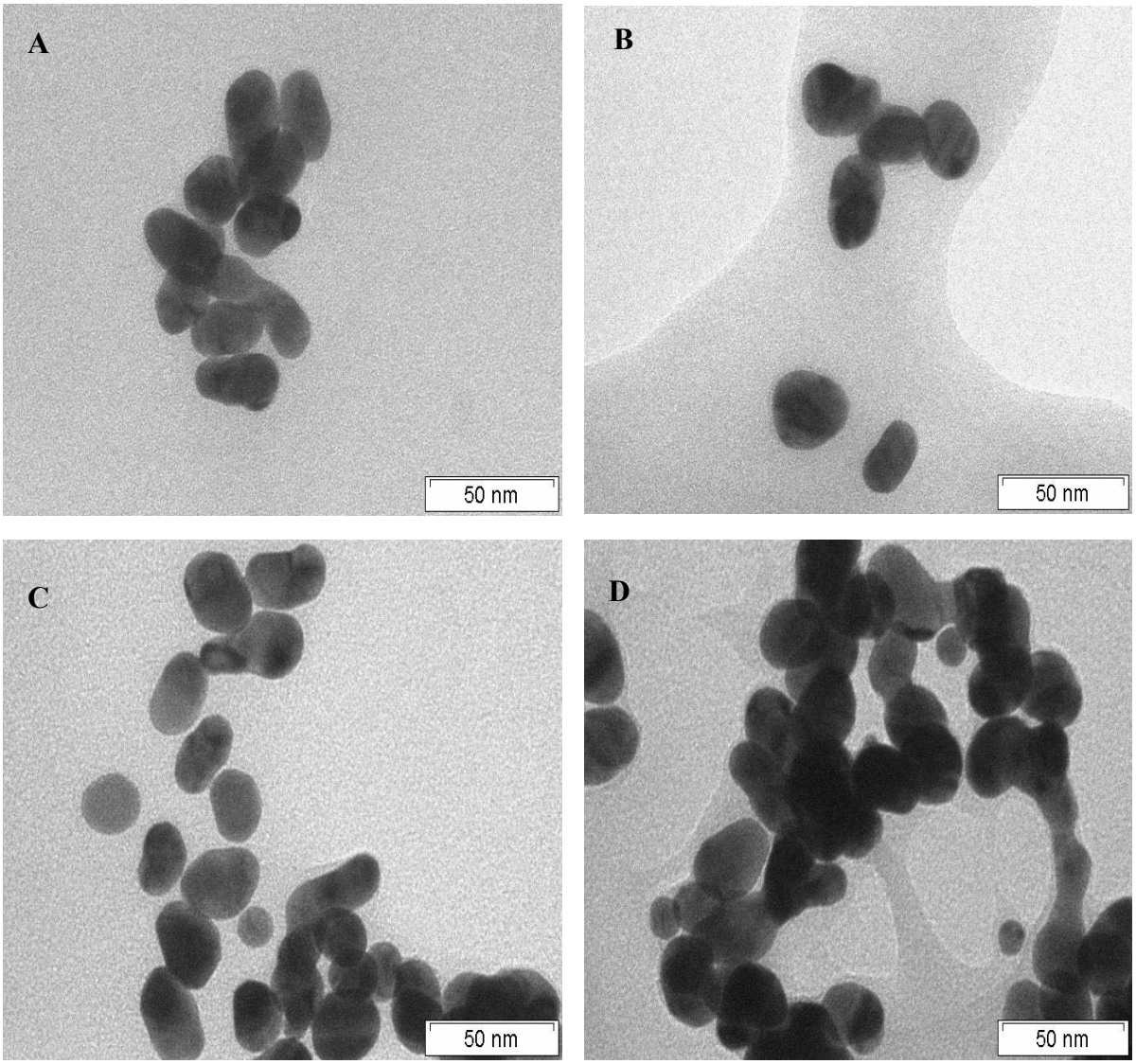

Figure 3.15: Transmission electron micrographs of FAuNPs: **A)** Au-PEI, **B)** Au-PEI/pDNA **C)** Au-PLL, **D)** Au-PLL/pDNA.

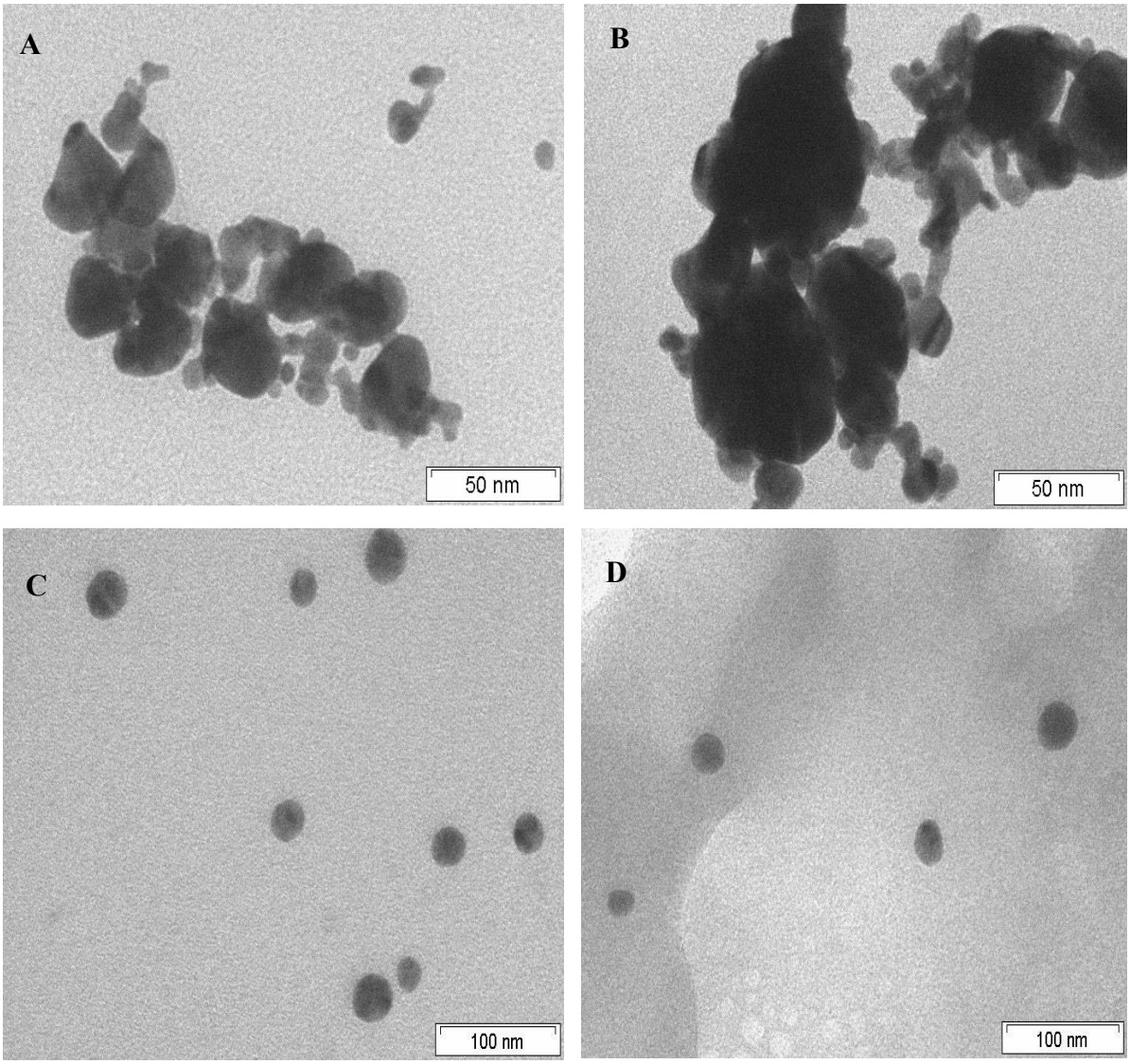

Figure 3.16: Transmission electron micrographs of: **A)** Au-Cys **B)** Au-Cys/pDNA **C)** Au-Chit **D)** Au-Chit/pDNA.

3.3.3 Band shift assays

Before proceeding with further biochemical assays it was of major importance to determine the minimum amount of FAuNP and CP that was needed to efficiently bind and compact a specific amount of the pCMV-luc plasmid DNA. The electrostatic binding ability of the gold based cationic nanoparticles to incorporate the negatively charged pDNA was investigated using the band shift assay, which is also commonly referred to as the agarose gel retardation assay. Electrostatic interactions between the negatively charged nucleic acids, cationic polymers and functionalized gold nanoparticles respectively induced formation of CP/pDNA and FAuNP/pDNA complexes as investigated by the agarose gel retardation assay. The control lane (lane 1) contained a fixed amount of either 0.25 µg or 0.5 µg uncomplexed pCMV-*luc* DNA. It produced three conformations namely circular, linear and supercoiled. The FAuNP and CP were able to completely retard pDNA mobility as summarized in Table 3.1, at specific nanocomplex ratios. This assay is based on the premise that pDNA which is completely bound to the nanoparticle will not migrate into the agarose gel matrix because the negative charges on the pDNA are completely neutralized by the positive charges on the nanoparticle. On the other hand, pDNA that was not completely complexed by the cationic nanoparticle easily migrated towards the anode. At the ratios stated in Table 3.1, there was complete pDNA compaction making it impossible for further migration to take place at higher ratios. The binding affinities of the polymers to the gold nanoparticle is dependent on the different chemical and surface properties of the different polymers.

The endpoint for each complex is indicated by an arrow. Lane 0 contained naked pDNA and lane 1-7 contained the respective CP/pDNA or FAuNP/pDNA at different weight ratios, as outlined in Table 2.1. At the optimal binding weight ratios as indicated by the arrows, the nanoparticles had completely condensed the pDNA forming an electroneutral complex. The point of electroneutrality or optimum binding weight ratios of the pCMV-*luc* DNA and FAuNPs ($^{w}/_{w}$) were: pDNA/Au-PEI (1:10), pDNA/Au-PLL (1:3.4), pDNA/Au-Cys (1:40) and pDNA/Au-Chit (1:0.08) and for the bare CP it was pDNA/PEI (1:4), pDNA/PLL (1:0.88), pDNA/Cys (1:37) and pDNA/Chit (1:0.05). The pDNA compaction by the FAuNPs had a strong influence on electrophoretic mobility within the gel. Due to the increased positive charges available on the CP, they were able to completely bind pDNA at lower weight ratios. As shown in Figure 3.17 A) PEI/pDNA was completely retarded and showed 100% binding at the lowest weight of 1 µg (lane 1). Hence, at the higher weight ratios there was no more DNA to bind the excess CPs, and hence the complex is retained in the well as evidenced by the fluorescence observed on the gel (Figure 3.17 B, lane 3), showing 100% retardation of Au-PEI at 2.5 µg. However Au-PLL and Au-Cys retarded at their first weight ratio (Figure 3.17 F, H). Further

dilutions were prepared to investigate binding at lower weight ratios, with no success as the complexes did not display any retarding ability. This could also be due to a decrease in the overall available charge of the nanoparticle thus preventing the nanoparticle from binding to the pDNA. Previous studies by McIntosh *et al.*, 2001 demonstrated that quaternary ammonium-functionalized gold colloids can recognize DNA strands. It is also expected that nanoparticles containing primary ammonium groups, pK10, on the surface could bind to DNA (anionic) via ion-pairing at physiological pH of 7.4.

Overall all CPs and FAuNPs showed strong binding at different weight ratios to the plasmid pCMV-*luc* DNA.

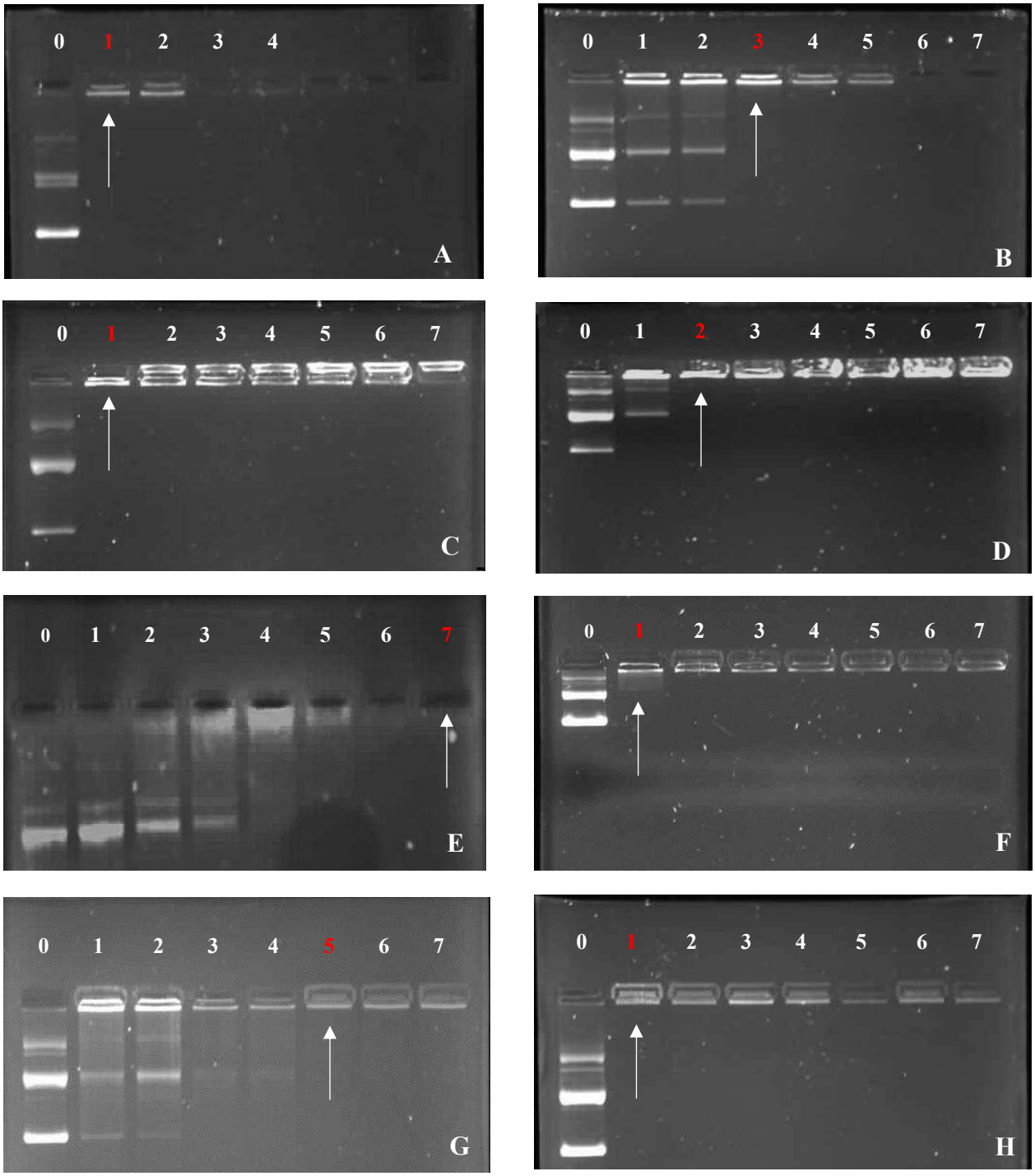

Figure 3.17: Band Shift Assays of nanocomplexes. pCMV-luc DNA was kept constant in lane 0 with A, B, C, D = 0.25µg and E, F, G, H = 0.5µg. Lanes 1-7 contained the respective nanocomplex using the mass (µg) as follows. The endpoint is indicated in red: **A)** PEI: (1, 1.5, 2, 2.5) **B)** Au-PEI: (1.5, 2, 2.5, 3, 3.5, 4, 4.5) **C)** Chitosan (0.01, 0.02, 0.04, 0.05, 0.06, 0.07, 0.09) **D)** Au-Chit (0.01, 0.02, 0.04, 0.05, 0.06, 0.07, 0.09) **E)** PLL (0.06, 0.12, 0.19, 0.25, 0.31, 0.37, 0.44) **F)** Au-PLL (1.60, 1.68, 1.76, 1.84, 1.92, 2, 2.08) **G)** Cysteine (16.5, 17, 17.5, 18, 18.5, 19, 19.5) **H)** Au-Cysteine (20, 20.5, 21, 21.5, 22, 22.5, 23).

3.3.4 Nuclease protection assay

The ultimate goal of gene therapy will be its clinical application. However, when the nanocomplexes are administered *in vivo*, the serum components in the biological fluid can influence the constitution of the complex, often leading to their degradation. Hence, it is compulsory that all investigations are carried out in the presence of serum to attain conclusive correlations between *in vitro* and *in vivo* efficiencies. A good nanovector should bind and protect its DNA cargo from degradation by serum nucleases. Previous research based on liposomal transfection efficiency (Simberg *et al*., 2003), state that serum proteins have a rich protein layer called a protein corona which associates with the surface of lipoplexes when they come into contact with serum. This could also apply to the interaction of our cationic polymers studied, and it is highly possible that the same behaviour is being mimicked. The polymers namely PEI, PLL, cysteine and chitosan generally resemble components that the serum proteins would recognize and attack. This can destabilize the nanocomplex structure thus exposing the pDNA to degradation as seen in Figure 3.18.

We evaluated the stability of the FAuNPs and CP/DNA complexes in the presence of serum using the nuclease protection assay. This assay showed the ability of the respective CPs and FAuNPs to protect their DNA cargo from digestion by the serum nucleases which would be encountered in an *in vivo* system. Often nanoparticles aggregate in saline and serum free medium because of the salt content in these solutions. The addition of serum can to some extent improve stability of these nanoparticles in the biological fluid by forming a protein halo or corona. Serum protein binding, however may alter the biological activity of some nanoparticles in more ways than just aggregation. Lacerda and colleagues showed that the binding kinetics between AuNPs and serum proteins is strictly size dependent. The bigger the particles, the higher the tendency to bind proteins (Lacerda *et al*., 2010). In this respect, it was our goal to develop an efficient non-toxic, non-viral vector that is safe and has favourable characteristics for gene delivery. Gold nanocomplexes were prepared with varying amounts of cysteine, poly-L-lyine, polyethylenemine and chitosan respectively and complexed with 0.25 µg of pCMV-*luc*. DNA is negatively charged and therefore requires specific masses of the nanoparticle to bring the entire nanocomplex to achieve electroneutrality. This was achieved by the gold nanoparticles serving as a scaffold for the DNA constructs.

The two controls utilised in this assay were control 1 (C1) that contained untreated naked pCMV-*luc* DNA and control 2 (C2) that contained naked pCMV-*luc* DNA treated with 10% foetal bovine serum (FBS). The aim of these controls was to monitor the extent of serum nuclease degradation in comparison to our nanocomplexes. Sodium dodecyl sulphate (SDS) was added to release the pDNA

from the nanocomplex after the incubation with serum. The DNA exposed to serum (C2) was fully digested as seen in lane 2 of all gels (Figure 3.18). Degradation of DNA to different extents can be seen in all the gels. The CP on their own were unable to fully sustain the protection of the bound pDNA, as no distinct DNA bands were visible on the gels. The FAuNP/pDNA gel patterns also show degradation and limited protection of the DNA. Au-PEI offered the highest degree of protection (Figure 3.18 B) as seen by the distinct intense fluorescent bands. Based on earlier results (Figure 3.13 A), it was expected that bands of the circular and linear forms will be detected in the gel due to the interaction of FAuNP with the different isoforms showing that gold had the potential to electroneutralize the nanocomplex making it suitable for gene delivery.

However, from the digestion assay, the Au-PEI was unable to fully protect the circular form here as it disappeared, and only the bands of the linear and super-coiled forms were predominantly visible. This could be partly due to the nicking of the circular form and possibly the supercoiled forms to that of a linear form by the nuclease enzyme. It is also possible that the proteins in the serum created a shield around the gold nanoparticles that "masked" its protection ability. In spite of the gold based cationic polymer binding strongly to the pDNA, it does not seem to provide the DNA with sufficient protection. In comparison to the plain CP where the DNA from the CP/DNA complexes were completely degraded by the serum nucleases, FAuNPs do provide partial protection to the DNA. Once again, when considering the degradation of the DNA, one has to take into account the DNA bending and strand separation possibility which exposed the pDNA. However, if successful transfection was eventually attained (section 3.4.3), then it is possible that the pDNA could not have been totally degraded and was able to enter the cell and the nucleus to effect transcription. This could also be due to a phenomenon of the gold's biophysical properties in the presence of serum that makes it difficult to view under the UV-light. Gold has been known to quench fluorophores and the serum proteins may have possibly clouded the light scattering ability of the gold. Furthermore, the AuNPs do not aggregate even under extreme pH in different ionic conditions or in the presence of proteins (Kanaras *et al.*, 2002).

Basically it can be assumed that the functionalized gold based nanoparticles were able to afford some protection to the pDNA compared to the cationic polymers on their own. The extent of the compaction of the pDNA by the nanoparticles which was investigated by the ethidium bromide intercalation assay (section 3.3.5) provides further evidence as to why some or most of the pDNA was degraded. From the results of these studies, it is clear that further studies and optimization of the FAuNPs are needed to ensure complete serum stability. One such optimization could be the addition of the polymer PEG (polyethylene glycol), which is known to increase stability of complexes in

serum and ensures their increased circulation times with view to *in vivo* gene delivery. PEG is often used as a ligand because of its colloidal stability which is assumed to be provided by a PEG brush like conformation on the surface of the nanoparticles preventing steric hindrance and opsonization by serum proteins.

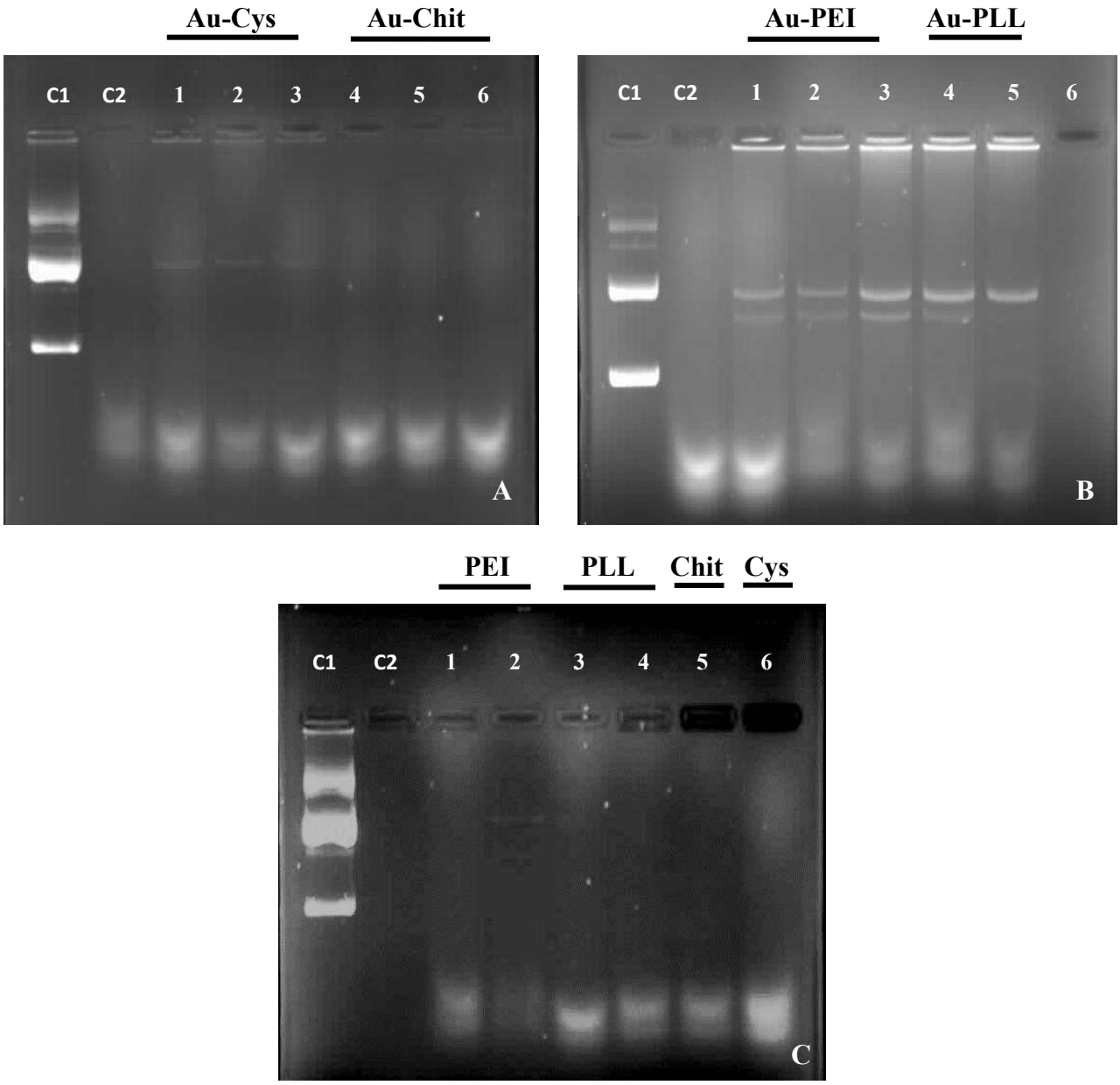

Figure 3.18: FCS-mediated digestion of FAuNPs. pDNA was kept constant in lane C1-C2 at 0.5 µg. Control 1 (C1) contained naked pCMV-*luc* and Control (C2) contained FCS-treated naked pCMV-*luc*. The respective nanocomplex using the mass (µg) is as follows: **A)** Au-Cys (20, 20.5, 21) and Au-Chit (0.01, 0.02, 0.04), B**)** Au-PEI (2, 2.5,) and Au-PLL (1.6, 1.68, 1.76) and the CP **C)** PEI (1, 1.5), PLL (0.37, 0.44), Chit (0.02) and Cys (18.5). (See weight ratios as outlined in Table 2.3 and 2.4).

3.3.5 Ethidium bromide intercalation assay

The EtBr intercalation assay investigated the binding efficiency of the CP and FAuNPs to pDNA. EtBr is an aromatic fluorophore whose emission intensity is approximately 10 fold higher when intercalated between base pairs compared to its fluorescence in water or buffer (Lakowicz, 1999). EtBr binds between the adjacent base pairs of dsDNA by a process termed intercalation. The pDNA then dynamically opens a space between its base pairs by unwinding its helix. This unwinding causes changes to the pDNA such as lengthening, twisting and elongating of the base pairs. EtBr dispels any water molecules as water is a highly effective quencher. This causes EtBr to fluoresce. A decrease in fluorescence indicates displacement of the EtBr and binding of the pDNA by the CP or FAuNP respectively, which would prohibit EtBr intercalation. As the amount of CP and FAuNP increases, greater amounts of EtBr are displaced from the DNA causing a gradual or in some cases a rapid decrease in fluorescence emission. Ratios in Table 3.1 reflect the points of inflection at which FAuNP and its corresponding CP maximally displayed the EtBr.

Results revealed that all the samples have compaction abilities because they successfully displaced EtBr and bound to pDNA at varying degrees. Samples were added in increments of 1 μg to the EtBr/pDNA until fluorescence readings reached a plateau. At this point maximum pDNA condensation had been reached. A trend was observed where the gold functionalized particles produced greater levels of fluorescence decay compared to its cationic polymer counterparts. In the case of the PEI, chitosan and the cysteine graph (Figure 3.19 A, B, D) a possible observation is that the cationic nature of the polymers saturated the pDNA thus inhibiting any further action by the cationic EtBr. On the other hand, with regards to the compacting nature of the pDNA by the FAuNPS, an interesting phenomenon that may have taken place is DNA strand bending. Railsback *et al*., 2012 investigated DNA interactions with functionalized AuNP and showed how binding events with these particles affect the structure of dsDNA. Nanoparticle binding can facilitate DNA compaction in addition to partial strand separation. It is of paramount importance to consider parts of strand unzipping due to strong interactions with the cationic ligands on the FAuNPs. The charge of a nanoparticle plays a crucial role in its ability to induce structural DNA changes. If a nanoparticle has a highly positive surface charge density the DNA is likely to wrap and bend upon binding to the nanoparticle as in the case of chromatin. Contrary to this finding if a nanoparticle is weakly charged it will not induce dsDNA compaction (Ke *et al*., 2007 and Torres and Baigl, 2011). This observation of compaction was confirmed in our band shift assay. Maximum percentage fluorescence decay for each FAuNP was: Au-PEI (79.3%), Au-PLL (51.6%), Au-Chit (46.4%) and Au-Cys (98.3%) and for the CPs: PEI (61.9%), PLL (50.4%), Chit (32.3%) and Cys (78.9%). The negative impact of high

degrees of DNA compaction could be unfavourable for transfection. Strongly associated pDNA enables the nanocomplex to safely transport its cargo to the cell but it becomes biochemically difficult when vector unpackaging is essential. On the other hand weak FAuNP/pDNA binding can trigger early dissociation resulting in degradation of the pDNA payload. Although, compaction and condensation of the DNA by all the nanoparticles was evident, from the results of the nuclease digestion studies where much of the DNA was degraded, suggests that the DNA may not have been very tightly complexed within the nanocomplex allowing access to the nucleases for some degradation to take place. Furthemore the sharp decline in fluorescence (Figure 3.19) for almost all the nanocomplexes but more for the FAuNPs also suggests that the complexes may not be very stable. Although DNA compaction is not as tight as expected from the band shift assays, it is possible that when it comes to transfection the proton-buffering capacity of the polymers such as PEI will be stimulated thereby promoting gene expression and enhancing transfection. There was no direct correlation between the EtBr and retardation assays with regard to the end point. End point ratios determined in gel retardation assays indicated a minimum amount of FAuNP and CP that was required to entirely bind a determined amount of pDNA.

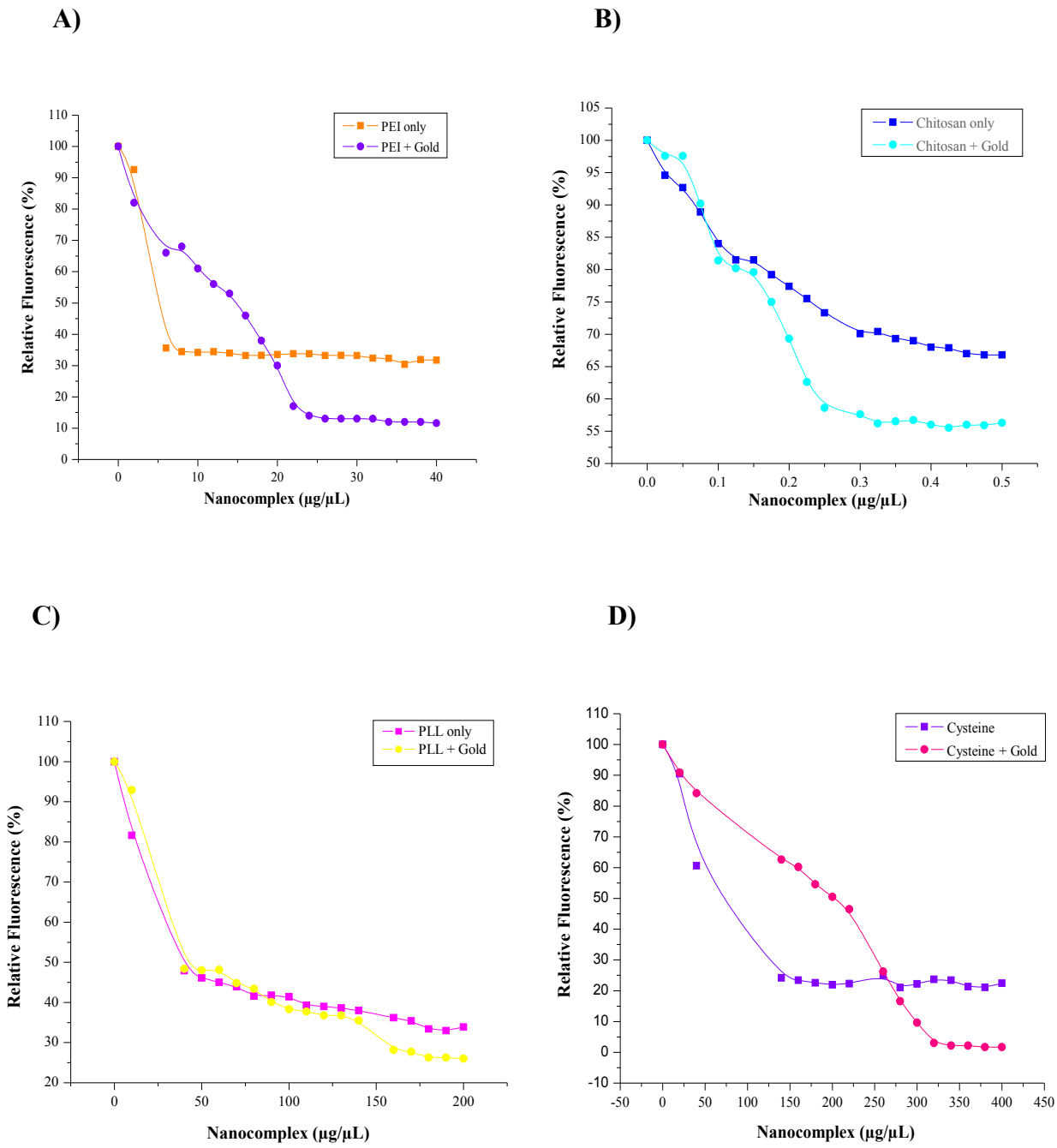

Figure 3.19: Ethidium Bromide intercalation assays of: **A)** Au-PEI and PEI **B)** Au-Chitosan and Chitosan **C)** Au-PLL and PLL **D)** Au-Cysteine and Cysteine.

3.4 *In vitro* cell culture assays

3.4.1 Cell lines

A four cell lines were successfully propagated in EMEM (with 10% FBS and antibiotics). Cells were monitored regularly with the required medium changes. Cells were trypsinized and plated for the various cell culture assays upon confluency. Of all the cell lines, the Caco2 cell line reached confluency much quicker and because the cells were in their mitotic phase they took up nutrients in the culture media very rapidly, requiring frequent replenishment of medium.

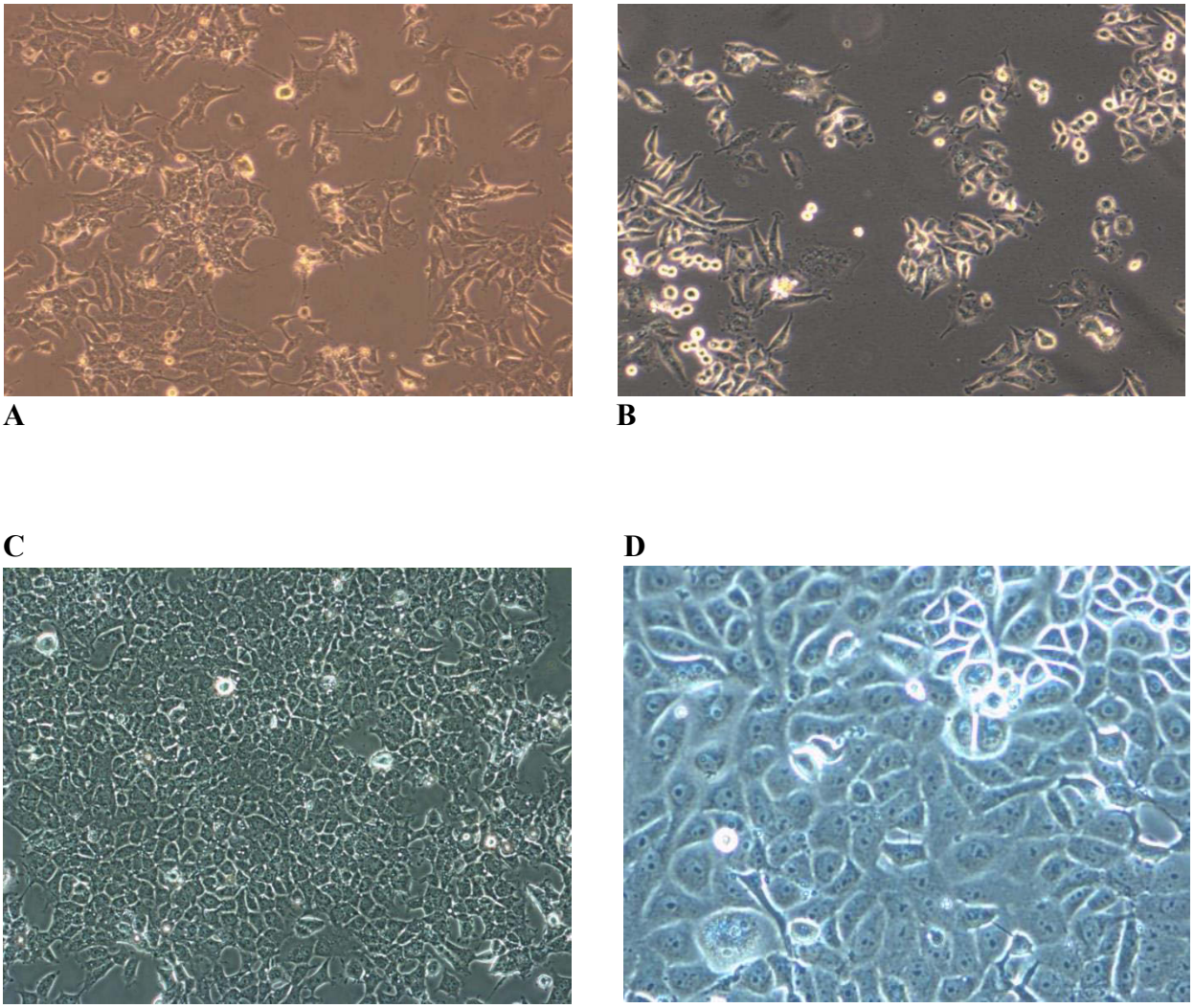

Figure 3.20: The cell lines used for *in vitro* studies were **A)** HEK293 **B)** HeLa **C)** HepG2 **D)** Caco2. Images cells were viewed as a monolayer at semi-confluency under a 10x magnification using a Nikon inverted phase contrast microscope.

3.4.2 *In vitro* MTT reduction assay

Cytotoxicity is an important obstacle in the application of non-viral vectors for clinical gene therapy. In many cases a suitable surface modification may render toxic nanoparticles less harmless to allow application in medical therapy. The principle of the MTT assay lies in the formation of formazan by mitochondrial succinate-reductases in metabolically active cells, which determines mitochondrial activity (Figure 3.21). The cytotoxicty of the FAuNPs and CPs were investigated in the human cell lines HEK 293, HeLa, HepG2 and Caco2.

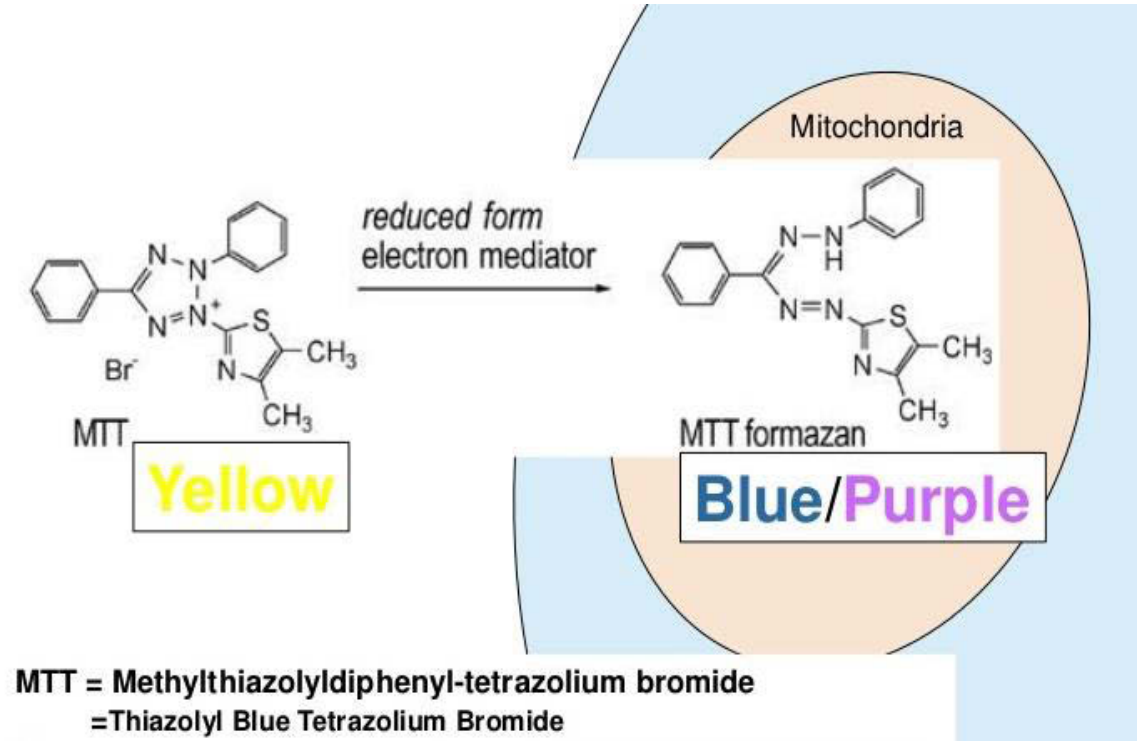

Figure 3.21: Metabolism of MTT-dye (yellow) to MTT-formazan crystals (blue) by mitochondrial dehydrogenases in living cells: (http://www.slideshare.net/AnVanRompay/overview-of-3dhuman-skin-reconstructed-models-for-irritation-and-corrosion-testing-by-an-van-rom) Accessed 18 Nov 2014.

Since for most cell populations the total mitochondrial activity is related to the number of viable cells, this assay can be broadly used to measure the *in vitro* cytotoxic effects of nanoparticles in cell lines (Van Meerloo *et al*., 2011). Cytotoxicity was evaluated at weight ratios that include their sub, optimal and supra-optimal ratios as obtained in the gel retardation studies. The overall goal of this study was to evaluate the underlying cytotoxic effects of FAuNPs and the CPs. Results were expressed as the percentage of cell viability with respect to a control (100%) corresponding to untreated cells. Changes in cell viability were detected by measuring the amount of formazan

(blue/purple) produced after the reduction of the MTT (yellow) (Figure 3.21). This was determined by obtaining the absorbance measurements of the DMSO solubilized formazan.

The control contained cells that were not treated with the nanocomplexes and is assumed to represent 100% cell viability. The maximum cell viability of functionalized nanocomplexes in HEK293 cells were, Au-PEI (95.4%); Au-Cys (84.8%); Au-PLL (74.9%) and Au-Chit (42.3%). In HeLa cells it ranged from, Au-PLL (104%); Au-Cys (98.1%); Au-PEI (94.9%) and Au-Chit (65.8%). In HepG2 cells the percentage cell survival was as follows: Au-Chit (126%); Au-PEI (98.2%); Au-Cyst (92.5%) and Au-PLL (85.5%). The Caco2 cell line cell viability was, Au-Cys (91.8%); Au-PEI (76.7%); Au-PLL (73.5%) and Au-Chit (48.2%). Au-PEI coated nanocomplexes in HEK293, HeLa and HepG2 cells showed a high percentage of cell viability with more than 90% cell survival (Figures 3.22 and 3.23), while cell viability in the Caco2 cells were just above 70%. The Dunnett comparison test revealed no statistical significance for the PEI functionalized polymers ($p>0.05$). Considering the non-toxic properties of gold nanoparticles and their biocompatibility with polymers (Shukla *et al.*, 2005) the Au-PEI displayed a much lower level of toxicity compared to the PEI polymer on its own. This can suggest that the use of functionalized gold can be a safe and relatively non-toxic vehicle for gene delivery as evidenced from its cell viability results. The PEI based nanocomplex did not produce very high cytotoxicity overall. Literature has noted that PEI on its own can exhibit some cytotoxicity (Kim *et al*., 2013), but upon complexation with gold, its cytotoxicity levels dropped.

The FAuNPs were relatively non-toxic with survival rates above 60% except for the Au-chit where levels in the HEK293, Hela and Caco2 cells at certain ratios were below 60%. However, Au-chit significantly promoted cell growth up to 126% ($p<0.01$) in HepG2 cells. A possible explanation behind this may be that when the Au-Chit nanocomplexes interacted with the cell membrane it stimulated growth factors. This promotion in cell growth is a sign that the cells were healthy and maintained their morphology and adhesion capacity. Chitosan is also known to have good biodegradability and a high biocompatibility for cells and has been used in the development of controlled drug delivery systems (Rajam *et al*., 2011). It is not totally clear as to why it proved to have the lowest viability in the three cell lines mentioned as opposed to the liver cells. This could be due to the presence of receptors on the HepG2 cell surface that have high affinities for the carbohydrate moieties such as galactose and were stimulated by the chitosan particles. Furthermore, the very low concentration of chitosan (0.01 μg/μL) used may have rendered it ineffective.

In the HeLa and HepG2 cells the higher the AuCP/DNA ratio the lower the cytotoxicity observed as indicated by the high cell viabilities (Fig 3.22 B and Figure 3.23 A). These results indicated that the nanocomplexes have a dose dependent cytotoxic effect on the cell lines and that cell viability was enhanced with all gold incorporated nanocomplexes.

Cells retained their viability over the 48 hour incubation period, and tolerated the gold nanocomplexes by encouraging cell growth as seen by the Au-PLL nanocomplexes in HeLa cells ($p>0.05$) and Au-Chit in HepG2 cells ($p<0.01$). In addition the cationic polymers on their own displayed a marked reduction in cell survival in some cell lines. This finding provides substantial evidence that across all four cell lines the FAuNps were relatively safe to administer. This is possibly because the polymers presented similar biochemical surface features as cells. The Caco2 cell line demonstrated significant stimulatory activity for all nanocomplexes ($p<0.01$). The importance of testing the safety and efficacy of gene nanovectors for cytotoxicity and biocompatibility is of crucial importance when developing biomaterials for *in vivo* applications. The MTT reduction assay confirmed that the FAuNPs used in this study are relatively safe and have good feasibility for future use *in vivo*.

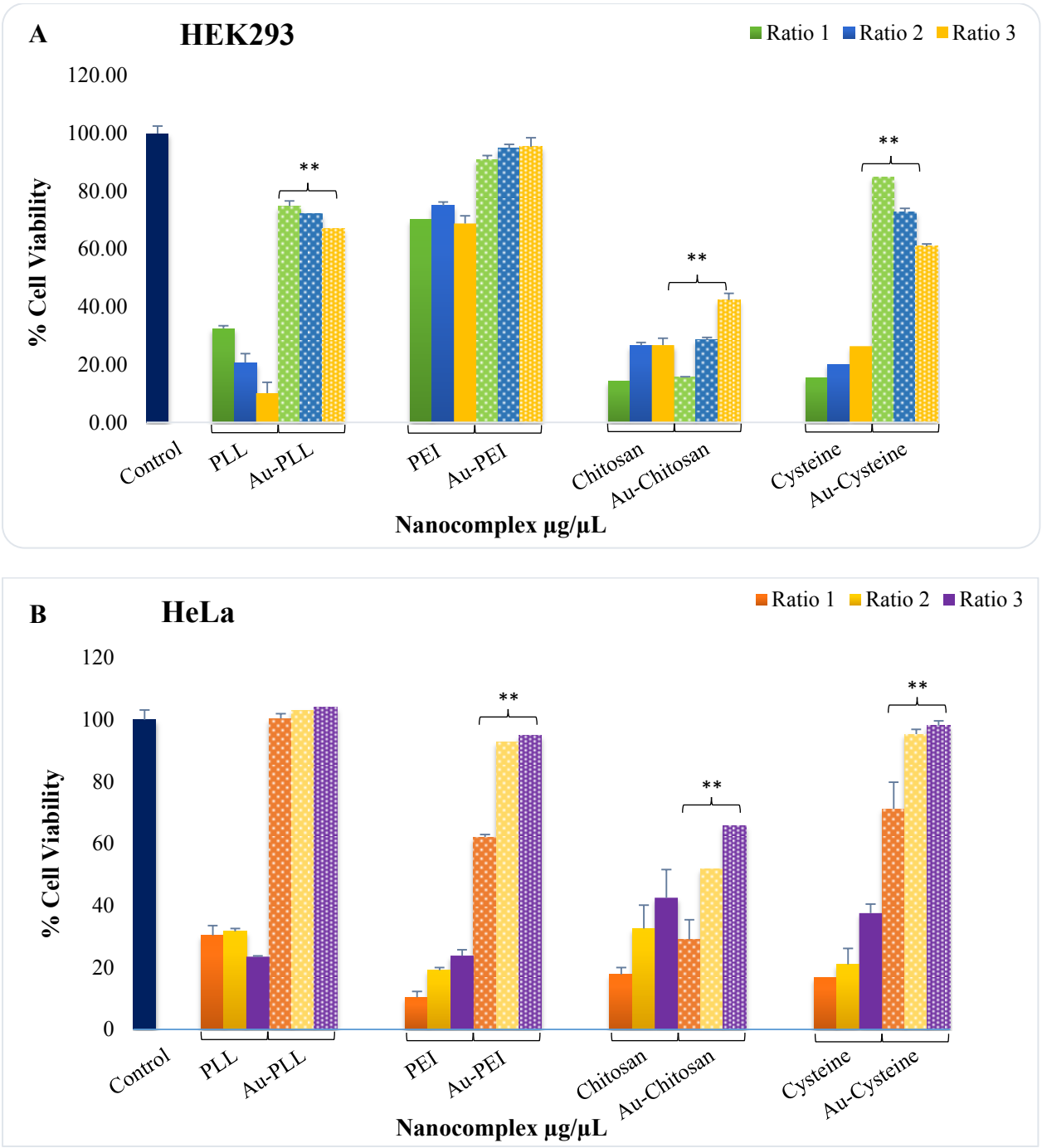

Figure 3.22: MTT cell viability assay in cell lines **A)** HEK293 and **B)** HeLa. Each column represents the mean ± SD (n = 3). *p<0.05 and **p<0.01 was considered statistically significant.

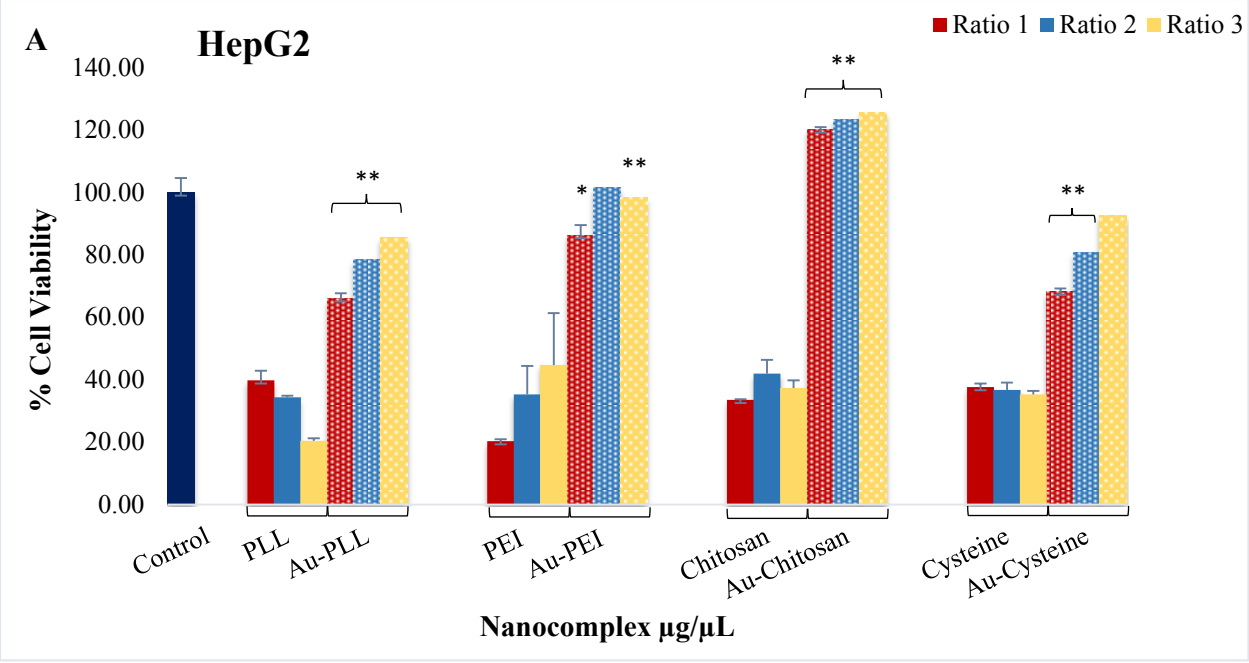

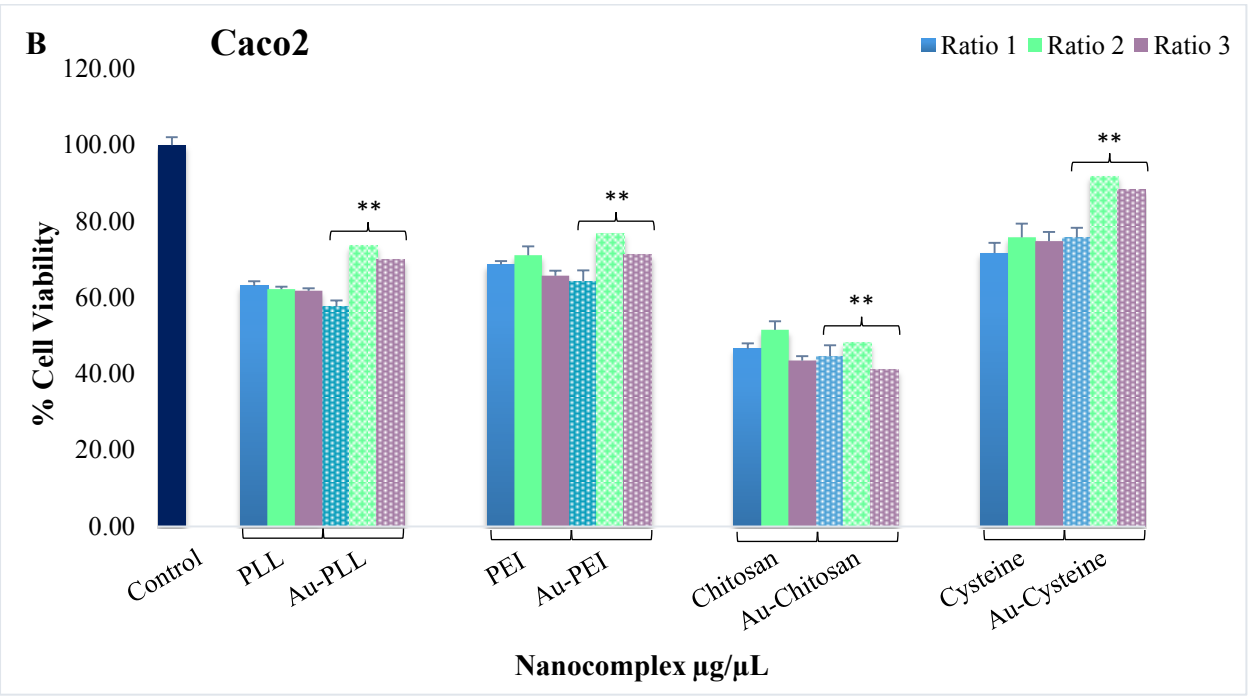

Figure 3.23: MTT cell viability assay in cell lines **A)** HepG2 and **B)** CaCo2. Each column represents the mean ± SD (n = 3). *p<0.05 and **p<0.01 was considered statistically significant. For the Caco2 cell line all the FAuNPS complexes were statistically significant (p<0.01) in relation to its corresponding CP complex.

3.4.3 *In vitro* transfection studies

The transfection of the four human cell lines HEK293, HeLa, HepG2 and Caco2, was assayed using the luciferase reporter gene assay (Promega). All cells displayed different tolerance levels to the nanocomplexes which may influence cellular uptake and hence transgene activity. The FAuNPs complexes exhibited an increased cellular uptake efficiency compared to the plain cationic polymers (Figure 3.24 and 3.25). Most of the nanocomplex assemblies showed variance throughout the cell lines. This was due to the difference in cell membrane properties (Callaghan *et al*., 1992 and Ruponen *et al*., 2004) and varied cell division rates which influenced nanocomplex cell membrane interaction and entry of pDNA into the nucleus (Zuhorn and Hoekstra, 2002). Each cell type also undergoes a different degree of electrostatic interaction with the nanocomplex producing variance in the cellular uptake efficiency of the different samples.

As shown in figures 3.24 and 3.25 all four cell lines displayed an increase in transgene activity as the concentration of FAuNPs increased. They exhibited a relatively rapid uptake of these nanocomplexes. The MTT cytotoxicity results had showed that the maximum reduction in cell viability was observed at the lowest Au:CP ratio for all nanocomplexes irrespective of the cell line. The enhancing effect of gold can be seen by the general trend in gene expression, where an increase in FAuNP concentration was complemented by an increase in luciferase activity. The activity of the nanocomplexes seemed to be cell line specific, and hence consistent with MTT cytotoxicity results, with the FAuNPs exhibiting higher transfection activity compared to the plain CPs. This can also be correlated to the cytotoxicity assay. Another contributing factor to the increase or decrease in transfection activity is to correlate particle size and the positive surface charge of the nanocomplexes with the negative charge of the cell membrane. Surface charge is one of the several factors that influences the cellular uptake mechanisms of phagocytsis and pinocytosis, with the culture medium also being responsible for modifying the surface charge (Mahmoudi *et al*., 2011). Bearing in mind zeta potential is just an estimation of the surface charge and most importantly provides information on the stability of the nanocomplex in solution, the poor transfection efficiency of Au-Cys in HEK293 and Caco2 cells could be due to the agglomerated particles as seen by TEM analysis (Figure 3.16 F). Even though they revealed above 70% cell viability, the TEM images show large particles which may have effected their entry into the cell. Hence, there was low transfection because the particles, if and, when they entered the cells were most likely only localized in the cytoplasm.

HeLa cells (Figure 3.24 B) revealed exceptional transfection activity (p>0.05) of 7.5 x 10^8 RLU/mg protein as demonstrated by the DNA:Au-Cys complex at weight ratio 2 (1:41 $^{w}/_{w}$). The thiol group

in the cysteine molecule stimulated the performance of gold as the delivery vehicle. In contrast using the unmodified cysteine resulted in no significant uptake (p>0.05). Gold incorporated polymers in the HeLa cell line (Figure 3.24 B) clearly enhanced transfection efficiency with regard to pDNA:Au-PLL (1:3.5 $^{w}/_{w}$) and pDNA:Au-Cyst (1:41 $^{w}/_{w}$). There was an immense 5 fold increase in gene expression when the concentration of Au-PLL was increased from 1.68 µg to 1.76 µg. This was due to its favourable size of 130 nm as well as the positive zeta potential of 47.9 mV. HEK293 cells showed strong resistance to transfection by PEI:pDNA nanocomplexes overall. The Au-PEI nanocomplex in HepG2 cells revealed an astounding 12 fold increase (p<0.001) in gene expression at weight ratio 3 (1:12 $^{w}/_{w}$) of 1.6 x 10^7 RLU/mg protein, which was only increased by 0.5 µg from that of weight ratio 2 (1:10 $^{w}/_{w}$) at 1.3 x 10^6 RLU/mg protein. Since cell membranes are negatively charged and the Au-PEI nanocomplex is positive (53.8 mV), the superior enhancing effect of the PEI on gene expression was most likely due to its proton buffering ability. At this specified nanocomplex concentration we may predict that the endosome ruptured due to the osmotic pressure gradient and released the Au-PEI nanocomplex into the cytoplasm (Kim *et al*., 2013). The chemical interaction between PEI and gold may have also contributed to mechanical effectiveness of the nanocomplex as compared to the plain polymer.

A possible reasoning to the low transfection in HepG2 cells could be due to the poor uptake of the nanocomplex and poor release of pDNA by the nanoparticle. Furthermore, there may have been degradation of the DNA by nucleases prior to its entry into the nucleus as was seen by the nuclease protection assay. The cellular dynamics at the time of cell growth may have also contributed to poor conditions for gene expression. HeLa cells (Figure 3.24 B) noticeably offered favourable cellular uptake compared to the HEK293 cells (Figure 3.24 A). Caco2 cells transfected by the Au-Chit nanocomplexes displayed the highest luciferase activity (p>0.05) and showed a 3 fold increase from ratio 1 (1:0.04 $^{w}/_{w}$) at 6.16 x 10^5 RLU/ mg protein to that of ratio 3 (1:0.16 $^{w}/_{w}$) at 1.8 x10^6 RLU /mg protein. The size of the nanocomplex was 186 nm and the zeta potential was 28.4 mV making it suitable for entry via the cell membrane. The second highest transfection efficiency was demonstrated by the Au-PEI nanocomplex with a 3 fold increase from weight ratio 2 (1:10 $^{w}/_{w}$) at 1.5 x 10^6 RLU/mg protein to weight ratio 3 (1:12 $^{w}/_{w}$) at 5.7 x 10^5 RLU/mg protein. The Au-PEI nanocomplex presented a size of 217 nm and a zeta potential of 53.8 mV. This was the highest zeta potential from all the samples and not only provided stability to the nanocomplex *en route* to the nucleus, but due to its positive surface charge gave rise to an electric field that attracted counter ions into the endosome. Consequently it also exhibited high transfection activity across all four cell lines. Chitosan introduces positive charges of amine functionalized groups into an acidic

microenvironment and due to its higher concentration they are easily internalized in cancer cells (Crayton and Tsourkas, 2011). Interestingly it is important to note that a similar trend is noticed throughout the nanocomplex assemblies in the Caco2 cell line where an increase in ratio from 1 to 2 did not produce a difference, but when the ratio increased from 2 to 3 so did the level of transfection change quite distinctively.

Perhaps it is safe to speculate from previous research (Balbino *et al*., 2012) that the dose dependent concentration of the nanocomplexes here induced saturation of the vesicles retaining pDNA and could have led to generation of new nanocomplex structures of the gold functionalized particles that elevated larger particles for gene expression. It is important to note that the Caco2 cells were actively dividing and this phase of cell division could have led to the impressive and consistent cellular uptake and expression. Caco2 cells also did not seem to tolerate nanocomplexes as well as the other 3 cell lines studied (Fig 3.23 B). Though positive complexes are found to be necessary for absorption onto the negatively charged phospholipid cellular membrane and optimum transfection, their positive potentials do not always guarantee high transfection levels.

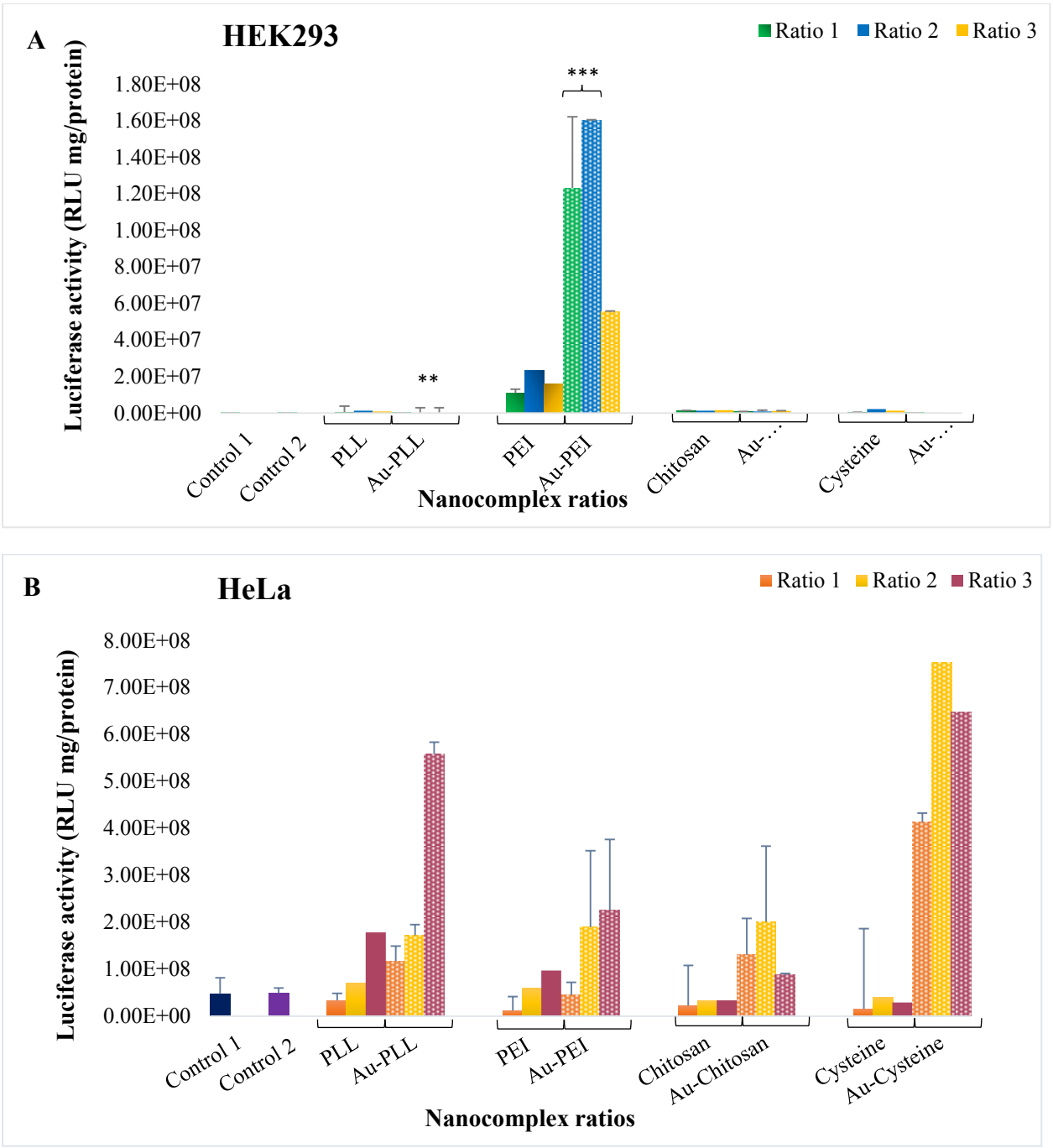

Figure 3.24: In vitro transfection activity in **a)** HEK293 and **b)** HeLa. Each column represents the mean ± SD (n = 3). Gene expression activity was measured in RLU/mg protein. ***p<0.001, **p<0.01 and *p<0.05 were considered statistically significant.

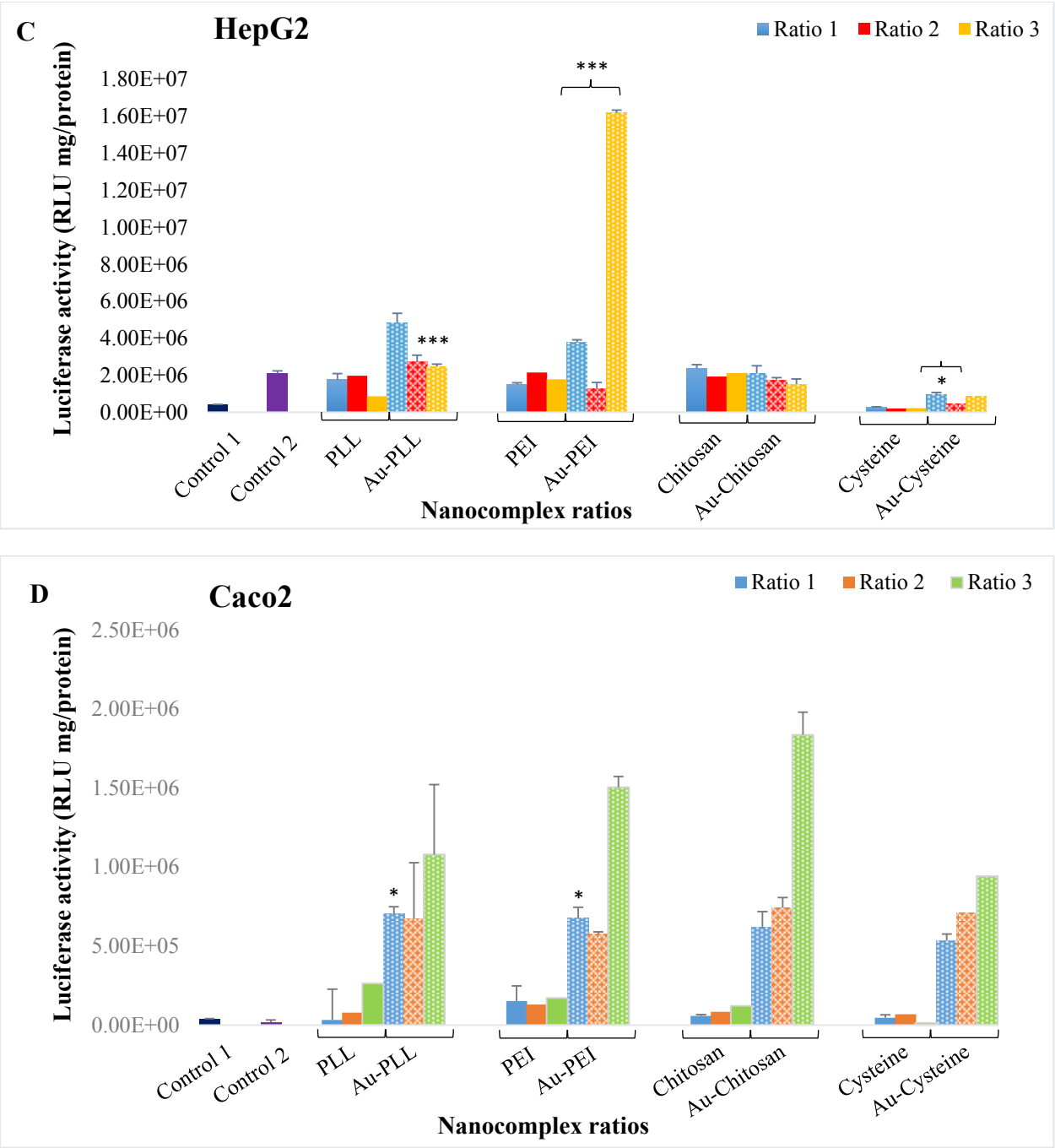

Figure 3.25: In vitro transfection activity in **c)** HepG2 and **d)** Caco2. Each column represents the mean ± SD (n = 3). Gene expression activity was measured in RLU/mg protein. ***p<0.001, **p<0.01 and *p<0.05 were considered statistically significant.

Chapter Four

Conclusion

Chapter Four

Conclusion and future work

Numerous non-viral gene delivery systems have been developed over the last two decades, however, therapeutic applications of these systems are rather limited despite their progress in vector design. To improve currently available systems and to develop new methods of gene delivery, continuous effort is needed that could lead to safer and more efficient non-viral gene-delivery. AuNPs present versatile synthetic scaffolds for efficient delivery of drugs and biomolecules. Cationic lipids and other naturally occurring compounds have proven to be effective for *in vitro* gene delivery, yet all of these cationic molecular based systems have shown to be unimpressive or have not to date been successful in clinical trials. The proposed way forward was the use of FAuNPs, because the combination of their low inherent cytotoxicity, photoluminescence properties, high surface area and tunable surface chemistry could prove favourable in gene delivery. This has contributed to their growing application in clinical practice. The outcomes herewith mentioned, hint at the potential of FAuNPs in both *in vitro* and future *in vivo* applications.

This thesis covered preliminary studies on the synthesis and electrokinetics of gold nanoparticles functionalized with the amino acid lysine and cationic polyelectrolytes, PEI and PLL, prior to looking at their biological activities *in vitro*. The use of L-lysine functionalized gold nanoparticles was discontinued since L-lysine exhibited positive electrophoretic mobility predominantly at pH 3, with binding at pH 7.4 and at neutral pH showing fairly weak complexation of L-lysine to gold and to plasmid DNA. Studies were further conducted with polymers, PLL, PEI, cysteine and chitosan.

One of the disadvantages of gene delivery applications is the size of the nanocomplex. In general poor sizes and binding affinities of negatively charged nanocomplexes promote the formation of large aggregates that hinder entry via the cell membrane and can accumulate leading to cytotoxicity. We have successfully demonstrated the functionalization of gold nanoparticles using polymers (PLL, PEI, cysteine and chitosan) which degrade through different mechanisms. Some of the advantages of these FAuNP complexes, include their relatively stable and small sizes as seen in TEM images and zeta sizing, their successful pDNA binding ability as evidenced by the band shift assay, their pDNA condensation properties (EtBr dye displacement assay) and their partial protection of pDNA cargo in the nuclease digestion assay. Furthermore, we have shown that these nanocomplexes were well tolerated by all the human cell lines studied. This has added to the overall understanding of the specificity of the cytotoxic responses and any potential detrimental outcomes from human exposure

to FAuNPs which was shown to be limited if any in *vitro*. Furthermore, the FAuNP complexes exhibited higher cell viability in a dose dependent fashion compared to the corresponding CP complexes. Au-PEI, Au-PLL, Au-Cys and Au-Chit complexes all promoted cell growth while Au-Chit showed the highest viability of 126% ($p<0.01$) and hence food growth promoting properties. The best performing nanocomplex was Au-PEI/pDNA that displayed consistently high cell viability (80%) across all four cells lines. Au-cys on the other hand exhibited significantly high cell viability of 91.8% in the colorectal cancer (Caco2) cells ($p<0.01$). Cytotoxicity also seemed to be cell specific with some cells showing greater tolerance to specific nanocomplexes. This cytotoxic study has yielded significant data which could be used in future research. However, not all FAuNP complexes that yielded high cell viability produced the corresponding high transfection results. The determination of transfection using the luciferase reporter gene assay showed good transgene activity in the human cell lines investigated. Transgene activity for the Au-PEI/pDNA complexes showed a 12 fold and a 9 fold increase ($p<0.001$) over that obtained with its corresponding CP ($p<0.001$) in the HEK293 cells and HepG2 cells respectively. This high transfection activity of Au-PEI complexes correlated to its cell viability where it achieved over 95% cell viability in both cell lines. The noticeably high gene expression of Au-PEI/pDNA in HEK293 and HepG2 indicated that these cell lines were able to take up the Au-PEI/pDNA nanocomplexes readily, and further allow for safe and efficient intracellular trafficking. PEI on its own is generally regarded as being toxic to cells, however, as seen from our studies its combination with Au nanoparticles has led to improved cytotoxicity and gene expression.

The results strongly suggest that these nanocomplexes demonstrate the potential for being efficient gene delivery vectors *in vitro* compared to their CP counterparts, possibly due to the electrokinetic stability of the gold core. The FAuNPs were however varied in their efficiency with Au-PEI>Au-PLL>Au-Cys ≥Au-Chit. Based on the results obtained it can be proposed that the mechanism of cellular uptake of the FAuNPs is different for the different classes of FAuNPs across the four cell lines, which may involve the activation of different sets of proteins and or cell surface receptors. This could follow from the diverse modifications of the AuNPs using the different CPs that allowed for the modulation of various physiochemical properties.

Future work could include the investigation of other combinations of CPs with the AuNPs and other possible transfection methods such as sonoporation and laser irradiation to control the release of genes before *in vivo* trials are strictly explored. Furthermore, the attachment of targeting ligands for cell specific targeting, and PEG for nanoparticle shielding in circulation are options for further optimization of these nanoparticles. One of the further advantages of using gold as the core of the

nanoparticles is that it can be tracked by imaging which is becoming a very important diagnostic tool in medicine. The accurate mechanisms of cellular uptake of FAuNPs should however be identified to facilitate optimization of them as platforms for efficient internalization. Considering the immense interest today in gold nanoparticles, this process may soon be elucidated.

In summary these functionalized gold nanoparticles were able to efficiently bind and deliver pDNA to three cancer (HepG2, HeLa and Caco2) and one normal cell line (HEK293) *in vitro*. Preliminary results do suggest the need for these complexes to be tested further in a range of mammalian cells to confirm and establish further their cytotoxicity, cell specificity and stability in order to eventually examine their efficacy in gene delivery *in vivo*.

Chapter Five

References

Reference Citations

- A. Jada, and M. Salou. 2002. Effects of the asphaltene and resin contents of the bitumens. *Journal of Petroleum Science and Engineering*. **33**: 185-193.
- Abdallah, B., Sachs, L., Demeneix. BA. 1995. Non-viral gene transfer applications in developmental biology and gene therapy. *Biology of the Cell.* **85**: 1–7.
- Ahmed, A., Deng, Z., Liu, S., Lafrenie, R., Kumar, A., Narain R. 2009. Cationic glyconanoparticles: their complexation with DNA, cellular uptake and transfection efficiencies. *Bioconjugate Chemistry.* **20**: 2169–2176.
- Aiken, III JD., Finke, RG. Applications in Catalysis. 1999. *Journal of Molecular Catalysis A: Chemical.* **145**: 1-44.
- Alhara, H., Miyazaka, J. 1998. Gene transfer into muscle by electroporation *in vivo*. *Natural Biotechnology.* **16**: 867–870.
- Ali, MR., Panikkanvalappil, SR., El-Sayed, MA. 2014. Enhancing the efficiency of gold nanoparticles treatment of cancer by increasing their rate of endocytosis and cell accumulation using rifampicin. *Journal of American Chemistry Society.* **136** (12):4464-4467.
- Alivisatos, AP., Johnsson, KP., Peng, XG., Wilson, TE., Loweth, CJ., Bruchez, MP Jr., Schultz., PG. 1996. Organization of 'nanocrystal molecules' using DNA. *Nature*. **382**: 609-611.
- Alkilany, AM., Murphy, CJ. 2010. Toxicity and cellular uptake of gold nanoparticles: what we have learned so far? *Journal of Nanoparticle Research*. **12**:2313–2333.
- Andree, C., Swain, WF., Page, CP., Macklin, MD., Slama, J., Hatzis, D., Eriksson, E. 1994. *In vivo* transfer and expression of a human epidermal growth factor gene accelerates wound repair. *Proceedings of the National Academy of Sciences USA.* **91**:12188–12192.
- Anson, DS., Smith, GJ., Parsons, DW. 2006. Gene therapy for cystic fibrosis airway disease – is clinical success imminent? *Current Gene Therapy.* **6** (2):161–179.
- Aryal, S., Remant, BKC., Dharmaraj, N., Bhattarai, N., Kim, CH., Kim, YK. 2006. Spectroscopic identification of S–Au interaction in cysteine capped gold nanoparticles. *Spectrochimica Acta Part A.* **63**:160–163.
- Balbino, TA., Gasperani, AAM., Oliveria, CLP., Azzoni, AR., Cavalcanti, LP., de La Torre, LG. 2012. Correlation of the physiochemical and structural properties of pDNA/ cationic liposome complexes with their in vitro transfection. *Langmuir*. **28**: 11535-11545.

- Banga, AK., Prausnitz, MR. 1998. Assessing the potential of skin electroporation for the delivery of protein and gene based drug. *Trends in Biotechnology.* **16**:408–412.
- Bartz, M., Kuther, J., Nelles, G., Weber, N., Seshadri, R., Tremel, W. 1999. Monothiols derived from glycols as agents for stabilizing gold colloids in water: preparation, self-assembly and use as crystallization templates. *Journal of Materials Chemistry.* **9**:1121–1125.
- Behr, JP. 1997. The proton sponge: a trick to enter cells the viruses did not exploit, *Chimia*, **51**: 34-36.
- Bianco A, Kostarelos K, Partidos CD, Prato M. 2005. Biomedical applications of functionalised carbon nanotubes. *Chemistry Communication.* **7**: 571–577.
- Bikerman, J. J. 1940. Chemistry and Physics of Interfaces. *Trans. Farad. Soc.* **36**, 154–159.
- Bonoiu, AC., Mahajan, SD., Ding, H., Roy, I., Yong, KT., Kumar, R., Hu, R., Bergey, EJ., Schwartz, SA., Prasad. PN. 2009. Nanotechnology approach for drug addiction therapy: gene silencing using delivery of gold nanorod–siRNA nanoplex in dopaminergic neurons. *Proceedings of the National Academy of Sciences USA.* **106** (14):1655–1656.
- Boyer, C., Priyanto, P., Davis, TP., Pissuwan, D., Bulmus, V., Kavallaris, M., Teoh, WY., Amal, R., Carroll, M., Woodward, R., Pierree. TS. 2010. Anti-fouling magnetic nanoparticles for siRNA delivery. *Journal of Material Chemistry.* **20**: 255-265.
- Brigger, I., Morizet, J., Aubert, G., Chacun, H., Terrier-Lacombe, MJ., Couvreur, P., Vassal, G. 2002. Poly (ethylene glycol)-coated hexadecylcyanoacrylate nanospheres display a combined effect for brain tumor targeting. *Journal of Pharmacology Experimental Therapeutics.* **303** (3):928–936.
- Brus, LE. 1984. Crystallites: The Size Dependence of the Lowest Excited Electronic State. *Journal of Chemical. Physics.* **80**: 4403-4409.
- Brust, M., Fink, J., Bethell, D., Schiffrin, DJ., Kiely, C. 1995. Synthesis and reactions of functionalized gold nanoparticles. *Journal of the Chemical Society, Chemical Communications.* **16**:1655–1656.
- Brust, M., Walker, M., Bethell, D., Schiffrin, DJ., Whyman, R. 1994. Synthesis of thiol-derivatised gold nanoparticles in a two-phase Liquid–Liquid system. *Journal of the Chemical Society, Chemical Communications.* **7**:801–802.
- Callaghan, R., LC van Gorkom., RM, Epand. 1992. A comparison of membrane properties and composition between cell lines selected and transfected for multi-drug resistance. *British journal of cancer* **66**: 781-786.

- Caruso, F. 2004. *Colloids and colloid assemblies*: *Synthesis, modification, organization and utilization of colloid particles*; Eds.; wiley-VCH: Weinheim.
- Cebrian, V., Martin-Saavedra, F., Yague, C., Arruebo, M., Santamaria, J., Vilaboa, N. 2011. Size-dependent transfection efficiency of PEI-coated gold nanoparticles. *Acta Biomaterialia.* **7:** 3645–3655.
- Check, E. 2002. Gene therapy: a tragic setback. *Nature.* **420**:116–118.
- Chithrani BD, Ghazani AA, Chan WC. 2006. Determining the size and shape dependence of gold nanoparticle uptake into mammalian cells. *Nano Letters.* **6**:662-668.
- Choi, WI., Kim, JY., Kang, C., Byeon, CC., Kim, YH., Tae, G. 2011. Tumor regression in vivo by photothermal therapy based on gold-nanorod-loaded, functional nanocarriers. *ACS Nano*. **5**:1995-2003.
- Conner, SD., Schmid, SL. 2003. Regulated portals of entry into the cell. *Nature*. **422**:37–44.
- Crayton, SH., Tsourkas, A., pH-titratable superparamagnetic iron oxide for improved nanoparticle accumulation in acidic tumor microenvironments. 2011. *Acs Nano.* **5** (12):9592–601.
- Crew, E., Rahman, S., Razzak-Jaffar, A., Mott, D., Kamundi, M., Yu, G., Tchah, N., Lee, J., Bellavia, M., Zhon C. 2012. MicroRNA conjugated gold nanoparticles and cell transfection, *Analytical Chemistry.* **84**: 26–29.
- Cushing, BL., Kolesnichenko, VL., O' Connor CJ. Recent advances in the liquid-phase syntheses of inorganic nanoparticles. *Chem. Rev*., 2004. **104**: 3893- 3946.
- Daniel, MC., Astruc, D. 2004. Gold nanoparticles: assembly, supramolecular chemistry, quantum-sized related properties and applications towards biology, catalysts and nanotechnology. *Chemistry Revised*. **104**:293–346.
- Dickerson EB, Dreaden EC, Huang X, El-Sayed IH, Chu H, Pushpanketh S. 2008. Gold nanorod assisted near-infrared plasmonic photothermal therapy (PPTT) of squamous cell carcinoma in mice. *Cancer Letters.* **269**: 57-66.
- Dobrovolskaia, MA., McNeil, SE. 2007. Immunological properties of engineered nanomaterials. *Natural Nanotechnology.* **2**:469–478.
- Drummond D.C., Meyer O., Hong K., Kirpotin D.B. and Papahadjopoulos D. 1991. Optimizing liposomes for delivery of chemotherapeutic agents to solid tumors. *Pharmacology Reviews.* **51** (4):691-743.
- Durcan, N., Murphy, C., Cryan, SA. 2008. Inhalable siRNA: potential as a therapeutic agent in the lungs. *Molecular Pharmaceutics.* **5**: 559-566.

- Durr, NJ., Larson, T., Smith, DK., Korgel, BA., Sokolov, K. 2007**.** Two-photon luminescence imaging of cancer cells using molecularly targeted gold nanorods. Nano Letters. **7** (4):941-945.
- Dutta., PK, Dutta., J, Tripathi., VS. 2004. Chitin and chitosan: chemistry, properties and applications. *Journal of Scientific and Industrial Research*. **63**: 20-31.
- Eghtedari, M., Oraevsky, A., Copland, J. A., Kotov, N. A., Conjusteau, A., Motamedi, M. 2007. *Nano Letters.***7**: 1914-1918.
- Elbakry, A., Zaky, A., Liebl, R., Rachel, R., Goepferich, A., Breunig, M. 2009. Layer by layer assembled gold nanoparticles for siRNA delivery. *Nano Letters.* **9**: 2059-2064.
- El-Sayed, IH., Huang, X., El-Sayed, MA. 2005. Surface plasmon resonance scattering and absorption of anti-EGFR antibody conjugated gold nanoparticles in cancer diagnostics: applications in oral cancer. *Nano Letters*. **5** (5):829–834.
- Erbacher P, Zou S, Bettinger T, Steffan AM, Remy JS. 1998. Chitosan-based vector/DNA complexes for gene delivery: biophysical characteristics and transfection ability. *Pharmaceutical Research*. **15**:1332–1339.
- Faraday, M. 1857. Experimental relations of gold (and other metals) to light, *Philosophical Transactions of the Royal Society*. **147**: 145-181.
- Ferrari, M. 2005. Cancer nanotechnology: opportunities and challenges. *Nature Reviews Cancer*. **5**: 161-171.
- Fievet, R., Lagier, JP., Blien, B., Boaudin, B., Figlarz, M., 1989. Nanocrystals: Synthesis, Properties and Applications. *Journal of Solid State Ionics*. **32**: 198.
- Freestone, I., Meeks, N., Sax, M., Higgitt C. 2007. The Lycurgus cup - a roman nanotechnology. *Gold Bulletin.* **40**: 270–277.
- Frens, G. Controlled nucleation for the regulation of the particle size in monodisperse gold suspensions. 1973. *Nature (London), Physical Science:* **241:** 20-22.
- Fuller, JE., Zugates, GT., Ferreira, LS., Ow, HS., Nguyen, NN., Wiesner, UB., Langer, RS. 2008. Intracellular delivery of core–shell fluorescent silica nanoparticles. *Biomaterials*. **29**:1526–1532.
- Gao, L., Nie, L., Wang, T., Qin, Y., Guo, Z., Yang, D., Yan, X. 2006. Carbon nanotube delivery of the GFP gene into mammalian cells, *ChemBioChem*. **7**: 239–242.
- Gao, X., Huang, L. 1993. Cytoplasmic expression of a reporter gene by co-delivery of T7 RNA polymerase and T7 promoter sequence with cationic liposomes. *Nucleic Acids Research.* **21**:2867–2872.

- Gao, X., Kim, KS., Liu, D. 2007. Nonviral gene delivery: what we know and what is next. *The American Physical Society Journal.* **9**:92–104.
- Gemeinhart, RA., Luo, D., Saltzman, WM. 2005. Cellular Fate of a Modular DNA Delivery System Mediated by Silica Nanoparticles. *Biotechnology Progress*. **21**: 532–537.
- Ghitescu, L., Fixman, A., Simionescu, M., Simionescu, N. 1986. Specific binding sites for albumin restricted to plasmalemmal vesicles of continuous capillary endothelium: receptor-mediated transcytosis. *Journal of Cell Biology.* **102**:1304-1311.
- Ghosh, PS., Kim, C., Han, G., Forbes, NS., Rotello, VM. 2008a. Efficient gene delivery vectors by tuning the surface charge density of amino acid-functionalized gold nanoparticles. *American Chemical Society Nano.* **2**: 2213–2218.
- Ghosh, PS., Kim, C., Han, G., Forbes, NS., Rotello. VM. 2008b. Gold nanoparticles in delivery applications. *Advanced Drug Delivery Reviews.* **60**:1307–1315.
- Giersig, M., Mulvaney, P. 1993. Preparation of ordered colloid monolayers by electrophoretic deposition. *Langmuir.* **9** (12):3408–3413.
- Giljohann, DA., Seferos, DS., Prigodich, AE., Patel, PC., Mirkin, CA. 2009. Gene regulation with polyvalent siRNA-nanoparticle conjugates. *Journal American Chemical Society*. **131**: 2072-2073.
- Godbey, WT., Kenneth, K., Wu, Antonios, WT., Mikos, G. 1999. Poly(ethylenimine) and its role in gene delivery. *Journal of Controlled Release* **60**: 149–160.
- Goldman CK, Soroceanu L, Smith N, Gillespie GY, Shaw W, Burgess S. 1997. In vitro and in vivo gene delivery mediated by a synthetic polycationic amino polymer. Nature Biotechnology. **15**:462–466.
- Gorov, AO., Richardson, HH. 2007. Generating heat with metal nanoparticles. *Nano Today.* **2**: 30-35.
- Green, M., O'Brien P. 2000**.** A simple one phase preparation of organically capped gold nanocrystals, *Chemistry Communication*. **3**: 183-184.
- Handley, D. A. 1989. *Colloidal Gold. Principles, Methods, and Applications,* Vol.1, Ed.; M.A. Hayat, Academic Press, New York. 13-32.
- Heller, LC., Ugen, K., Heller, R. 2005. Electroporation for targeted gene transfer. *Expert Opinion on Drug Delivery*. **2**:255–268.
- Higby, GJ. 1982. Gold in medicine: a review of its use in the West before 1900. *Gold Bulletin*. **15**:130–140.

- Hirn, S., Semmler-Behnke, M., Schleh, C., Wenk, A., Lipka, J., Schaffler, M., Takenaka, S., Moller, W., Schmid, G., Simon, U., and Kreyling, WG. 2011. Particle size-dependent surface charge-dependent biodistribution of gold nanoparticles after intravenous administration. *European Journal of Pharmaceutics and Biopharmaceutics*. **77**: 407–416.
- Holmes, JD., Smith, PR., Evans-Gowing, R., Richardson, DJ., Russell ,DA,., Sodeau, J.R. 1995. Energy-dispersive x-ray analysis of the extracellular cadmium sulfide crystallites of *Klebsiella aerogenes*. *Archives of Microbiology*. **163**: 143-147.
- http://www.slideshare.net/AnVanRompay/overview-of-3dhuman-skin-reconstructed-models-for-irritation-and-corrosion-testing-by-an-van-rompay (Accessed 18 Nov 2014).
- http://www.wired.co.uk/news/archive/2012-10/16/gold-nanoparticles-cancer-dogs (Accessed 31 October 2014).
- Huang, L., Hung, MH., Wagner, E. 1999. Non-viral vectors for gene therapy. *In:* Huang, L., Hung, MH., Wagner, E., ed. Vol. **2**. Academic Press: California.
- Ipe, BI., George Thomas, K., Barazzouk, S., Hotchandani, S., Kamat, PV. 2002. "Photoinduced Charge Separation in a Fluorophore-Gold Nanoassembly", *Journal of Physical Chemistry B*. **106**: 18-21.
- Islam, MM., Masum, SM., Rahman, MM., Molla, MAI., Shaikh, AA., Roy., SK. 2011. Preparation of Chitosan from Shrimp Shell and Investigation of Its Properties. *International Journal of Basic & Applied Sciences.* **11** (1): 1-18.
- Jain, R., Shah, NH., Malick, AW., Rhodes, CT. 1998. Controlled drug delivery by biodegradable poly(ester) devices: different preparative approaches. *Drug Development and Industrial Pharmacy.* **24**:703–727.
- Jans, H., Liu, X., Huo, Q. 2009. Dynamic light scattering as a powerful tool for gold nanoparticle bioconjugation and biomolecular binding studies. *Analytical Chemistry.* **81**:9425–9432.
- Jeong, SJ., So, YK., Sang Bong, L., Kyung Ok, K., Joong Soo, H., Young Moo, L. 2006. Poly(ethylene glycol)/poly (ε-caprolactone) diblock copolymeric nanoparticles for non-viral gene delivery: the role of charge group and molecular weight in particle formation, cytotoxicity and transfection. *Journal of Controlled Release.* **113**:173–182.
- Joshi, H., Shirude, PS., Bansal, V., Ganesh, KN., Sastry, M. 2004. Isothermal titration calorimetry studies on the binding of amino acids to gold nanoparticles. *Journal of Physical Chemistry B.* **108**:11535–11540.

- Kanaras, AG., Kamounah, FS., Schaumburg, K., Kiely, CJ., Brust, M. 2002. Thioalkylated tetraethylene glycol: a new ligand for water soluble monolayer protected gold clusters. *Journal of the Chemical Society, Chemical Communications.* **20**:2294–2295.
- Kattumuri, V., Katti, K., Bhaskaran, S., Boote, EJ., Casteel, SW., Fent, GM., Robertson, DJ., Chandrasekhar, M., Kannan, R., Katti, KV. 2007. Gum arabic as a phytochemical construct for the stabilization of gold nanoparticles: *in vivo* pharmacokinetics and X-ray-contrast-imaging studies. *Small.* **3**(2):333–341.
- Kauffman, GB. 1985. The role of gold in alchemy. *Gold Bulletin.* **18**:31–44.
- Ke, CF., Hou, S., Zhang, HY., Liu, Y., Yang, K., Feng, XZ. 2007. Quantitative Emergence of Hetero [4] rotaxanes by Template-Directed Click Chemistry. *Chemical Communication*. **14**: 3374-3376.
- Keating, A., Toneguzzo F. 1990. Gene transfer by electroporation: a model for gene therapy. *Progress in Clinical Biological Research*. **333**:491–498.
- Kiang, T., Wen, J., Lim, HW., Leong, KW. 2004. The effect of the degree of chitosan deacetylation on the efficiency of gene transfection. Biomaterials. **25**:5293–301.
- Kim**,** D., Park, S., Lee, JH., Jeong, YY., Jon, S. 2007. Antibiofouling polymer-coated gold nanoparticles as a contrast agent for in vivo X-ray computed tomography imaging. *Journal of American Chemical. Society***. 129**: 7661.
- Kim, H., Lyerly, J., DaMaio, M. 1993. Gene delivery systems in surgery. *Archives of Surgery.* **128**:1197–1205.
- Kim, TH., Choi, H., Yu, GS., Lee, J., Choi, JS. 2013. Novel hyperbranched polyethyleneimine conjugate as an efficient non-viral gene delivery vector. *Macromolecular Research.* **21**(10):1097–1104.
- Kima, T., Jianga, H., Jerea, D., Parka, I., Chob, M., Nahc, J., Choia, Y., Akaiked, T., Choa. C. 2007. Chemical modification of chitosan as a gene carrier in vitro and in vivo. *Progress in. Polymer. Science.* **32**: 726–753.
- Klein, TM., Wolf, ED., Wu, R., Sanford, JC. 1987. High-velocity microprojectiles for delivering nucleic acids into living cells. *Nature.* **327**:70–73.
- Kneuer C, Sameti M, Bakowsky U, Schiestel T, Schirra H, Schmidt H. 2000**.** A nonviral DNA delivery system based on surface modified silica-nanoparticles can efficiently transfect cells in vitro. *Bioconjugate Chem.* **11**: 926–932.

- Kohlmann, O., Steinmetz, WE., Mao, X-A., Wuelfing, WP., Templeton, AC., Murray, RW., Johnson Jr, CS. 2001. NMR diffusion, relaxation, and spectroscopic studies of water soluble, monolayer protected gold nanoclusters. *Journal of Physical Chemistry B.* **105**:8801–8809.
- Krishna, SA., Amarehwar, P. 2011. Preparation of chitosan coated nanoparticles by emulsion polymerization technique. *Asian Journal of Pharmaceutical and Clinical Research*. **4**: Supplementary 1.
- Kupfer, JM., Ruan, XM., Liu, G., Matloff, J., Forrester, J., Chaux, A. 1994. High-efficiency gene transfer to autologous rabbit jugular vein grafts using adenovirus-transferrin/polylysine-DNA complexes. *Human Gene Ther*apy. **5**:1437–1443.
- Lacerda, SH., Park, JJ., Meuse, C., Pristinski, D., Becker, ML., Karim, A., Douglas, JF. 2010. Interaction of gold nanoparticles with common human blood proteins. ACS Nano 4, 365–379.
- Lakowicz, JR. 1999. Principles of fluorescence spectroscopy. 2nd ed., Kluwer academic/plenum publishers, USA.
- Lawrie, A., Brisken, AF., Francis, SE., Cumberland, DC., Crossman, DC., Newman, CM. 2000. Microbubble-enhanced ultrasound for vascular gene delivery. *Gene Therapy.* **7**: 2023–2027.
- Lazarus, GG., Revaprasadu, N., López-Viota., J., Singh M**.** 2014. The electrokinetic characterization of gold nanoparticles, functionalized with cationic functional groups, and its' interaction with DNA. *Colloids and Surfaces B: Biointerfaces.* **121**: 425–431.
- Lee, HY., Kim, SM., Kim, JY., Youn, SK., Choi, JS., Park, SM., 2002. Effect of addition of chitosan on improvement for shelf-life of bread. *Journal of the Korean Society of Food Nutrition*. **31**: 445–450.
- Lee*,* M. 2007. Apoptosis Induced by Polyethylenimine/DNA Complex in Polymer Mediated Gene Delivery. *Bulletin of the Korean Chemical Society.* **28** (1). 95-98.
- Lee, SH., Bae, KH., Kim, SH., Lee, KR., Park, TG. 2008. Amine-functionalized gold nanoparticles as non-cytotoxic and efficient intracellular siRNA delivery carriers. *International Journal of Pharmaceutics.* **364**: 94−101.
- Leo Y. T. Chou , Kevin Ming and Warren C. W. Chan. 2011. Strategies for the intracellular delivery of nanoparticles. *Chemistry Society Review.* **40**: 233-245.
- Lévy, R., Shaheen, U., Cesbron, Y., Sée, V. 2010. Gold nanoparticles delivery in mammalian live cells: a critical review. *Nano Reviews.* **1**:4889–4907.

- Li, J., Revol, JF., Marchessault, RH. 1996. Rheological properties of aqueous suspension of chitin crystallites. *Journal Colloid Interface Science*.**183**: 365–73.
- Liu, F., Song, Y., Liu, D. 1999. Hydrodynamics-based transfection in animals by systemic administration of plasmid DNA. *Gene Therapy.* **6**:1258–1266.
- Luo, D., Saltzman, WM. 2000a. Synthetic DNA delivery systems. *Nature Biotechnology*. **18**:33–37.
- Luo, D., Saltzman, WM. 2000b. Enhancement of transfection by physical concentration of DNA at the cell surface. *Nature Biotechnology.* **18**:893–895.
- Lyklema, J., Minor, M., 1998. On surface conduction and its role in electrokinetics. *Colloids Surfaces. A.* **140**: 33–41.
- Mahmoudi, K., Azadmanesh, K., Shokrgozar, MA., Journeay, WS., Laurent, S. 2011. Effect of nanoparticles on the cell life cycle, *Chemistry Review*. **111**: 3407–3432.
- Majzika, A., Fülöpb, L., Csapóa, E., Bogárb, F., Martinekc, T., Penkea, B., Bíród, G., Dékánya., I. 2010. Functionalization of gold nanoparticles with amino acid, -amyloid peptides and fragment. *Colloids and Surfaces B: Biointerfaces* **81**: 235–241.
- Makhsin, SR., Razak, KA., Noordin, R., Dyana Zakaria N., Chun. TS. 2012. The effects of size and synthesis methods of gold nanoparticle-conjugated MαHIgG_4 for use in an immunochromatographic strip test to detect brugian filariasis. *Nanotechnology.* **23**: 49-57.
- Mangeney, C., Ferrage, F., Aujard, I., Marchi-Artzner, V., Jullien, L., Ouari, O., Rekai, E-D., Laschewsky, I., Vikholm, JW., Sadowski, J. 2002. Synthesis and properties of water-soluble gold colloids covalently derivatized with neutral polymer monolayers. Journal of the *American Chemical Society.* **124**:5811–5821.
- Mann, MJ. 1999. Pressure-mediated oligonucleotide transfection of rat and human cardiovascular tissue. *Proceedings of the National Academy of Sciences USA.* **96**:6411–6416.
- Mao, HQ., Roy, K., Troung-Le, VL., Janes, KA., Lin, KY., Wang, Y., August, JT., Leong, KW. 2001. Chitosan–DNA nanoparticles as gene carriers: synthesis, characterization and transfection efficiency, *Journal of Control. Release* **70:** 399–421.
- Mao, S., Sun, W., Kissel, T. 2010. Chitosan-based formulations for delivery of DNA and siRNA. *Advanced Drug Delivery Reviews* **62**:12–27.
- Mariko, U., Mariko, HS., Kingo, U., Yasuhide, N. 2005. Photo-control of the polyplexes formation between DNA and photo-cation generatable water-soluble polymers. *Current Drug Delivery* **2**:207–214.

- Maruyama, K., Takizawa, T., Takahashi, N., Tagawa, T., Nagaike, K., Iwatsuru, M. 1998. Targeting efficiency of PEG-immunoliposome-conjugated antibodies at PEG terminals. *Advanced Drug Delivery Reviews.* **24**:235–242.
- Massimo SF., Mitchel SB., Krystof SB. 2011. The Use of Convection-Enhanced Delivery with Liposomal Toxins in Neuro-oncology. *Toxins* **3** (4), 369-397.
- Mayya, K.S., Patil, V., Sastry, M. 1997. On the stability of carboxylic acid derivatized gold colloidal particles: the role of colloidal solution pH studied by optical absorption spectroscopy. *Langmuir.* **13**:3944–3947.
- McIntosh, CM., Esposito, EA., Boal, AK., Simard, JM., Martin, CT., Rotello, VM. 2001. Inhibition of DNA transcription using cationic mixed monolayer protected gold clusters. *Journal of the American Chemical Society.* **123**:7626–7629.
- Mohr, L., Geissler, M. 2002. Gene therapy: new developments. *Praxis.* **91**:2227–2235.
- Morille, M., Passirani, C., Vonarbourg, A., Clavreul, A., Benoit, J-P. 2008. Progress in developing cationic vectors for non-viral systemic gene therapy against cancer. *Biomaterials.* **29**: 3477–3496b.
- Muller, RH., Mader, K., Gohla, S. 2000. Solid lipid nanoparticles (SLN) for controlled drug delivery – a review of the state of the art. *European Journal of Pharmaceutics and Biopharmaceutics*. **50**:161–177.
- Murashov, V., John Howard. 2011, *Nanotechnology Standards*, Springer.
- Murphy, CJ., Sau, TK., Gole, AM., Orendorff, CJ., Gao, JX., Gou, L., Hunyadi, SE., Li, T. 2005. Anisotropic metal nanoparticles: synthesis, assembly, and optical applications. *Journal of Physical Chemistry B*. **109**:13857–13870.
- Nair, B., Pradeep, T. Coalescence of nanoclusters and formation of submicron crystallites assisted by lactobacillus strains. 2002. *Crystal Growth and Design*. **2**: 293-298.
- Neumann, E., Schaefer-Ridder, M., Wang, Y., Hofschneider, PH. 1982. Gene transfer into mouse lyoma cells by electroporation in high electric fields. *European Molecular Biology Organization Journal*. **1**:841–845.
- Nguyen, TT., Shklovskii, BI. 2001a. Complexation of a polyelectrolyte with oppositely charged spherical macroions: giant inversion of charge. *Journal of Chemical Physics.* **114**:5905–5916.
- Nguyen, TT., Shklovskii, BI. 2001b. Complexation of DNA with positive spheres: phase diagram of charge inversion and reentrant condensation. *Journal of Chemical Physics.* **115**:7298–7308.

- Niidome, T., Nakashima, K., Takahashi, H., Niidome, Y. 2004. Preparation of primary amine-modified gold nanoparticles and their transfection ability into cultivated cells. *Journal of the Chemical Society, Chemical Communications.* **17**:1978–1979.
- Nikoobakht, B., El-Sayed, MA. 2003. Surface-enhanced Raman scattering studies on aggregated gold nanorods. *Journal of Physical Chemistry A*. **107**:3372–3378.
- Ogawa, Y. 1997. Injectable microcapsules prepared with biodegradable poly (α -hydroxy) acids for prolonged release of drugs. *Journal of Biomaterial Science, Polymer Edition*. **8**:391–409.
- Oshima, Y., Sakamoto, T., Yamanaka, I., Nishi, T., Ishibashi, T., Inomata, H. 1998. Targeted gene transfer to corneal endothelium in vivo by electric pulse. *Gene therapy.* **5**:1347–1354.
- Pan, Y., Neuss, S., Leifert, A., Fischler, M., Wen, F., Simon, U., Schmid, G., Brandau, W., and Jahnen-Dechent, W. 2007. Size-dependent cytotoxicity of gold nanoparticles. *Small.* **3**: 1941–1949.
- Papasani, MR., Wang, G., Hill, RA., 2012. Gold nanoparticles: the importance of physiological principles to devise strategies for targeted drug delivery. *Nanomedicine: Nanotechnology, Biology, and Medicine.* **8:** 804–814.
- Pearson, S., Lu, H., Stenzel, MH. 2015. Glycopolymer Self-Assemblies with Gold (I) Complexed to the Core as a Delivery System for Auranofin, *Macromolecules,* **48** (4), 1065-1076.
- Pei, R., Yang, X., Wang, E. 2001. Enhanced surface plasmon resonance immunosensing using a streptavidin- biotinylated protein complex. *Analyst*, **126**: 4–6.
- Petean, I., Tomoaia, GH., Horovitz, O., Mocanu, A., Tomoaia-Cotisel, M. 2008. Cysteine mediated assembly of gold nanoparticles. *Journal of optoelectronics and advanced materials*, **10**: 2289-2292.
- Pissuwan, D., Niidome, T., Cortie, MB. 2011. The forthcoming applications of gold nanoparticles in drug and gene delivery systems. *Journal of controlled release.* **149**: 65-71.
- Pouton, CW., Seymour, LW. 2001. Key issues in non-viral gene delivery. *Advanced Drug Delivery Reviews.***46**:187-203.
- Prasad, BLV., Stoeva, SI., Sorensen, CM., Klabunde, K. 2003. Digestive-ripening agents for gold nanoparticles: alternatives to thiols. *Chemistry of materials*. **15** (4): 935-942.
- Railsback, JG., Singh, A., Pearce, RC., McKnight, TE., Collazo, R., Sitar, Z., Yingling, YG., Melechko, AV. 2012. Weakly charged cationic nanoparticles induce DNA bending and strand separation. *Advanced Materials.* **24** (31):4261-4265.

- Rajam, M., Pulavendran, S., Rose, C., Mandal. AB. 2011. Chitosan nanoparticles as a dual growth factor delivery system for tissue engineering applications. *International Journal of Pharmaceutics*. **410**: 145-152.
- Remant Bahadur, KC., Thapa, B., Bhattarai, N**.** 2013. Gold nanoparticle-based gene delivery: promises and challenges. *Nanotechnology Reviews.* **3**: 269-280.
- Rizzuto G, Cappelletti M, Maione D. 1999. Efficient and regulated erythropoietin production by naked DNA injection and muscle electroporation. *Proceedings of the National Academy of Sciences.* USA. **96**. 6417-6422.
- Rodríguez-Pulido, A., Mart´ın-Molina, A., Rodríguez-Beas, C., Llorca, O., Aicart, E., Junquer E. 2009. A Theoretical and Experimental Approach to the Compaction Process of DNA by Dioctadecyldimethylammonium Bromide/Zwitterionic Mixed Liposomes. *Journal of Physical Chemistry. B.* **113**. 15648–15661.
- Rosi, NL, Mirkin, CA. 2005. Nanostructures in Biodiagnostics. *Chemistry Reviews*. **105**: 1547–1562
- Rosi, NL., Giljohann, DA., Thaxton, CS., Lytton-Jean, AK., Han, MS., Mirkin, CA**.** Oligonucleotide-modified gold nanoparticles for intracellular gene regulation. 2006. *Science.* **312**: 1027-30.
- Rossi, JJ. RNAi as a treatment for HIV-1 infection. 2006. *BioTechniques.* **40**: 25-29.
- Ruponen, M., Honkakoski, P., Tammi, M., Urtti. A. 2004. Cell-surface glycosaminoglycans inhibit cation-mediated gene transfer. *Journal of gene medicine*. **6**: 405-414.
- Sandhu, KK., McIntosh, CM., Simard, JM., Smith, SW., Rotello, VM. 2002. Gold nanoparticle-mediated transfection of mammalian cells. *Bioconjuguate Chemistry.* **13**:3–6.
- Sau, TK., Murphy, CJ. 2004a. Room temperature, high-yield synthesis of multiple shapes of gold nanoparticles in aqueous solution. *Journal of the American Chemical Society.* **126** (28): 8648-8649.
- Sau, TK., Murphy, CJ. 2004b. Seeded high yield synthesis of short Au nanorods in aqueous solution. *Langmuir*. **20**: 6414–6420.
- Schaaff, TG., Knight, G., Shafigullin, MN., Borkman, RF., Whetten, RL. 1998. *Journal of Physical Chemistry B.* **102**: 10643–10646.
- Semmler-Behnke, M., Kreyling, WG., Lipka, J., Fertsch, S., Wenk, A., Takenaka, S. Schmid, G., and Brandau, W. 2008. Biodistribution of 1.4- and 18-nm gold particles in rats. *Small.* **4**: 2108–2111.

- Sennato, S., Bordi, F., Cametti, C. 2004. On the phase diagram of reentrant condensation in polyelectrolyte-liposome complexation. *Journal of. Chemical Physics.* **121**: 4936-4940.
- Shaw, CF. 1999. Gold-based therapeutic agents, *Chemical. Reviews*. **99**: 2589-2600.
- Simberg, DS., Weisman, Y., Talmon, A., Faerman, T., Shoshani, Barenholtz, Y. 2003. The role of organ vascularization and lipo-plex serum initial contact in intravenous murine lipofection. *Journal of Biological Chemistry*. **278:** 39858-39865.
- Sonavane, G., Tomoda, K., Makino, K. 2008. Biodistribution of colloidal gold nanoparticles after intravenous administration: Effect of particle size. *Colloids and Surfaces. B. Biointerfaces.* **66**: 274–280.
- Sun, WH., Burkholder, JK., Sun J., Culp, J., Lu, XG., Pugh, TD., Ershler, WB., Yang, NS. 1995. In vivo cytokine gene transfer by gene gun reduces tumor growth in mice. *Proceedings of the National Academy of Sciences.* USA. **92**: 2889-2893.
- Sun. Y., Migueliz, I., Navarro, G., Tros de Ilarduya, C. 2009. Structural and morphological studies of cationic liposome-DNA complexes. *Letters in drug design and discovery*. **6**: 33-37.
- Suzuki, R., Takizawa, T., Negishi, Y., Utoguchi, N., Maruyama. K. 2008**.** Effective gene delivery with novel liposomal bubbles and ultrasonic destruction technology, *International journal of Pharmacy*. **354**: 49–55.
- Templeton, AC., Chen, S., Gross, SM., Murray, RW**.** 1999. Water-soluble gold clusters protected by tiopronin and coenzyme a monolayers. *Langmuir.* **15:** 66-76.
- Templeton, AC., Wuelfing, MP., Murray, RW. 2000. Monolayer protected cluster molecules. *Accounts of Chemical Research.* **33**: 27–36.
- Teranishi T. and Miyake M. 1998. Size Control of Palladium Nanoparticles and Their Crystal Structures. *Chemistry Materials*. **10**: 594-600.
- Thomas, M., Klibanov, A.M., 2003. Conjugation to gold nanoparticles enhances polyethyleneimine transfer of plasmid DNA into mammalian cells, *Proceedings of the National. Academy of Science. USA*. **100**: 9138-9143.
- Tiwari, PM., Vig, K., Dennis, VA., Singh, SR**.** 2011. Functionalized gold nanoparticles and their biomedical applications. *Nanomaterials*: **1:** 31-63.
- Torres, AE, Baigl. D. 2011. DNA compaction: fundamentals and applications. *Soft Matter.* **7**: 6746-6756.
- Turkevich, J., Stevenson, P.C., Hillier, J. 1951. A study of the nucleation and growth processes in the synthesis of colloidal gold. *Discussions of the Faraday Sociey* **II:** 55-75.

- Uson, R**.** 1978. The chemistry of gold. *Synthesis ad Reactivity in Inorganic, Metal-organic and nano-metal chemistry*: **8**: 503-504.
- Van Meerloo, J., Kaspers, GJ., Cloos, J. 2011. Cell sensitivity assays: the MTT assay. *Methods Molecular Biology*. **731**: 237-245.
- Viota, JL., Arroyo, FJ., Delgado, AV., Horno, J. 2010. Electrokinetic characterization of magnetite nanoparticles functionalized with amino acids. *Journal of colloid and interface science.* **344**:144-149.
- Von Maltzahn G, Park JH, Agrawal A, Bandaru NK, Das SK, Sailor MJ. 2009**.** Computationally guided photothermal tumor therapy using long-circulating gold nanorod antennas. *Cancer Research*. **69**: 3892-900.
- Wang, J., Zhang, W., Li, Y. 2014a. Treatment of metastatic breast cancer by combination of chemotherapy and photothermal ablation using doxorubicin-loaded DNA wrapped gold nanorods. *Biomaterials* **35**: 8374-8384.
- Wang, S., Lee, C., Chiou, A., Wei, P., Wang. 2010. Size-dependent endocytosis of gold nanoparticles studied by three-dimensional mapping of plasmonic scattering images. *Journal of Nanobiotechnology*. **8**:33
- Watzky M.A. and Finke R.G., 1997. Transition Metal Nanocluster Formation Kinetic and Mechanistic Studies. *Journal of American. Chemical Society*. **119**: 10382-10400.
- Webster A, Coupland P, Houghton FD, Leese HJ, Aylott JW**.** 2007. The delivery of PEBBLE nanosensors to measure the intracellular environment. *Biochemistry Society Transactions.* **35**: 538-543.
- Weir, B., Zhao, X., Meyerson, M. 2004. Somatic alterations in the human cancer genome. *Cancer Cell*. **6** (5):433-438.
- Weisbecker, CS., Merritt, MV., Whitesides, GM. 1996. Molecular self-assembly of aliphatic thiols on gold colloids. *Langmuir*. **12**: 3763-3772.
- Wieber, AT., Selzer, J., Kreuter, J. 2012. Physiochemical characterization of cationic liposomes as drug delivery system for a hydrophilic decapeptide before and after freeze-drying. *European journal of pharmaceutics and biopharmaceutics*. **80**: 358-367.
- Wolff, JA., Malone, RW., Williams, P. 1990. Direct gene transfer into mouse muscle in vivo. *Science.* **247:** 1465-1468.
- Wong, T.K and Neumann, E. 1997. Electric field mediated gene transfer. *Biochemical and, Biophysical. Research. Communication*. **107**: 584-587.

- Xiang JJ, Tang JQ, Zhu SG, Nie XM, Lu HB, Shen SR. 2003. IONP-PLL: a novel nonviral vector for efficient gene delivery. *Journal Gene Medicine*. **5**:803–817.
- Yang, NS and Sun WH. 1995. Gene gun and other non-viral approaches for cancer gene therapy. *Nature Medicine.* **1**: 481-483.
- Yang, NS., Burkholder, J., Roberts, B., Martinell, B., McCabe, D. 1990. In vivo and in vitro gene transfer to mammalian somatic cells by particle bombardment. *Proceedings in Natural. Academy of Science*. USA. **87**: 9568-9572.
- Yang, ZR., Wang, HF., Zhao, J., Peng, YY, Wang, J., Guinn, BA. Huang, LQ. 2007. Recent developments in the use of adenoviruses and immunotoxins in cancer gene therapy. *Cancer Gene Therapy*. **14**: 599–615.
- You, CC., De, M., Han, G., Rotello, VM. 2005. *Journal of Analytical Chemistry Society.* **127**: 12873-12881.
- Zhang, G., Budker, V., Wolff, JA. 1999. High levels of foreign gene expression in hepatocytes after tail vein injections of naked plasmid DNA. *Human Gene Therapy*. **10**: 1735-1737.
- Zhang, X and Godbey, W.T. 2006. Viral vectors for gene delivery in tissue engineering, *Advanced Drug Delivery. Review.* **58**: 515–534.
- Zhang. XD., Wu.D., Shen, X., Chen, J., Sun, YM., Liu, PX., Liang, XJ. 2012. Size-dependent radio sensitization of PEG-coated gold nanoparticles for cancer radiation therapy. *Biomaterials* **33**: 6408-6419.
- Zhou, X., Klibanov, A., Huang, L. 1991. Lipophilic poly-lysines mediate efficient DNA transfection in mammalian cells. *Biochimica. Biophyica. Acta.* **1065:** 8-14.
- Zuhorn, IS., Kalicharan, R., Hoekstra, D., 2002. Lipoplex mediated transfection of mammalian cells occurs thought the cholesterol-dependent clathrin-mediated pathway of endocytosis. *Journal of Biological Chemistry.* **277**: 18021-18028.

Appendix A

Appendix B

Colloids and Surfaces B: Biointerfaces 121 (2014) 425–431

Contents lists available at ScienceDirect

Colloids and Surfaces B: Biointerfaces

journal homepage: www.elsevier.com/locate/colsurfb

The electrokinetic characterization of gold nanoparticles, functionalized with cationic functional groups, and its' interaction with DNA

Geraldine Genevive Lazarus[a,b,c,*], Neerish Revaprasadu[b], Julián López-Viota[c,1], Moganavelli Singh[a]

[a] Discipline of Biochemistry, University of KwaZulu-Natal, Private Bag X 54001, Durban 4000, South Africa
[b] Department of Chemistry, University of Zululand, Private Bag X1001, KwaDlangezwa 3886, South Africa
[c] Department of Applied Physics, Hospital Universitario San Cecilio, University of Granada, Granada, Spain

ARTICLE INFO

Article history:
Received 2 December 2013
Received in revised form 14 May 2014
Accepted 12 June 2014
Available online 19 June 2014

Keywords:
Gold nanoparticles
Cytotoxicity
Electrophoretic mobility
DNA

ABSTRACT

Gold nanoparticles have attracted strong biomedical interest for drug delivery due to their low toxic nature, surface plasmon resonance and capability of increasing the stability of the payload. However, gene transfection represents another important biological application. Considering that cellular barriers keep enclosed their secret to deliver genes using nanoparticles, an important step can be achieved by studying the functionalization of nanoparticles with DNA. In the present contribution the synthesis of nanoparticles consisting of a gold core coated with one or more layers of amino acid (L-lysine), and cationic polyelectrolytes (poly-ethyleneimine and poly-L-lysine) is reported. All nanoparticles were subjected to dynamic light scattering, electrophoretic mobility measurements, UV–vis optical spectrophotometry analysis and transmission electron microscopy imaging. In addition, the adsorption of DNA plasmid (pSGS) with linear and supercoiled configurations was studied for those gold nanoparticles under the most suitable surface modifications. Preliminary results showed that the gold nanoparticles functionalized with poly-ethyleneimine and poly-L-lysine, respectively, and bound to linear DNA configurations, present in absolute value a higher electrophoretic mobility irrespective of the pH of the media, compared to the supercoiled and nicked configuration. The findings from this study suggest that poly-ethyleneimine and poly-L-lysine functionalized gold nanoparticles are biocompatible and may be promising in the chemical design and future optimization of nanostructures for biomedical applications such as gene and drug delivery.

1. Introduction

Gold nanoparticles (AuNPs) have sparked much interest in the fields of chemistry, physics, biology, medicine and biomaterial sciences. They are bioinert, non-toxic and readily synthesized [3] and their small size allows them to penetrate cells and tissues, making their application in medicine far reaching. They have become one of the most interesting sensing materials because of their unique size and shape dependent optical properties, high extinction coefficient and super-quenching capability. AuNPs hold the promise for efficient gene or drug delivery into cells by absorbing and resonantly scattering visible and near-infrared light upon excitation of their surface plasmon-oscillation [14]. AuNPs do not have target recognition abilities necessary for selective binding of analytes of interest. In order to selectively detect analytes of interest antibodies, short-chain organic acids, proteins or DNA molecules have been used to modify the surface properties of AuNPs to provide target recognition sites [20]. These molecules can be incorporated into AuNPs through electrostatic attraction or covalent bonding. It is an effective way to enhance specificity and efficacy of nanoparticle based delivery systems [17]. For them to be successfully utilized in medical applications their fundamental properties such as the forces that are responsible for nanoparticle-drug stabilization must be understood.

AuNPs are also currently being used as delivery vehicles to transport siRNA into cells for efficient knockdown of target genes

* Corresponding author at: University of KwaZulu-Natal, Discipline of Biochemistry, Durban, South Africa. Tel.: +27732293126.
E-mail addresses: geraldinelazarus@yahoo.co.uk, geraldinelazarus@gmail.com (G.G. Lazarus).
[1] Departamento de Física Aplicada, Avenida Fuente Nueva S.N., 18071 Granada, Spain.

http://dx.doi.org/10.1016/j.colsurfb.2014.06.032
0927-7765/

without significant cytotoxicity. They demonstrated high stability and effective transfection in multiple myeloma cells ([8] and [2]). These particles can also be carriers of peptides and proteins. They present strategies for the treatment of genetic as well as acquired diseases. The release of gold nanoparticles is vitally important for effective therapy. This release could be triggered by internal (e.g. gluthathione), pH or external stimuli such as light [6].

Electrokinetic characterization was carried out first, because in order to design a carrier, one needs to know the features and properties of the system that one is working with. These include hydrophobicity/hydrophilicity, size and most importantly charge. It is important to note that each time the surface of a nanoparticle is functionalized, any one of these (or all three at the same time) properties may change. Adsorption on the surface commonly results in a modification of the charge. Therefore electrophoretic mobility (U_e) studies were carried out to determine and optimize the preparation conditions of the final surface charge. Complementary to this feature, dynamic light scattering was also performed in order to confirm the surface modification of the nanoparticle with an external agent. Size and surface charge of DNA complexes are two important factors in determining the efficiency of cellular uptake. Although there is a common theme in all vectors, each vector has to be suitably tailored and optimized to meet the needs of a specific application.

This was seen when attaching a functional group such as lysine to a nanoparticle, the p*K*a values (2.2, 8.5, and 10.28) had to be considered in order to determine at which pH this amino acid needed to be prepared. Depending on the physical orientation of its side chains, lysine may form bridges with the citrate ions enclosing the AuNP and resulting in aggregation. This may account for the negative or decreased electrophoretic mobility observed. Lysine contains 1 carboxylic group and 2 amine groups so a fully protonated lysine molecule has a +2 net charge. The two ε-amino groups have p*K*a's of 9.0 and 10.2 respectively which are significantly higher.

2. Materials and methods

Water (Milli-Q Academic, Millipore, France) was used in the preparation of all suspensions. Gold(III) chloride trihydrate, trisodium citrate dehydrate, ethanol, L-lysine, polyethyleneamine (PEI branched, 25 kDa) and poly-L-lysine (PLL) were purchased from Sigma Aldrich. Citric acid was from Pancreac (Spain). All chemicals were of analytical quality. DNA plasmid pSGS was amplified at Hospital Universitario San Cecilio, Granada. The following instruments were used. Nanosight Nanoparticle Tracking Analysis (NTA) Version 2.2 Build 0377, Zetasizer Nanoseries Nano-ZS Model ZEN 3600 (Malvern Instruments, U.K), Eppendorf Centrifuge 5418, NanoDrop 2000c spectrophotometer (Thermo Scientific, Wilmington, USA), Hettich Zentrifugen Mikro ZZ0R, Gel electrophoresis apparatus, pH meter, Perkin Elmer Lambda 20 UV–vis spectrophotometer, Transmission electron microscope Jeol (T 1010), iTEM Soft Imaging Systems (SIS) MegaView III side-mounted 3 megapixel digital camera.

2.1. Synthesis of colloidal gold nanoparticles by citrate reduction

0.45×10^{-3} M of an aqueous colloidal gold solution was prepared by $HAuCl_4$ reduction with sodium citrate using the method of [18]. A solution consisting of 0.11 mL gold colloidal in 25 mL water was boiled for 15 min and thereafter 1 mL of 1% sodium citrate was added rapidly to the vortex of the solution. On addition of the citrate into the boiling tetrachloroaurate solution the colour changed from pale yellow to dark blue within the first 3 min and then ruby red after 15 min of reaction time. It was boiled for a further 5 min on the heating mantle, thereafter removed and left to cool down to room temperature. It was stored in a dark bottle.

2.2. UV–vis optical spectrophotometry analysis

The qualitative analysis in particle uniformity and stability of each gold nanoparticle was followed up by examining the absorption spectra of the individual nanoparticles and to confirm in agreement with literature that the expected SPR absorption of the nano-sized gold particles occurs at 534 nm. UV–vis absorption measurements were conducted and the spectra recorded by measuring dilute samples in a quartz cell with a path length of 1 cm.

2.3. TEM and size analysis

The morphology of gold nanoparticles was observed by TEM. The zeta potentials and mean sizes of the gold nanoparticles were analyzed using a Zetasizer. The zeta potential measurements were performed in triplicate at pH 7.

2.4. Functionalization with amino acid and cationic poly-electrolytes

Different concentrations of the amino acid lysine (0.01, 0.1, 5, 10, 100, 200 and 500 mg/mL) and cationic poly-electrolytes; poly-L-lysine (1, 5, 10 and 100 mg/mL) and poly-ethyleneimine (1, 10 and 100 mg/mL) were prepared by dissolving the required amount into water according to the desired pH. Adsorption was carried out by slowly adding the gold colloidal solution dropwise to each amino acid and poly-electrolyte solution under constant and moderate vortexing. They were washed three times to remove any free polyelectrolytes that remained in solution.

2.5. Electrokinetic characterization

Zeta potential is a powerful tool that is used to analyse the electrostatic forces within the bulk solution and on the surface of the nanoparticles and nanocomplexes, respectively [15]. One drop of the gold suspension coated by the respective amino acid and poly-electrolyte as described in Section 2.4, was added to 10 mL of an aqueous solution of respective pH 3–9 and desired ionic strength. After 24 h of incubation, the pH was re-adjusted and the electrophoretic mobility was measured. Citric acid and sodium hydroxide were used to adjust the pH.

2.6. Ionic strength studies

Ionic strength studies were performed to determine the compactness of the adsorbed layer. To achieve this we investigated the effect of electrolyte concentrations on the U_e. Essentially in the presence of layers the mobility should tend towards zero because of the electric double layer compression at high ionic strength. The dispersion medium, sodium chloride, was prepared in different ionic salt concentrations of (1×10^{-4}; 1×10^{-3}; 2.5×10^{-3}; 5×10^{-3}; 7.5×10^{-3}; 1×10^{-2}; 2.5×10^{-2}; 5×10^{-2} mg/mL).

3. Results and discussion

3.1. Gold nanoparticle synthesis by citrate reduction

The transition in colour of the AuNPs from pale yellow to ruby red confirmed the formation of citrate-capped gold nanoparticles [18]. When the pale yellow colour fades it signifies the formation of the gold atoms which nucleate to form dark red nanowires. The

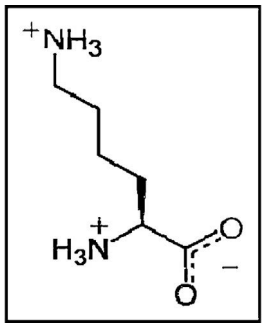

Fig. 1. Structural orientation of L-lysine.

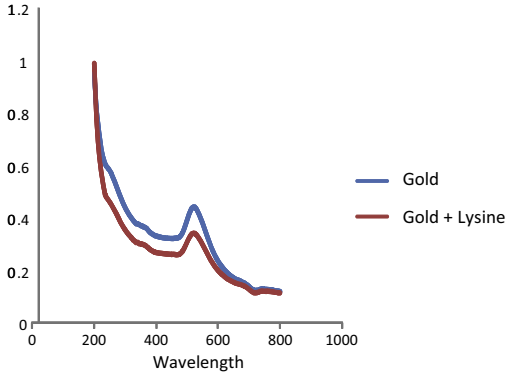

Fig. 2. UV–vis spec of Au and Au-Lys NP (100 mM).

nanowires destabilize with an increase in size followed by fragmentation and cleavage to form the citrate-capped AuNPs.

3.2. UV–vis spec

Figs. 2 and 3 show the UV–vis absorption spectra and TEM analysis, respectively, of the citrate-reduced colloidal nanoparticles synthesized. The surface plasmon resonance (SPR) absorption of the nanoparticles was observed at 534 nm. This is in agreement with the expected SPR absorption of the nanosized gold particles at this wavelength. The absorption of lysine onto the surface of the gold particle was confirmed by a decrease in the absorbance peak to 519 nm. A blue shift can be observed by the decrease in wavelength which denotes a decrease in particle size. Size and shape of the nanoparticles is of major importance to the efficiency of cellular uptake in transfection studies. From the TEM micrographs, the nanoparticles appear spherical with a smooth shape and surfaces that are homogenous in the nano-sized range of 30–50 nm. Subsequent observations showed no structural modifications such as aggregation or absorption changes for the particles after 6 months at room temperature.

3.3. Electrophoretic mobility measurements

3.3.1. Effect of pH and concentration of cationic functional groups

PEI and PLL were used to investigate their interaction and relationship with gold nanoparticles and to determine whether gold may reduce its toxicological effects. The AuNP's were combined with PEI to prepare (1, 2, 5, 7 and 10 mg/mL) of PEI-coated AuNP's and PLL (1, 10 and 100 mg/mL) of PLL-coated AuNP's. PEI displayed sizes in the range 70–120 nm (Fig. 5b) which is more acceptable compared to PLL 350–500 nm (Fig. 5a). Au-Lys-PEI nanoparticles were coupled to DNA of 3 different isophorms. The DNA conjugates with the nanoplexes were found to be positively charged with a considerable increase in particle size. Fig. 4a and b shows the electrophoretic mobility of Au-PLL and Au-PEI as a function of its concentration in solution. The results obtained show a considerable increase in electrophoretic mobility of the cationic functionalized groups when adsorbed onto gold nanoparticles. The increase in electrophoretic mobility is due to the cationic character of both polymers. In the case of poly-L-lysine the higher the concentration the greater the positive charge. Note in the case of polyethyleneimine for the concentration range studied, the gold nanoparticles were already close to the saturation region predicted in the law of Lambert Beer. It was not necessary to prepare the Au-PLL and Au-PEI complexes at varying pH's as they are positively charged entities.

Lysine exhibited positive electrophoretic mobility predominantly at pH 3 (Fig. 6). This correlates to previous literature [19]. The researchers investigated the adsorption of amino acids onto the surface of magnetite cores by measuring the electrophoretic mobility of the amino acid-coated magnetite particles and comparing the results with the ones obtained for the unmodified magnetite cores. Likewise in order to explain lysines' particular pH dependence and its effect on U_e, we coated the gold nanoparticles with lysine and took into consideration the p*K*a of its ionized groups. Lysine has p*K*a values of 2.2; 8 and 10. At pH 3 the Au-lys NP's are protonated and lysine has an overall +2 net charge (Fig. 1). Therefore there is attraction and adsorption between the two particles. The isoelectric point with minimum electrostatic repulsion, shifted 4 units back (pH 3) from the norm (pH 7) after the gold was put into contact

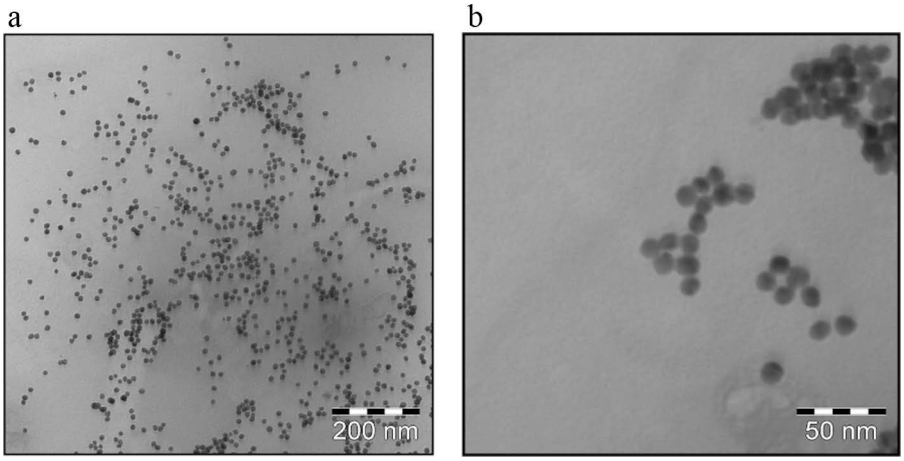

Fig. 3. Transmission electron microscopy analysis of AuNP at (a) 40 000× and (b) 60 000×.

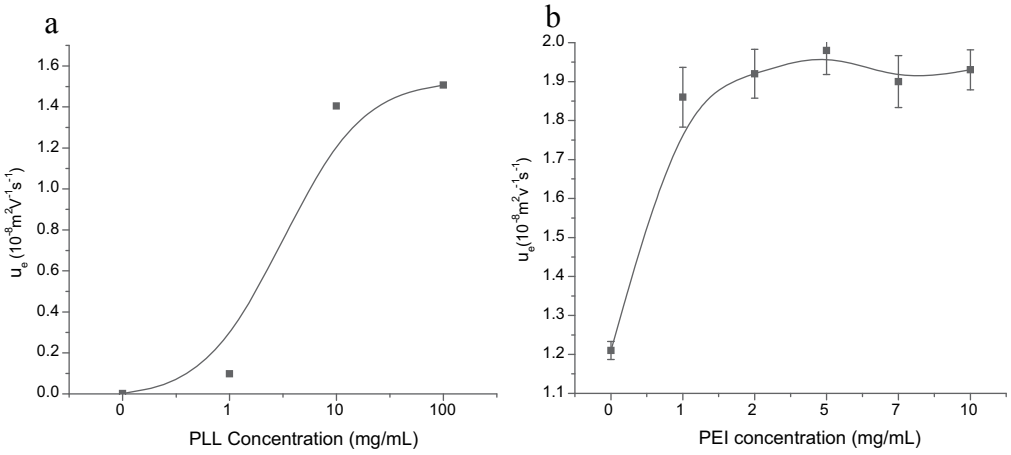

Fig. 4. (a) Electrophoretic mobility U_e of Au-PLL and (b) Au-PEI as a function of its concentration in solution. Error bars represents the mean ± SD, $n = 3$.

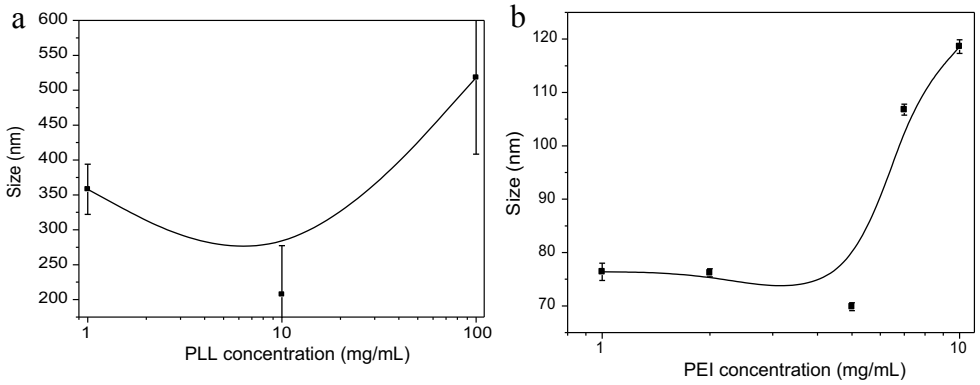

Fig. 5. (a) Zeta sizing by dynamic light scattering of Au-PLL and (b) Au-PEI as a function of its concentration in solution. Error bars represents the mean ± SD, $n = 3$.

with lysine. At pH 7 the U_e is negative because the lysine bound to gold forms cross bridges with each other resulting in aggregation (Fig. 6). As the pH increases to 9, deprotonation occurs, hence the negative U_e. The Au-Lys NP experiences repulsion, resulting in little or no adsorption taking place.

The difference in pH trend was further studied by modifying the surface adsorption of the AuNP and varying the concentration of lysine in solution. As a result, at low lysine concentrations of 0.01 and 0.05 mg/mL the values correspond to the bare gold particles. In Fig. 6 there is a distinct adsorption on the bare AuNP with the lysine coated particles showed a significant negative mobility

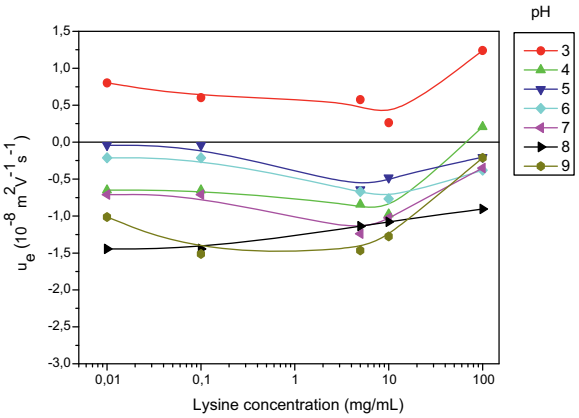

Fig. 6. Electrophoretic mobility (U_e) of Au-lys as a function of pH. Error bars represents the mean ± SD, $n = 3$.

irrespective of pH. This again can be attributed to the fact that at high pH lysine is deprotonated and any further increase in the concentration of lysine in solution leads to saturation of the AuNP resulting in cross-binding, aggregation and negative mobility (Fig. 7a). The size distribution (Fig. 7b) by intensity correlates to the size by zeta sizing. This is evident by the colour changes of the nanocomplex in solution (Fig. 8a). It shows a distinct change from red to purple. It is likely that an increase in lysine concentration may have caused bridging leading to aggregation. At the lowest concentration of lysine (1–5 mg/mL) the colour is a ruby red. Red is indicative of small particles of 20–40 nm in size. After 24 h the Au-lys of small size (Fig. 8b and c) turned purple indicating aggregation and instability. As the concentration of lysine was increased (6–10 mg/mL) the colour changed to a deeper purple which indicated the formation of clusters and larger particles around 70–80 nm.

3.3.2. *Au-Lys-PLL and its interaction with DNA*

Nanoparticle binding can facilitate DNA compaction in addition to partial strand separation [5]. We did not incubate the Au-Lys NP with DNA because lysine was positive only at pH 3 which is too acidic for the body to optimally function in. The pH of blood is 7.4 and in order for the nanocomplexes to circulate in the body it has to be neutral or slightly positive. Although PEI revealed size distributions within our desired size range and positive electrophoretic mobility, PEI was not employed further with DNA plasmids since previous literature had shown some toxicity to cells. Hence further studies with Au-PLL were conducted and Au-PLL incubated with DNA pSGS. It exhibited size distributions in the range of

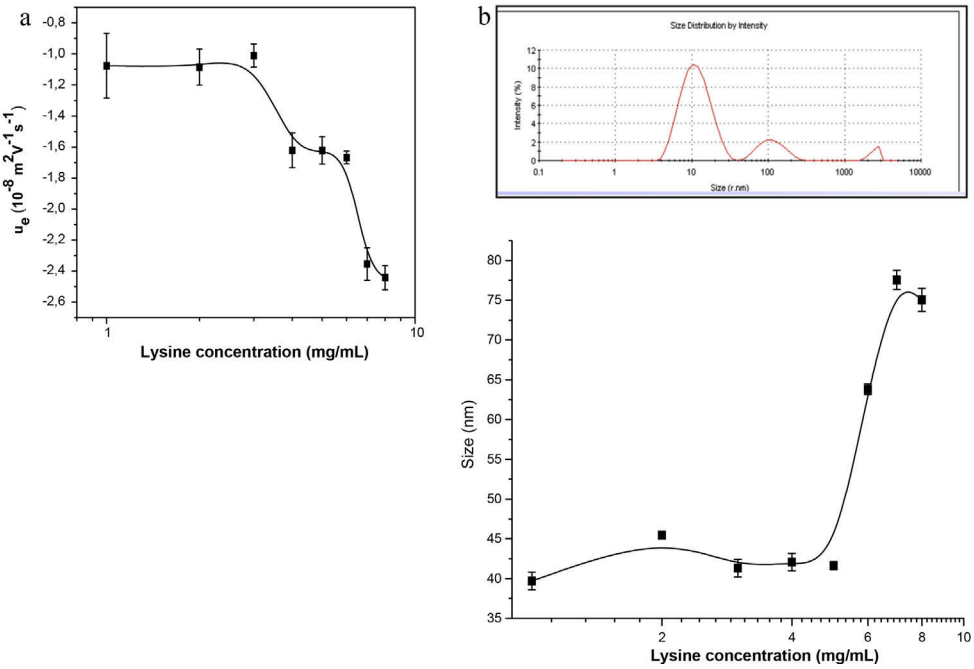

Fig. 7. (a) Electrophoretic mobility (U_e) and (b) Size distribution of Au-lys as a function of lysine concentration. Error bars represents the mean ± SD, $n = 3$.

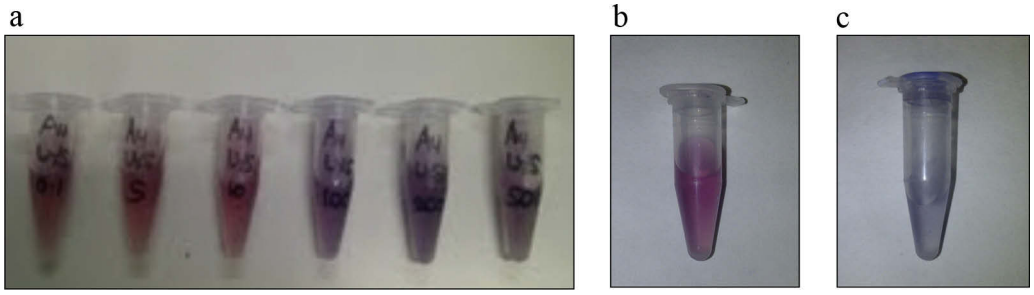

Fig. 8. (a) Colour changes of AuNPs after addition of lysine at varying concentrations (0.1, 5, 10, 100, 200 and 500 mg/mL); (b) Au-Lys and (c) Au-Lys after 24 h.

110–290 nm (Fig. 9a). As the concentration of PLL was increased the DNA strands wrapped tighter around the Au-PLL complex thereby compacting it as seen in the TEM images (Fig. 10) with a size decrease of more than 50% (Fig. 9a). Given that the smallest particle size is at 10 mg/mL, the Au-PLL NP that was prepared accordingly and incubated with DNA pSGS of different isophorms as a function of their concentration. The results obtained (Fig. 9b) indicate that the U_e of linear and supercoiled isophorms tended towards zero. When supercoiled DNA was complexed to PLL it yielded a much lower effective negative charge than linear DNA since the polyelectrolyte is compacted with a large amount of counter ions.

3.3.3. *Effect of ionic strength*

The results show that at high ionic strength electroneutrality was achieved, this can be interpreted to mean that the electric double layer was compact and stable. When the surface of the gold core

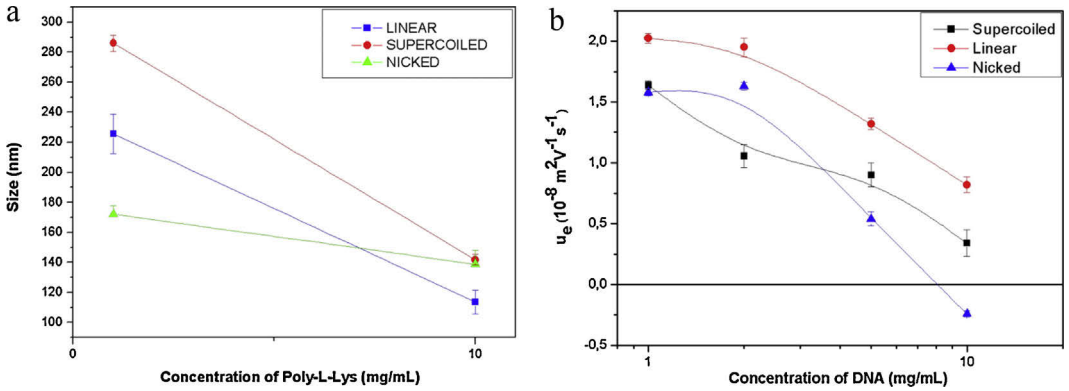

Fig. 9. (a) Size distribution of Au-PLL and DNA pSGS as a function of PLL concentration and (b) U_e of Au-PLL and DNA pSGS as a function of DNA concentration. Error bars represents the mean ± SD, $n = 3$.

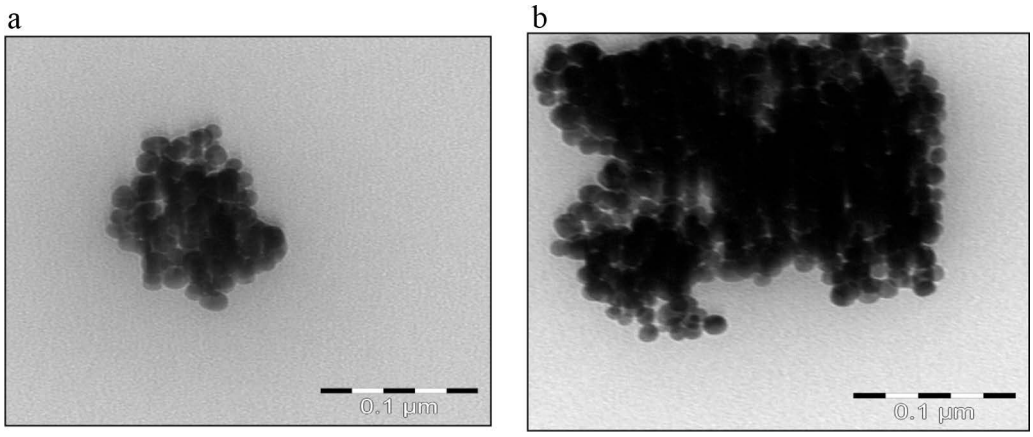

Fig. 10. (a) TEM of lysine bound to gold showing aggregates (b) Au-Lys DNA complex.

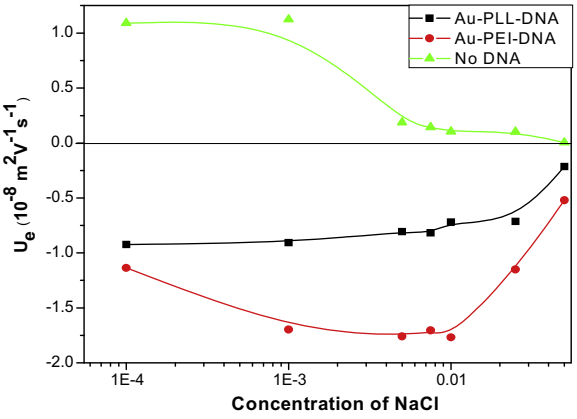

Fig. 11. U_e of Au-PLL, Au-PEI and its interaction with supercoiled DNA as a function of ionic strength. Error bars represents the mean ± SD, $n = 3$.

was covered by PLL-DNA and PEI-DNA (Fig. 11), the particles did not display soft electrokinetic behaviour. Using the formalization derived by [16] which is in turn based on the complexation theory recently developed by [10,11], it describes the complexation of long polyelectrolytes with oppositely charged spherical bodies to a single negative molecule of DNA. The theory predicts that in a system, equilibrium is reached by the DNA concentration with lipoplexes. The same can be said for metal nanoparticles which allows us to predict the isoelectric point where the nanocomplex is almost neutrally charged [15].

4. Conclusion

We described the synthesis and electrokinetics of gold nanoparticles functionalized with amino acid lysine and cationic polyelectrolytes, poly-ethyleneimine and poly-L-lysine. In view of previous applications of lysine functionalized gold nanoparticles, we report findings that at predominantly high concentrations of lysine there is only a slight increase in negative electrophoretic mobility. Lysine exhibited positive electrophoretic mobility predominantly at pH 3, which correlates to previously published literature [19]. However required binding of lysine at pH 7.4 and at neutral pH show that the complexation of lysine to gold is fairly weak as confirmed by [7]. Since positivity was not achieved at high lysine concentrations and hence no DNA interaction, further binding studies were not conducted.

With regards to PEI, it displayed strong positive U_e (Fig. 4b) compared to PLL, with favourable size distributions due to compaction with DNA. The U_e tended towards zero, meaning the overall surface charge was neutral which is required for further use in transfection studies. At high ionic concentrations the U_e tended towards zero owing to the electric double layer, confirming a compact molecule ([4,12]). Ref. [13]recently revealed that when the isolelectric point is reached in a system an inversion of electrophoretic mobility sign takes place. This behaviour was previously found in works of cationic lipoplexes. In this study no charge inversion was reported at the desired concentration. This means that within the concentration range the gold nanoparticles neutralized the charge of DNA in the system. This may be due to the different and unique properties of gold nanoparticles compared to liposomes. In accordance, Ref. [9], confirms the significance of the isoneutrality point which is defined as the ratio at which the positive charge of the liposomes, which in our study is the cationic coated gold nanoparticle that neutralizes the negative charge coming from the phosphate group of DNA. This makes it a potential cell transfecting agent. It was observed that when supercoiled, linear and nicked DNA were complexed to PLL respectively, supercoiled DNA yielded a much lower effective negative charge than linear and nicked DNA. This is confirmed with results recently published by Barran-Berdon and co-workers in 2012. In summary PLL functionalized AuNPs show promising characteristics for use as a non-viral gene delivery system. In vitro cytotoxicity and transfection studies in mammalian cells are currently being conducted.

Acknowledgments

The authors are grateful to the National Research Foundation (NRF, South Africa) and the Erasmus Mundus Fellowship for financial assistance.

References

[1] A.L. Barran-Berdon, M. Munoz-Ubeda, C. Aicart-Ramos, L. Perez, M.R. Infante, P. Castro-Hartman, A. Martin-Molina, E. Aicart, E. Junquera, Ribbon-type and cluster-type lipoplexes constituted by a chiral lysine based cationic Gemini lipid and plasmid DNA, Soft Matter 8 (28) (2012) 7368–7380.
[2] E. Crew, S. Rahman, A. Razzak-Jaffar, D. Mott, M. Kamundi, G. Yu, N. Tchah, J. Lee, M. Bellavia, C. Zhon, MicroRNA conjugated gold nanoparticles and cell transfection, Anal. Chem. 84 (2012) 26–29, http://dx.doi.org/10.1021/ac202749p.
[3] M.C. Daniel, D. Astruc, Gold nanoparticles: assembly, supramolecular chemistry, quantum-sized related properties and applications towards biology, catalysts and nanotechnology, Chemistry (Revised) 104 (2004) 293–346.
[4] A.V. Delgado, Interfacial Electrokinetics and Electrophoresis;, Marcel Dekker, New York, NY, 2002, pp. 106.
[5] P.S. Ghosh, C. Kim, G. Han, N.S. Forbes, V.M. Rotello, Efficient gene delivery vectors by tuning the surface charge density of amino acid-funcionalized gold nanoparticles, Am. Chem. Soc. 2 (2008) 2213–2218.
[6] P.S. Ghosh, C. Kim, G. Han, N.S. Forbes, V.M. Rotello, Gold nanoparticles in delivery applications, Adv. Drug Delivery Rev. 60 (2008) 1307–1315.

[7] H. Joshi, P.S. Shirude, V. Bansal, K.N. Ganesh, M. Sastry, Isothermal titration calorimetry studies on the binding of amino acids to gold nanoparticles, J. Phys. Chem. B 108 (2004) 11535–11540.
[8] S.H. Lee, K.H. Bae, S.H. Kim, K.R. Lee, T.G. Park, Int. J. Pharm. 364 (2008) 94–101.
[9] M. Munoz-Ubeda, A. Rodríguez-Pulido, A. Nogales, O. Llorca, M. Quesada-Perez, A. Martín-Molina, E. Aicart, E. Junquer, Gene vectors based on DOEP/DOPE mixed cationic liposomes: a physiological study, Soft Matter 7 (2011) 5991.
[10] T.T. Nguyen, B.I. Shklovskii, J. Chem. Phys. 114 (2001) 5905.
[11] T.T. Nguyen, B.I. Shklovskii, J. Chem. Phys. 115 (2001) 7298.
[12] H. Ohshima, K. Furusawa, Electrical Phenomena at Interfaces. Fundamentals, Measurements, and Applications;, Marcel Dekker, New York, NY, 1998.
[13] D. Paiva, A. Martin-Molina, I. Cardosa, M. Quesada-Perez, M. Carmo Pereira, S. Rocha, The effect of a fluorinated cholesterol derivative on the stability and physical properties of cationic DNA vectors, Soft Matter 9 (2013) 401.
[14] D. Pissuwan, T. Niidome, M.B. Cortie, The forthcoming applications of gold nanoparticles in drug and gene delivery system, J. Controlled Release 149 (2011) 65–71.
[15] A. Rodríguez-Pulido, A. Martín-Molina, C. Rodríguez-Beas, O. Llorca, E. Aicart, E. Junquer, A theoretical and experimental approach to the compaction process of DNA by dioctadecyldimethylammonium bromide/zwitterionic mixed liposomes, J. Phys. Chem. B 113 (2009) 15648–15661.
[16] S. Sennato, F. Bordi, C. Cametti, J. Chem. Phys. 121 (2004) p4936.
[17] P.M. Tiwari, K. Vig, V.A. Dennis, S.R. Singh, Functionalized gold nanoparticles and their biomedical applications, Nanomaterials 1 (2011) 31–63.
[18] J. Turkevich, P.C. Stevenson, J. Hillier, A study of the nucleation and growth processes in the synthesis of colloidal gold, Discuss. Faraday Soc., 11 (1951) 55–75.
[19] J.L. Viota, F.J. Arroyo, A.V. Delgado, J. Horno, Electrokinetic characterization of magnetite nanoparticles functionalized with amino acids, J. Colloid Interface Sci. 344 (2010) 144–149.
[20] Y. Zhang., G. Liu, C. Hou, J. Chen, J. Wang, Y. Pan, Preparation pf cationic gold nanoparticles and their transfection ability into cultivated cells, Nanoscience 12 (2007) 49–53.

iCBBE

International Conference on Bioinformatics and Biomedical Engineering

Beijing, China, Sep 26th -28th, 2013 **http://www.icbbe.org**

Attendance Confirmation

October 30, 2013

Dear Ms G.G Lazarus,

Thank you very much for your participating to the 7th International Conference on Bioinformatics and Biomedical Engineering (iCBBE 2013) which has been held in Beijing, China from September 26 to 28, 2013.

This is to confirm that you have participated in iCBBE2013 and made an oral presentation for your paper:
ID: 80316
TITLE: The electrokinetic characterization of gold nanoparticles, functionalized with cationic functional groups, and its' interaction with DNA

This conference is organized by the Engineering Information Institute and co-sponsored by the Scientific Research Publishing. It dedicates to creating a stage for exchanging the latest research results and sharing the advanced research methods. There are many distinguished scholars from all over the world to join this meeting, and you can see many exciting new fronts in all areas of Bioinformatics and Biomedical Engineering.

Thanks again for your kind support to iCBBE2013!

Best regards,
iCBBE Organizing Committee
Email: submit@icbbe.org
Tel : +86-13264702230